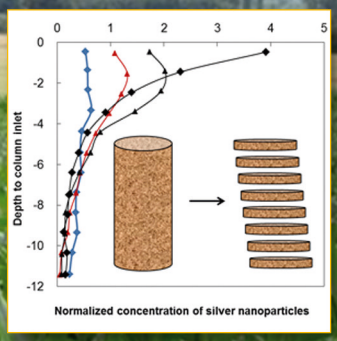

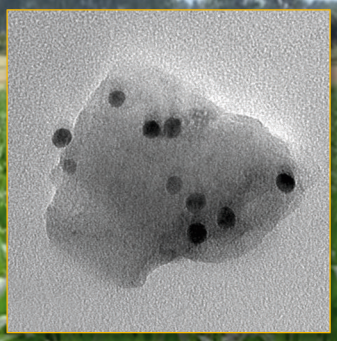

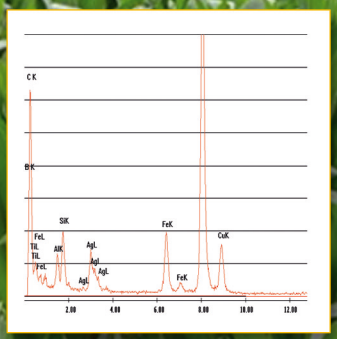

Transport and Retention of Stabilized Silver Nanoparticles in Porous Media

Yan Liang

Member of the Helmholtz Association

JÜLICH
FORSCHUNGSZENTRUM

Schriften des Forschungszentrums Jülich
Reihe Energie & Umwelt / Energy & Environment Band / Volume 212

Forschungszentrum Jülich GmbH
Institute of Bio- and Geosciences (IBG)
Agrosphere (IBG-3)

Transport and Retention of Stabilized Silver Nanoparticles in Porous Media

Yan Liang

Schriften des Forschungszentrums Jülich
Reihe Energie & Umwelt / Energy & Environment Band / Volume 212

ISSN 1866-1793 ISBN 978-3-89336-957-7

Bibliographic information published by the Deutsche Nationalbibliothek.
The Deutsche Nationalbibliothek lists this publication in the Deutsche Nationalbibliografie; detailed bibliographic data are available in the Internet at http://dnb.d-nb.de.

Publisher and Distributor: Forschungszentrum Jülich GmbH
Zentralbibliothek
52425 Jülich
Tel: +49 2461 61-5368
Fax: +49 2461 61-6103
Email: zb-publikation@fz-juelich.de
www.fz-juelich.de/zb

Cover Design: Grafische Medien, Forschungszentrum Jülich GmbH

Printer: Grafische Medien, Forschungszentrum Jülich GmbH

Schriften des Forschungszentrums Jülich
Reihe Energie & Umwelt / Energy & Environment, Band / Volume 212

D 82 (Diss., RWTH Aachen University, 2014)

ISSN 1866-1793
ISBN 978-3-89336-957-7

The complete volume is freely available on the Internet on the Jülicher Open Access Server (JUWEL) at www.fz-juelich.de/zb/juwel

Acknowledgments

First of all I would like to thank the China Scholarship Council (CSC) for the financial support for my Ph.D. This work was carried out at the Agrosphere Institute (IBG-3) in Forschungszentrum Jülich, Germany and funded by the NanoFlow project supported by German Federal Ministry of Education and Research (BMBF).

I would like to express the deepest appreciation to my doctoral advisor Prof. Dr. Erwin Klumpp for all his support during the past four years. His excellent advice, constructive ideas, and insightful comments helped me to go through the difficulties in the work. A special thank goes to Dr. Scott A. Bradford at USDA-ARS U.S. Salinity Laboratory and Prof. Dr. Jiří Šimůnek at University of California, Riverside for their constant support with regard to the numerical simulation and paper writing.

Thanks to Prof. Dr. Andreas Schäffer at RWTH Aachen University for being a referee of my Ph.D. dissertation and for the valuable discussions on my study.

I would like to thank Prof. Dr. Harry Vereecken for the support, discussion, and critical comments on the presentations and half-year reports. I enjoyed the pleasant working atmosphere in the institute and I am very grateful to the staff of the IBG-3 for their contributions to the assistance of the experimental setup and technical issues. I express my gratitude to Herbert Philipp, Claudia Walraf, Peter Klahre, Stephan Köppchen, Ursula Paffen, Dr. Hans-Dieter Narres, Dr. Lutz Weihermüller, Prof. Sander Huisman, and Ansgar Weuthen for their support. Thanks to Dr. Marc Heggen at the Ernst Ruska Centre, Forschungszentrum Jülich GmbH for the support on the measurement by transmission electron microscope. I would like to thank Prof. Michael Burkhardt from HSR, University of Applied Sciences, Rapperswil, Switzerland for his valuable suggestions at the beginning of my work.

I would also like to express my sincere appreciation to Daniela Kasel, Sebastian Rudolph, Alexandre kisner, Stephan Sittig and Joanna Makselon for all the help. Thanks a lot to Dr. Xiaoyi Xu, Prof. Chengliang Li, Dr. Canlan Jiang, Miaoyue Zhang, and Xiaoqian Jiang for their help and company during my stay in Germany. Thanks to my family for their unconditional love and support during my Ph.D study.

Abstrakt

Aufgrund der weit verbreiteten Verwendung von Silbernanopartikeln (AgNPs) besteht das Potential des Eintrags in die Umwelt. Daher sind Informationen über deren Transport und Verbleib in der Umwelt für die Risikoabschätzung unerlässlich. Häufig werden AgNPs durch funktionelle Gruppen, Tenside oder Polymere modifiziert um die Stabilität in Flüssigkeiten zu erhöhen. Diese Oberflächenmodifizierung beeinflusst das Umweltverhalten der AgNPs. Das Ziel dieser Studie ist es daher den Transport und die Retention tensidstabilisierter AgNPs unter umweltrelevanten Bedingungen zu untersuchen. Dazu wurden Experimente mit wassergesättigten Quarzsand-Säulen, zu 90% wassergesättigten Bodensäulen und einem Lysimeter durchgeführt. Die Konzentrationen von AgNPs, Ca^{2+}, K^{+}, Fe und Al wurden mittels induktiv gekoppeltem Plasma-Massenspektroskop bzw. -optischem Emissionsspektrometer (ICP-MS/OES) bestimmt. Die experimentellen Durchbruchskurven (BTCs) und Tiefenprofile (RPs) aus den Säulenversuchen wurden mittels eines Models beschrieben, dass zeit- und tiefenabhängige Retention annimmt. Säulenversuche mit Quarzsand wurden außerdem in Gegenwart von Tensiden durchgeführt um deren Einfluss auf den Transport von AgNPs zu ermitteln. Dabei spielt insbesondere die räumliche Verteilung der AgNPs in der Säule eine Rolle. Außerdem wurde die Remobilisierung retardierter AgNPs in ungestörtem Boden untersucht um die Wechselwirkungen zwischen AgNPs und der Umweltmatrix besser zu verstehen. Hierzu wurde die chemische Zusammensetzung der Lösung (z.B. unterschiedliche Kationen, Ionenstärke) variiert.

Die Versuchsergebnisse der gesättigten Säulenversuche zeigten, dass die normalisierte Eluatkonzentration der BTCs für AgNPs mit abnehmender Ionenstärke der Lösung (IS) sowie zunehmender Fließgeschwindigkeit (q), Sandkorngröße und Inputkonzentration (C_o) zunahm. Im Gegensatz zur konventionellen Filtrationstheorie zeigten die RPs uniforme, nicht-monotone oder hyper-exponentielle Formen die sensitiv gegenüber den physiko-chemischen Bedingungen waren. Der simulierte Retentionskoeffizient (k_1) und die maximale Retentionskonzentration (S_{max}) nahmen mit der IS bei abnehmender Korngröße und/oder C_o zu. In feinerem Sand und bei geringerer C_o waren die RPs mehr hyper-exponentiell aufgrund der höheren Werte für S_{max}, was auf eine höhere Retentionskapazität hinweist. Im Gegensatz dazu waren die RPs nicht-monoton oder uniform bei höherer C_o und in gröberem Sand aufgrund geringerer Werte für S_{max}. Bei geringeren Fließgeschwindigkeiten und höherer IS tendierten die RPs zu höheren Peak-Konzentrationen. Diese Beobachtungen deuten darauf hin, dass uniforme und nicht-monotone RPs auftreten wenn S_{max} aufgefüllt ist. Die Sensitivität der nicht-monotonen RPs auf die Ionenstärke und die Fließgeschwindigkeit in gröberem Sand weisen darauf hin, dass die AgNPs teilweise in einem sekundären Minimum nach der Derjaguin-Landau-Verwey-Overbeek (DLVO) Theorie interagieren. Nichtsdestotrotz führte die Eliminierung durch das sekundäre Minimum nur zu einer geringen Wiederfindung (<10%) der

retardierten AgNPs. Diese Ergebnisse implizieren, dass AgNPs stark irreversibel in einem primären Minimum assoziiert mit der mikroskopischen Heterogenität des porösen Mediums interagieren. Nicht-monotone RPs zeigten Peakkonzentrationen bei größeren Distanzen wenn größere Mengen Tenside zu der AgNPs-Suspension zugefügt wurden. Dies deutet darauf hin, dass die Konkurrenz zwischen AgNPs und Tensiden beim Füllen der Retentionsplätze zu einer Reduktion von S_{max} am Säuleneinlass führten. Wenn Tenside vor dem Säulenversuch aufgegeben wurden um das poröse Medium zu ummanteln, wurde die Retentionskapazität für AgNPs in Abhängigkeit der Tensidkonzentration und der Abfolge von AgNPs- und/oder Tensidapplikation auf die Säule herab gesetzt.

Die experimentellen und simulierten Ergebnisse der ungestörten Bodensäulen zeigten ähnliche Trends bezüglich des Einflusses physiko-chemischer Faktoren. Darunter fällt der erhöhte Transport mit abnehmender Ionenstärke der Lösung, zunehmender AgNPs-Ausgangskonzentration und Fließgeschwindigkeit. So nehmen k_1 und S_{max} mit zunehmender IS und abnehmendem C_o zu. Im Gegensatz zu den gesättigten Säulen wurden hier in fast allen Transportversuchen signifikante Verzögerungen der AgNPs-BTCs sowie hyper-exponentielle RPs beobachtet. Ein Großteil der injizierten AgNPs wurde in den ersten 3 cm der Säule zurück gehalten. Der hohe k_1 resultierte in verzögerten BTCs bis S_{max} aufgefüllt war und dadurch in höheren Eluatkonzentrationen. Hyper-exponentielle Tiefenprofile wurden vermutlich durch hydro-dynamische Effekte am Säuleneinlass verursacht welche zu einem konzentrierten AgNP-Fluss zur Festphasenoberfläche führten. Höhere IS und geringere C_o führten zu mehr hyper-exponentiellen RPs aufgrund höherer Werte für S_{max}. Der Lysimeterversuch ließ vermuten, dass der Hauptanteil der AgNPs nach 12 Monaten bei unterbrochener Beregnung in den obersten Schichten (20 cm) retardiert wurde. Dennoch kann eine Grundwasserkontamination nicht vollständig ausgeschlossen werden.

Die Ergebnisse von Remobilisierungsversuchen wiesen darauf hin, dass die Retention von AgNPs in Gegenwart von Ca^{2+} deutlich stärker ausgeprägt war als von K^+ bei derselben IS. Außerdem war die Freisetzung von AgNPs bei einer Abnahme der IS bei K^+ stärker ausgeprägt als bei Ca^{2+}. Die stärkere Wechselwirkung von AgNPs in der Gegenwart von Ca^{2+} wird auf die Bildung von Kationenbrücken zurückgeführt. Eine weitere Freisetzung von AgNPs und Ton aus dem Boden wurde durch Ionenaustausch (K^+ für Ca^{2+}) verursacht. Dies wird auf reduzierte Brückenbildung und IS durch Vergrößerung der elektrischen Doppelschicht zurückgeführt. Untersuchungen mit Transmissionselektronenmikroskopie und energie-dispersiver Röntgenspektroskopie sowie die Korrelation zwischen freigesetzten Bodenkolloiden und AGNPs zeigten, dass ein Teil der im Säuleneluat gefundenen AgNPs an die freigesetzte Tonfraktion gebunden war. Co-Transport von AgNPs durch Bodenkolloide kann daher von großer Bedeutung für deren Transportverhalten in der Umwelt sein.

Abstract

Due to the widespread application of silver nanoparticles (AgNPs) and the resulting potential exposure in the environment, information about their environmental transport and fate is essential for risk assessment. AgNPs are commonly modified with functional groups, surfactants, or polymers to increase their stability in liquids and the surface modification greatly influences the environmental behavior of AgNPs. The aim of this study is therefore to investigate the transport and retention of surfactant-stabilized AgNPs under environmentally relevant conditions. Experiments were conducted with water-saturated columns packed with quartz sand, around 90% water-saturated columns filled with undisturbed loamy sand soil, and a lysimeter. Inductively coupled plasma-mass spectrometry/optical emission spectrometry (ICP-MS/OES) was used to analyze the concentrations of AgNPs, Ca^{2+}, K^{+}, Fe, and Al. The experimental breakthrough curves (BTCs) and retention profiles (RPs) from column experiments were described using a numerical model that considers time- and depth-dependent retention. Column experiments with quartz sand packing were also conducted in the presence of surfactant to deduce the influence of surfactant on AgNP transport, especially on the spatial distribution of retained AgNPs that determines the long-term transport potential. In addition, to better understand the interactions of AgNPs and the matrix in the environment, remobilization of retained AgNPs from undisturbed soil was studied by changing the solution chemistry such as change of cation types and ionic strength reduction.

Experimental results showed that the normalized concentration in BTCs for AgNPs obtained from water-saturated columns increased with a decrease in solution ionic strength (IS), and an increase in flow velocity (q), sand grain size, and input concentration (C_o). In contrast to the conventional filtration theory, RPs in sand exhibited uniform, nonmonotonic, or hyperexponential shapes that were sensitive to physicochemical conditions. The simulated retention rate coefficient (k_1) and maximum retained concentration on the solid phase (S_{max}) increased with IS and as the grain size and/or C_o decreased. The RPs were more hyperexponential in finer textured sand and at lower C_o because of their higher values of S_{max}, which indicated a larger retention capacity of the porous media. Conversely, RPs were nonmonotonic or uniform at higher C_o and in coarser sand that had lower values of S_{max}, and tended to exhibit higher peak concentrations in the RPs at lower flow velocities and at higher solution IS. These observations indicate that uniform and nonmonotonic RPs occurred under conditions when S_{max} was filled. The sensitivity of the nonmonotonic RPs to IS and flow velocity in coarser textured sand indicates that AgNPs were partially interacting in a secondary energy minimum according to the Derjaguin-Landau-Verwey-Overbeek (DLVO) theory. However, elimination of the secondary minimum only produced recovery of a small portion (<10%) of the retained AgNPs. These results imply that AgNPs were largely irreversibly interacting in a primary minimum associated with microscopic heterogeneity of the porous

media. Nonmonotonic RPs had peak concentrations at greater distances when larger amounts of surfactant were added to AgNP dispersion, suggesting that the competition for filling retention sites between AgNPs and surfactant reduced S_{max} close to the column inlet. The introduction of surfactant to pre-cover porous media resulted in stronger mobility than adding it to AgNP dispersion. These findings demonstrated that the occupation of retention sites by surfactant reduced the retention capacity for AgNPs to different degrees depending on the surfactant concentration and the sequence of AgNP and/or surfactant application to the column.

Experimental and simulated results for undisturbed soil columns showed similar trends with regard to the effects of physicochemical factors, e.g., enhanced transport with decreasing solution IS, increasing AgNP input concentration and flow velocity, and increased k_1 and S_{max} with increasing IS and decreasing C_o. In contrast, a significant retardation of AgNP breakthrough and hyperexponential RPs were observed in almost all the transport experiments with soil. A major portion of the injected AgNPs was retained in the first 3 cm of the soil column. The high k_1 resulted in retarded BTCs until S_{max} was filled and then high effluent concentrations were obtained. Hyperexponential RPs were likely caused by the hydrodynamics at the column inlet which produced a concentrated AgNP flux to the solid surface. Higher IS and lower C_o produced more hyperexponential RPs because of larger values of S_{max}. Lysimeter experiments indicated that the major removal of AgNPs occurred in the top layers (first 20 cm) after 12 months intermittent irrigation, but the potential contamination of the groundwater by AgNPs may not be fully excluded.

Results from remobilization experiments indicated that retention of AgNPs was much more pronounced in the presence of Ca^{2+} than of K^+ at the same IS, and the amount of AgNP released with a reduction in IS was larger for K^+ than Ca^{2+} systems. The stronger AgNP interactions in the presence of Ca^{2+} were attributed to cation bridging. Further release of AgNPs and clay from the soil was induced by cation exchange (K^+ for Ca^{2+}) that reduced the bridging interaction and IS reduction that expanded the electrical double layer. Results with transmission electron microscopy and energy-dispersive X-ray spectroscopy, and the correlations between released soil colloids and AgNPs indicated that some of the released AgNPs were associated with the released clay fraction. Co-transport of the AgNPs by soil colloids may therefore be of importance for their transport behavior in the environment.

Table of contents

Abbreviations

AgNPs	silver nanoparticles
BET	Brunauer-Emmett-Teller
BTCs	breakthrough curves
DLS	dynamic light scattering
EDX	energy-dispersive X-ray spectroscopy
EPM	electrophoretic mobility
HPLC	high-performance liquid chromatography
ICP-MS	inductively coupled plasma-mass spectrometry
ICP-OES	inductively coupled plasma-optical emission spectroscopy
IS	ionic strength
NPs	nanoparticles
RPs	retention profiles
SEM	scanning electron microscopy
TDR	time-domain reflectrometry
TEM	transmission electron microscopy
XDLVO	extended Derjaguin-Landau-Verwey-Overbeek
XRD	X-ray diffraction

Symbols

A_{11}	Hamaker constant for stabilized silver nanoparticles [J]
A_{22}	Hamaker constant for the collector surface [J]
A_{33}	Hamaker constant for water [J]
A_{123}	combined Hamaker constant in the system [J]
C	aqueous phase nanoparticle concentration [mg L^{-1}]
C_o	nanoparticle input concentration [mg L^{-1}]
D	hydrodynamic dispersion coefficient [cm^2 min^{-1}]
d	brush layer [nm]
d_{50}	median grain size of the porous medium
d_p	diameter of nanoparticles [nm]
e	electron charge [C]
h	separation distance between the nanoparticle and the interface of interest [nm]
k_b	Boltzmann constant [J/K]
k_1	first-order retention coefficient [min^{-1}]
l^{-1}	electrophoretic softness [nm]
M_{eff}	mass percentage recovered from effluent
M_{sand}	mass percentage recovered from sand
M_{total}	mass percentage recovered from total
M_w	molecular weight of the surfactant [g mol^{-1}]
n_{j0}	number concentration of ions in the bulk solution
n^{∞}	bulk number concentration of the electrolyte

q	Darcy water flux [cm min^{-1}]
r_1, r_2	radii of a particle and the second sphere, respectively [nm]
R^2	Pearson's correlation coefficient
S	solid phase nanoparticle concentration [g g^{-1}]
S_{max}	maximum solid phase concentration of deposited nanoparticles [g g^{-1}]
S_{max}/C_o	normalized maximum solid phase concentration of deposited nanoparticles [cm^3 g^{-1}]
S_w	water saturation
t	time [min]
T_k	absolute temperature [K]
V_{ed}	energy of electrostatic double layer interaction [kT]
V_{Tmax}	maximum of the total XDLVO energy [kT]
V_{vdW}	energy of van der Waals [kT]
$(V_{vdw}+ V_{ed})_{max}$	maximum energy of van der Waals (V_{vdW}) and electrostatic double layer interaction (V_{ed}) [kT]
y	year
z	distance from the column inlet [cm]
z_e	ion valence
β	an empirical parameter controlling the shape of the spatial distribution of retained nanoparticles
ε_o	permittivity of free space [C/V_m]
ε_r	relative permittivity
ζ^a	predicted core surface potential of silver nanoparticles [mV]
ζ^b	measured zeta potential of quartz sand [mV]

η	dynamic viscosity of water
η_o	single-collector efficiency
θ_w	volumetric water content
κ	Debye parameter [m^{-1}]
κ_m	Debye-Hückel parameter of the coating layer [nm]
λ	dispersivity [cm]
λ_{vdW}	characteristic wavelength, 100 nm
μ	electrophoretic mobility [mV]
v	volume of a solvent molecule [nm^3]
σ	volumetric fixed charge density
ρ	density of adsorbed surfactant layer [g cm^{-3}]
ρ_b	soil bulk density [g cm^{-3}]
Γ_{max}	maximum attained surface excess concentration
φ	porosity
χ	Flory-Huggins solvency parameter
ψ	function to account for time- and depth-dependent blocking
ψ_{DON}	Donnan potential in the coating layer
Φ	volume fraction of coating

1 Introduction*

Nanoparticles (NPs) are defined as particles with at least one dimension with a length of 1-100 nm (Oberdorster 2005). Because of their extremely fine size, NPs may have enhanced or even unique physicochemical and biological properties that differ from the individual atoms, molecules, or bulk materials (Foss Hansen et al. 2007; Klaine et al. 2008). Engineered NPs have been widely used in household and industrial applications, e.g., cosmetics, health care products, paint, plastics, recreational equipment, and electronics (Nowack and Bucheli 2007; Lowry and Casman 2009). The engineered NPs used will potentially be released into the environment.

The pathways and processes of NPs in the environment are depicted in Figure 1.1 (Wiesner et al. 2006 ; Nowack and Bucheli 2007). The release of NPs into the environment may originate from point sources such as landfills or manufacturing, nonpoint sources such as storms and wet deposition, accidental release during production or transport, and intentional release such as zero-valent iron NPs injected into the groundwater for remediation purposes. The released NPs will end up in waters, sediments, or soils through sewage treatment facilities, waste handling, or aerial deposition. Aggregation of NPs increases the removal of suspended NPs in aqueous phase by the sedimentation of the larger particles. NPs may also be attached onto other particles such as natural colloids or taken up by plants or animals. Potential exposure of human to NPs through the environment or the food chain has also been considered.

* Contains parts from Liang, Y.; Bradford, S. A.; Simunek, J.; Vereecken, H.; Klumpp, E., Sensitivity of the transport and retention of stabilized silver nanoparticles to physicochemical factors, Water Research 2013, 47 (7) 2572-2582 and Liang, Y.; Bradford, S. A.; Simunek, J.; Heggen, M.; Vereecken, H.; Klumpp, E., Retention and Remobilization of Stabilized Silver Nanoparticles in an Undisturbed Loamy Sand Soil. Environmental Science & Technology, 2013, 47 (21), 12229-12237 with permissions from Elsevier and American Chemical Society, respectively.

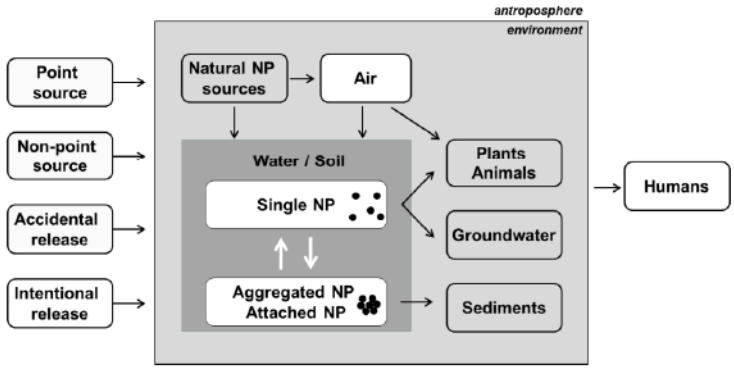

Figure 1.1. Nanoparticle pathways from the anthroposphere into the environment, reactions in the environment, and exposure of humans. Modified from Nowack and Bucheli (2007).

1.1 Silver nanoparticles and the environment

Silver in the environment commonly exists as nanoparticles or clusters that are frequently associated with sulfide (Nowack et al. 2011). Silver nanoparticles (AgNPs) have been registered as a biocidal material in the United States since 1954 and actually have been used for more than 100 years as colloidal silver (Nowack et al. 2011). Currently, AgNPs are widely used in various nanotechnology-based commercial products because of their strong antimicrobial activity (Kang et al. 2011). The application of AgNPs consists of a wide range, e.g., textiles, filters, paints, cosmetics, tooth brushes, food packaging, kitchen surfaces, and medical equipment, as well (Gottschalk et al. 2010; Li et al. 2010). The presence of nanosilver has been confirmed in silver-embedded household products by scanning electron microscopy (Benn et al. 2010). They are potentially released from the products into the environment as colloidal silver or silver ions (Benn and Westerhoff 2008; Geranio et al. 2009; Liu and Hurt 2010; Cleveland et al. 2012). Benn et al. (2010) demonstrated that up to 45 µg of silver, with size fractions of both larger and smaller than 100 nm, was released from 1 g household products. Release of silver from textiles and biocidal plastics in the form of NPs or ions may account for around 15% of the total silver released into waters (Blaser et al. 2008). In textile such as socks, even nearly 100% release of the total silver content in products was observed depending on the

manufacturing processes (Benn and Westerhoff 2008). According to the limited information (Gottschalk et al. 2009), AgNPs in surface water (U.S. and Europe) are predicted to range from 0.088 to 2.63 ng/L. In sediments, the estimated concentrations are between 0.7 and 2.2 μg/kg, and their concentration can be even higher in sludge-treated soil.

AgNPs have been shown to be toxic to cells, bacteria, fungi, and other microorganisms (Lee et al. 2007 ; Choi et al. 2009; Fabrega et al. 2009; Kennedy et al. 2010), e.g., AgNPs could penetrate into chorionic space via pore canals of zebra fish embryos by Brownian diffusion. Toxicity of AgNPs is dependent on various factors such as the surface charge, size, concentration, shape of the particles, and the capping agent (El Badawy et al. 2010). Unique hazards of AgNPs to microorganisms may be attributed to the nanoscale size because their toxicity is potentially increased with decreasing particle size (Kennedy et al. 2010; Shaw and Handy 2011). This is because smaller NPs, compared to larger particles, are able to penetrate cell membranes more easily and reduce the permeability of membranes and hinder the respiration process (Zook et al. 2011). Similarly, antibacterial ability of AgNPs was found to decrease in the presence of divalent ions (such as Ca^{2+}) due to precipitation and formation of large aggregates (Fabrega et al. 2009; Zhang et al. 2012). Conversely, although the dissolved natural organic matter such as humic acid tends to stabilize NP dispersion and decrease aggregation, it may reduce the toxicity of AgNPs by creating a physical barrier between NPs and bacteria when it is adsorbed on the NP surface (Zhang et al. 2012). It has been confirmed that the reproduction activity of bacteria used for wastewater treatment could be halted by AgNPs (Liang et al. 2010). Furthermore, AgNPs may extend their antimicrobial effects to ecosystem due to the fact that the main portion of silver released into wastewater treatment plants is incorporated into sewage sludge and potentially be spread to soils (Blaser et al. 2008). Consequently, there is concern that the antimicrobial effect of released AgNPs may adversely impact ecosystem influenced by the properties of AgNPs and the environmental conditions (Choi et al. 2010).

1.2 Surface modification of nanoparticles

Surface modification of NPs is common and important to enhance the stability of NPs in liquid phase (Sarkar et al. 2005; Jaisi et al. 2008) because many NPs will lose their unique properties or be less effective once they have aggregated and precipitated from dispersion (Darlington et al. 2009). Charge or steric stabilization is common to form barriers between two NPs that are necessary for the stability of particle dispersion (Kvitek et al. 2008). Frequently, the ways to functionalize NPs are to produce them with surface coatings, including a wide range of metal ions, small molecules, surfactants, polymers, and charged functional groups (Henglein and Giersig 1999; Jaisi et al. 2008; Kvitek et al. 2008). In the case of surfactant as the coating, it is an equilibrium state between the interaction of NPs, NP- bounded surfactant molecules, and free surfactant molecules (Christian et al. 2008). This equilibrium may shift and result in instability or precipitation when the system is interrupted such as excessive dilution of the surfactant, and hence the concentration of the free surfactant molecules should be maintained at the critical micelle concentration to prevent aggregation (Christian et al. 2008). Functionalization highly changes the properties of NP surface. It has been confirmed that Suwannee River humic acid molecules adsorbed on the surface of iron oxide NPs may neutralize the positive charge or enhance the negative charge depending on the solution pH, and thus lead to a shift in the point of zero charge (Baalousha 2009).

The surface modification of NPs and the presence of stabilizers can significantly influence their transport behavior under environmental conditions and potentially extend their toxicity in ecosystems (Christian et al. 2008; Jaisi et al. 2008; Jeong and Kim 2009; Phenrat et al. 2010; Wang et al. 2012). In general, particles with a surface charge similar to that of the collector surface are transported, while those with opposite charges tend to be retained in the porous media more easily (Darlington et al. 2009). However, surface coating may play a dual role in the transport behavior of NPs. On one hand, surface modification can generally enhance NPs mobility due to increased steric or electrostatic repulsions. On the other hand, it may promote NP retention in porous media by bridging effect (Lin et al. 2012). It was found that the

attachment efficiency of fullerene NPs onto a flat silica surface or in a porous medium packed with glass beads was considerably decreased in the presence of 1 mg L^{-1} (as total organic carbon) Suwannee River humic acid (Chen and Elimelech 2006) or tannic acid (Grolimund et al. 2007), respectively. Due to the stabilization by surface coatings, the potentials of enhanced NP transport and the extended ecotoxicity to the ecosystem are also concerned (Kanel et al. 2007; Kvitek et al. 2008).

In the case of AgNPs, surface functionalization is common because aggregation can lead to a loss of antibacterial activity (Kvitek et al. 2008; Zhang et al. 2012). The increased stability in aqueous phase and mobility in porous media by surface modification have been recently discussed (Kvitek et al. 2008; Tian et al. 2010; Lin et al. 2011; Song et al. 2011; Flory 2012; Thio et al. 2012; Zhang et al. 2012). The presence of natural organic matter and/or stabilizers such as surfactants and polymers generally increases the repulsive potentials between two particles according to extended Derjaguin-Landau-Verwey-Overbeek theory (DLVO), and thus increases the stability of NPs in aqueous phase (Song et al. 2011). Furthermore, repulsive forces arising from the adsorption of these stabilizing materials onto AgNP or collector surface tend to enhance the particle mobility in porous media by means of reduced aggregation and/or attachment. These studies indicate that the role of surface modification of AgNPs on their fate is critical and may even act as a key factor to control their transport and retention behavior. Surface coatings can also affect the bactericidal properties of NPs. Toxicity of AgNPs coated with branched polyethyleneimine show higher toxicity to *bacillus* species than coated with citrate due to the different electrostatic barriers between particles and *bacillus* cells (El Badawy et al. 2010). Knowledge on the mobility of stabilized AgNPs in porous media is therefore of importance when assessing the risk of exposure to the ecosystem and developing appropriate regulatory strategies of waste management and remediation techniques.

1.3 Transport of silver nanoparticles in porous media

Information on the stability and aggregation of AgNPs in aqueous media is important to assess their transport and fate in the environment. The surface properties of AgNPs and the solution chemistry significantly influence their stability (Thio et al. 2012). The presence of divalent cations (e.g., Ca^{2+} and Mg^{2+}) generally decreases the coagulation concentration (CCC) of AgNPs and produces larger aggregates more easily compared to monovalent cations (Zhang et al. 2012). In contrast, the presence of organic matter or surface coating tends to increase CCC and reduce aggregation by steric or electrostatic repulsion (Lin et al. 2012; Thio et al. 2012). According to the study from Badawy et al. (2010), AgNP aggregation was affected by a combination of ionic strength, cation types, and pH to various degrees with different surface coatings. The aggregation of polyvinylpyrrolidone (PVP)-coated AgNPs was not influenced by a wide range of ionic strength, solution pH, and electrolyte type, whereas the surface charge and aggregation of branched polyethyleneimine-coated AgNPs were more sensitive to pH (Badawy et al. 2010).

The interaction with porous media is a crucial process that determines the transport and retention of AgNPs after exposure to the environment. Previous studies with quartz sands (Tian et al. 2010; Lin et al. 2011; Song et al. 2011; Lin et al. 2012; Thio et al. 2012) or soils (Sagee et al. 2012) have demonstrated that AgNP transport is sensitive to the surface properties of both AgNPs and porous media, and chemical composition the of solution, e.g. surface modification of AgNP and collector surface, the pH value, and the type of cations. Surface modification and/or the presence of organic matter such as surfactant or humic acid tends to enhance the mobility of AgNPs (Tian et al. 2010; Lin et al. 2012; Thio et al. 2012), while higher ionic strength and divalent cations promote aggregation and retention due to the compressed diffuse layer/weakened electrical double layer and the bridging effect, respectively (Badawy et al. 2010; Lin et al. 2011; Thio et al. 2012; Zhang et al. 2012). Tian et al. (2010) investigated the transport of sodium dodecylbenzene sulfonate (SDBS)-dispersed AgNPs in quartz sand treated by two methods (washed by water and by 10% nitric acid) and pointed out that the presence of

surfactants and the treated porous media enhanced AgNP mobility. It was also concluded that the presence of SDBS caused deviations from DLVO and filtration theory. Lin et al. (2012) demonstrated that the coatings on both of the NPs and collector were necessary to reduce NP deposition. In particular, an apparent affinity and a high sensitivity (to ionic strength) of coated AgNP onto the collector surface may result from a shift of attachment location from the core surface by a distance of coating thickness, then lowered the electrical double layer repulsion that must be overcome for attachment (Lin et al. 2012). The heterogeneity of collector surface has also been demonstrated to strongly influence AgNP transport. Lin et al. (2011) investigated the transport of AgNPs in different mixing mass ratios of unmodified and iron oxide-modified glass beads under pH 5.0 and pH 8.3 with a variety of ionic strengths. They found a linear correlation between the composition of a surface fraction and the NP affinity for this heterogeneous grain surface. At a pH lower than the point of zero charge of iron oxide, the retention of AgNPs in an iron oxide-modified porous medium was higher than in an unmodified media. Song et al. (2011) showed that the hydrophobicity of surface coatings was important to the attachment efficiency of AgNPs to hydrophobic collector surfaces. A study on AgNP transport in soil showed a high mobility with effluent relative concentrations ranging from 30% to 70% (Sagee et al. 2012). Mechanical straining and chemical interactions between AgNPs and the soil surfaces were suggested to play important roles in the retention process (Sagee et al. 2012). Similar with in sand, AgNP retention in soil was also reduced in the presence of humic acid and increased at a lower flow rate (Sagee et al. 2012). Furthermore, properties of interacting surfaces have been clearly demonstrated to influence the dissolution, aging, and transformation (e.g. into silver sulfide NPs) of AgNPs that are released into the environment (Benn and Westerhoff 2008; Geranio et al. 2009; Kim et al. 2010; Nowack 2010; Cornelis et al. 2012; Coutris et al. 2012; Levard et al. 2012; Li and Lenhart 2012). Kim et al. (2010) studied the nature of Ag-containing NPs in sewage sludge collected from a municipal wastewater treatment plant and found that these NPs were present as silver sulfide nanocrystals in a size range of 5-20 nm. Kaegi et al. (2011) studied the behavior of AgNPs in a pilot waste water treatment plant and also found that most of the Ag in both of the effluent and the sludge was in

the form of silver sulfate, and pointed out that the transformation process could occur quickly (less than 2 hours).

The interaction of AgNPs with natural soil colloids can be of importance to determine NP removal due to attachment, straining, physical filtration, and release of retained NP by co-transport with soil colloids in the environment. Zhou et al. (2012) investigated the interactions of AgNPs and montmorillonite and demonstrated that the heteroaggregation of these mixed particles depended on both pH and ionic strength, e.g., montmorillonite reduced the stability of negatively charged AgNPs when pH values were below the isoelectric point of montmorillonite edge site, increased coagulation occurred within an intermediate range of the ionic strength. In addition, the charge heterogeneity enabled the clay minerals strongly interact with NPs. Consequently, the natural clay may destabilize or immobilize NPs and potentially be used for decontamination of nanomaterial (Zhou et al. 2012). Cornelis et al. (2012) studied the retention of AgNPs onto natural soils and indicated that the clay mineral edges and oxides of metals such as iron and aluminum provided preferentially adsorption sites for negatively charged AgNPs. Both the surface properties of the solid phase and the physical structure of the matrix can be altered when soil colloids are suspended in the pore water and/or released into the flowing liquid phase. Accordingly, the potential impacts on NP transport (due to the released natural colloidal particles and the corresponding physical and chemical changes of matrix) can be of importance to determine the fate of AgNPs within the subsurface and the aquatic systems.

2 Theory and background*

As the wide application of NPs and the risk of exposure to the ecosystem, the transport and fate of NPs in the subsurface environment have been a topic of significant scientific interest because soils and aquifers act as the primary filter systems to protect water resources (Nowack and Bucheli 2007). Increasing studies toward understanding the NP transport processes, the dominant mechanisms, and the importance of various effects from physicochemical conditions have been recently reported (Jaisi et al. 2008; Wang et al. 2012). A growing body of research carried out with laboratory-scale transport experiments demonstrates the high mobility of NPs under environmentally relevant conditions, implying a risk potential of groundwater contamination (Song et al. 2011; Wang et al. 2012; Kasel et al. 2013). The mobility of colloidal particles in the subsurface environment is generally considered to be determined by physicochemical interactions and size-related processes (Jaisi et al. 2008; Jaisi and Elimelech 2009; Sagee et al. 2012). Researchers have demonstrated a complex coupling between many physicochemical factors (e.g., grain size, flow velocity, the chemistry of aqueous and solid phases, organic matter, particle concentration, functionalized surfaces) and the environmental transport of NPs (Jaisi et al. 2008; Liu et al. 2009; Tong et al. 2010; Godinez and Darnault 2011; Wang et al. 2012). The quantitative evaluation of these complex effects of various environmental factors on the transport behavior of NPs accounts for a crucial part in the risk assessment of contamination. Therefore, the theoretical and numerical descriptions of the NP stability (in aqueous phase) and transport (in porous media) are of fundamental interest in the research.

* Contains parts from Liang, Y.; Bradford, S. A.; Simunek, J.; Vereecken, H.; Klumpp, E., Sensitivity of the transport and retention of stabilized silver nanoparticles to physicochemical factors, Water Research 2013, 47 (7) 2572-2582 and Liang, Y.; Bradford, S. A.; Simunek, J.; Heggen, M.; Vereecken, H.; Klumpp, E., Retention and Remobilization of Stabilized Silver Nanoparticles in an Undisturbed Loamy Sand Soil. Environmental Science & Technology, 2013, 47 (21), 12229-12237 with permissions from Elsevier and American Chemical Society, respectively.

2.1 Extended DLVO theory

The interfacial interaction between colloid and substrate in aqueous media and the colloid deposition in saturated porous media are commonly described by the colloid filtration theory (CFT) (Yao et al. 1971). CFT assumes that colloid immobilization occurs as irreversible deposition in a primary energy minimum that can be determined by the Derjaguin-Landau-Verwey-Overbeek (DLVO) theory (Verwey 1947; Derjaguin and Landau 1993). This theory explains the aggregation of colloidal dispersions and quantitatively describes the force between two charged surfaces in the aqueous phase. In the classical DLVO theory, the interaction energy accounts for attractive potential of van der Waals interaction (V_{vdW}) and repulsive potential of electrostatic double layer interaction (V_{ed}).

The interaction energy barriers between NP-NP and NP-collector therefore play an important role in the stability of NP suspensions and in determining the attachment potential of particles to collectors. Based on the DLVO theory, the total interaction energy between particles consists of the sum of V_{vdW} and V_{ed}, which can be calculated as (Hogg et al. 1966; Gregory 1981):

$$V_{\mathrm{vdW}}(h) = -\frac{A_{123} r_1 r_2}{6h(r_1 + r_2)}\left(1 + \frac{14h}{\lambda_{\mathrm{vdW}}}\right)^{-1} \tag{2.1}$$

$$A_{123} = \left(\sqrt{A_{11}} - \sqrt{A_{33}}\right)\left(\sqrt{A_{22}} - \sqrt{A_{33}}\right) \tag{2.2}$$

$$V_{\mathrm{ed}}(h) = \frac{\pi \varepsilon_r \varepsilon_o r_1 r_2}{(r_1 + r_2)}\left\{2\psi_1\psi_2 \ln\left[\frac{1 + \exp(-\kappa h)}{1 - \exp(-\kappa h)}\right] + (\psi_1^2 + \psi_2^2)\ln[1 - \exp(-2\kappa h)]\right\} \tag{2.3}$$

$$\kappa = \sqrt{\frac{e^2 \sum_i n_{\mathrm{j0}} z_e^2}{\varepsilon_r \varepsilon_o k_{\mathrm{b}} T_{\mathrm{k}}}} \tag{2.4}$$

where r_1 and r_2 are the radii of a particle and the second sphere, respectively, h is the separation distance between the nanoparticle and the interface of interest, λ_{vdW} is the characteristic wavelength, usually taken as 100 nm, A_{123} is the combined Hamaker constant in the system, which can be calculated from eq. (2.2) where A_{11} is the Hamaker constant for NPs, A_{22} is the Hamaker constant for the collector surface, A_{33} is the Hamaker constant for water (3.7×10^{-20} J). In eq. (2.3), ε_o is the permittivity of free space, ε_r is the relative permittivity, ψ_1 and ψ_2 are the zeta potentials of the NPs and sand grain, respectively. The Debye parameter (κ) is expressed in eq. (2.4), e is the electron charge, n_{j0} is the number concentration of ions in the bulk solution, z_e is the ion valence, k_b is the Boltzmann constant, and T_k is the absolute temperature. A sphere-sphere interaction is normally calculated in NP-NP systems and a sphere-plate interaction is used in NP-collector systems. The same size values were used for r_1 and r_2 in eqs. (2.1) and (2.3) when calculated sphere-sphere interaction (NP-NP), whereas r_1 replaced the quantity $(r_1\, r_2)/(r_1+ r_2)$ for sphere-plate interaction (NP-sand) (Bradford and Torkzaban 2008).

Consequently, the total interaction energy as a function of distance between two interacting surfaces can be calculated by the above equations. However, significant discrepancies and deviations are reported between theoretical predictions and experimental observations regarding the colloid stability, retention, and adhesion in both simplified and natural systems (Tufenkji and Elimelech 2004; Hoek and Agarwal 2006). Consequently, non-DLVO interactions have been considered to address these differences, e.g., hydration force, hydrophobic interaction, and steric and Lewis acid/base interactions (Grasso et al. 2002). The combination of the non-DLVO interactions with van der Waals and electrostatic interactions is commonly referred to the extended DLVO (XDLVO). The XDLVO theory is able to describe the interaction between two particles in a system with various factors that are neglected in DLVO theory such as surface roughness (Hoek and Agarwal 2006) and the presence of organic matter (Phenrat et al. 2010)

2.2 Nanoparticle transport in porous media

Simplified systems are typically employed to determine the fundamental mechanisms and models for colloid/NP transport and deposition in the environment. For example, quartz sands or glass beads are often used as idealized porous media and monovalent salts are used in electrolyte solutions. Most research studies therefore frequently apply idealized systems consisting of repacked, homogeneous, coarse textured porous media and monovalent salts to minimize any disturbance from other physicochemical parameters (Jaisi et al. 2008; Liu et al. 2009; Wang et al. 2012). This previous research has provided fundamental knowledge and understanding of the influence of many physicochemical factors on particle transport and retention. The important deposition mechanisms of colloids/NPs in porous media is schematically described in Figure 2.1, including Brownian diffusion (a), interception (b), gravitational sedimentation (c), and straining (d) when the agglomerates are too big to pass through the medium pores. In contrast, the blocking effect (e) decreases NP retention due to the repulsive potential between the previously deposited and the approaching particles. The importance of these interaction processes dependents on the physicochemical properties of colloids/NPs, collector, and solution chemistry. Attachment or interception of NPs onto collectors is strongly influenced by the chemistry of NP and solution (Kanel and Choi 2007; Jaisi et al. 2008; Jeong and Kim 2009; Phenrat et al. 2010). Increased ionic strength can result in electrostatic double layer compression, which leads to increased aggregation and deposition of particles, thus reduce NP mobility (Jaisi et al. 2008; Tian et al. 2010; Lin et al. 2011; Wang et al. 2011). Removal of NPs by straining and physicochemical filtration may also depend on ionic strength, e.g., the deposition of single-walled carbon nanotubes is dominated by physicochemical filtration at higher ionic strength, while both straining and physicochemical filtration control the deposition at low ionic strength (<3.0 mM) (Jaisi et al. 2008). Mass transfer of NP to porous media is also significantly affected by grain size and by flow velocity under certain conditions. Decreasing grain size tends to increase NP deposition by the enhanced magnitude of straining (Gargiulo et al. 2007; Torkzaban et al. 2008; Wang 2009). Increase in

flow velocity can lead to increased transport due to greater drag force and hydrodynamic force that may break up aggregates or cause more attached particles release from collector (Lecoanet and Wiesner 2004; Chowdhury et al. 2011; Godinez and Darnault 2011). Flow rate has also been demonstrated to control the density and location of retention in porous media, e.g., the deposition can be diffused over a larger area in porous media at a higher velocity (Jeong and Kim 2009). Li et al. (2005) investigated retention and release of microspheres as a function of flow velocity and demonstrated a decreased retention because of the higher flow rates employed under unfavorable attachment conditions. The authors also proposed that the retention capacity for secondary-minimum-associated particles can be reduced under higher flow rate due to a reduction of stagnation flow zone volumes and an increase of collision potential between mobile and retained colloids (Li et al. 2005).

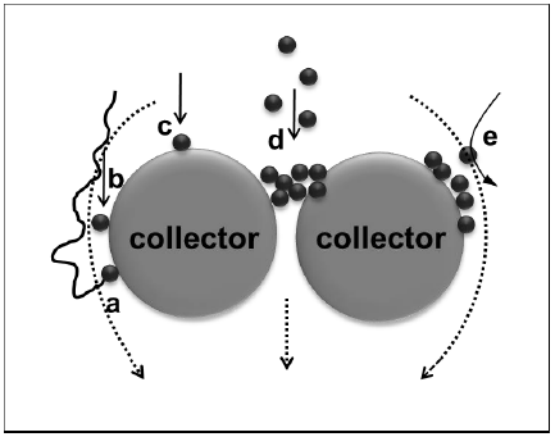

Figure 2.1. Schematic depiction for transport of colloids/nanoparticles in porous media. The particles can attach to the collector surface through (a) Brownian diffusion, (b) interception, (c) gravitational sedimentation, and (d) straining. Blocking effect (e) will reduce particle deposition. The small dots, dotted lines, and solid lines with arrows represent the particles, fluid directions, and the paths/directions of particle movement, respectively. Modified from Lin et al. (2010) and Zhang et al. (2012).

However, the simplified porous media are not able to account for the full complexity and heterogeneity of natural soils (e.g., pronounced surface roughness, highly nonuniform distribution of grain size, complex pore structure, and surface chemical heterogeneity due to a wide variety of inorganic and organic compounds). Previous studies concerning the mobility of colloids/NPs in soils have indicated that the pore structure and soil properties strongly affect particle retention in the subsurface environment (Kjaergaard et al. 2004; Jaisi and Elimelech 2009; Sagee et al. 2012). The pore structure of undisturbed soil and the leaching of naturally occurring particles during infiltration are important factors that affect contaminant migration (Jacobsen et al. 1997; Kjaergaard et al. 2004). The presence of different electrolyte types, which generally occurs in soils, has been proven to play an important role in NP stability and mobility in porous media (Badawy et al. 2010; Huynh and Chen 2011; Sagee et al. 2012). In particular, divalent cations can enhance NP deposition in comparison to monovalent ions (Jaisi and Elimelech 2009; Torkzaban et al. 2012). The complex combination of various cations in natural soils is thus crucial for NP mobility. Therefore, although the application of simplified system is able to investigate the coupled effect from different experimental conditions, conduction of NP transport experiments in undisturbed soil is crucial for better understanding of the interaction between NPs and the environment.

2.3 Modeling of transport and deposition of nanoparticles/colloids

The development of numerical simulation is crucial to predict the transport and retention of colloids/NPs after being released into the environment. Accordingly, a number of mathematical approaches have been proposed and applied to describe the removal of colloidal particles in porous media and the removal mechanisms (Tufenkji 2007). Classical filtration theory (CFT) (Yao *et al.* (1971) is most commonly used to assess the removal rate of particles in deep-bed filtration water treatment systems. According to this theory, a first order traditional advection-dispersion equation (ADE) can be applied to predict the attachment of colloidal particles to the collectors (Yao et al. 1971; Oberdorster 2005):

$$\frac{\partial C}{\partial t}+\frac{\rho_b}{\theta_w}\frac{\partial S}{\partial t}=\frac{\partial}{\partial z}\left(D\frac{\partial C}{\partial z}\right)-v\frac{\partial C}{\partial z} \tag{2.5}$$

$$\frac{\rho_b}{\varepsilon}\frac{\partial S}{\partial t}=kC \tag{2.6}$$

where C is the NP/colloid concentration in the aqueous phase [N_c L^{-3}], t is the time [min], ρ_b is soil bulk density [g mL^{-1}], θ_w is the volumetric water content, S is the solid phase concentration of particles [N_c M^{-1}], v is the flow rate [mL cm^{-1}], z is the spatial coordinate [cm], D is the dispersion coefficient [cm^2 min^{-1}], and ε is the bed porosity.

According to CFT, colloid/NP transport from the bulk solution to the collector surface and the subsequent interactions between particle and collector can be described by attachment efficiency (k_1) in eq. (2.7) and single coefficient (η_o) in eq. (2.8), respectively. The first-order attachment coefficient generally be calculated as (Logan et al. 1995):

$$k_1=\frac{3(1-\theta_w)}{2d_{50}}v\alpha\eta_o \tag{2.7}$$

where d_{50} is the diameter of the sand grains [L], v is the pore-water velocity [LT^{-1}], α is the

sticking efficiency [-], and η_o is the single-collector efficiency [-] (Rajagopalan and Tien 1976):

$$\eta_o = 4\,A_s^{1/3} N_{Pe}^{-2/3} + A_s N_{Lo}^{1/8} N_R^{15/8} + 0.00338 A_s N_G^{1.2} N_R^{-0.4} \quad (2.8)$$

where A_s is a correction factor [-], N_{Pe} is the Peclet number [-], N_{Lo} is the contribution of particle London-van der Walls attractive forces to particle removal [-], N_R is the interception number [-], and N_G is the gravitation number [-]. The first, second, and third terms on the right hand side of eq. (2.8) represent the removal by diffusion, interception, and gravitational sedimentation, respectively. The particle transport from the bulk solution to collector surface is therefore mainly determined by removal mechanisms described in eq. (2.8). Further, the transport process is influenced by various physical factors such as grain size, particle size, flow velocity, and porosity, while the interactions between particle and collector surface are governed by van der Waals attraction and electrical double layer repulsive forces. CFT is frequently applied to evaluate colloid/NP attachment kinetics based on breakthrough curves obtained from laboratory column experiments (Jaisi et al. 2008). Previous studies have revealed that the retention behavior of colloidal particles is in good agreement with CFT predictions when the experimental conditions are favorable for deposition (Li and Johnson 2005; Tufenkji and Elimelech 2005).

However, deviations have frequently been reported between filtration theory predictions and experimental observations for both NPs and colloids (Adamczyk et al. 1995; Ko and Elimelech 2000; Tufenkji and Elimelech 2005). CFT predicts an exponential distribution of retained NPs with distance, whereas hyperexponential, nonmonotonic (a peak in particle retention down gradient from the column inlet) and uniform retention profiles have been commonly reported (Li et al. 2004; Li and Johnson 2005; Tong et al. 2005; Bradford et al. 2006). A wide variety of factors have been demonstrated to contribute to deviations of RPs between filtration theory predictions and experimental observations including: heterogeneity of the

particle and collector surfaces (Tufenkji and Elimelech 2005), roughness (Kretzschmar et al. 1997), the presence of stabilizing agents (Wang et al. 2012), straining (Li et al. 2004), aggregation (Bradford et al. 2006), and hydrodynamic drag (Li and Johnson 2005; Johnson et al. 2007). Most previous research has been directed to explain the occurrence and causes of hyperexponential RPs, whereas relatively little attention has been directed at studying nonmonotonic RPs (Tong et al. 2005; Yuan and Shapiro 2011). CFT employs an empirical sticking efficiency (α) to account for the fraction of the NPs that is immobilized on the collector surface. Colloid deposition is implicitly assumed to occur irreversibly (deposition in the primary minimum). In reality, only a small portion of the collector surface may contribute to NP retention under unfavorable attachment conditions (Bradford et al. 2009), and this "favorable" area can change with solution chemistry and velocity (Adamczyk et al. 1995; Ko and Elimelech 2000). Enhanced retention of colloids and/or NPs occurs at locations associated with surface roughness, grain-grain contacts, and locations of chemical heterogeneities because of lower flow velocities or increased adhesion (Li et al. 2005; Wang et al. 2011). Particles in unfavorable regions can be slowly transported along the collector surface by hydrodynamic forces to these "favorable" locations (Li et al. 2005; Xu et al. 2008). Particle retention in "favorable" locations will decrease over time as these locations are blocked or filled, which is known as "blocking effect" (Ko and Elimelech 2000). The rate of filling of these "favorable" locations will depend on the particle concentration. Higher particle concentrations will fill these "favorable" retention sites more rapidly under unfavorable attachment and thereby increase their transport potential (Camesano et al. 1999; Bradford et al. 2009; Chowdhury et al. 2011). In contrast, particle retention would be enhanced as increasing time/input concentration through process such as filter ripening if retained particles are favorable for attachment (Li et al. 2005; Tong et al. 2008), or when greater agglomeration occurs at a higher concentration (Phenrat et al. 2010). Consequently, the previously deposited particles can play an important role on the deposition rate, whereas the particles are typically assumed to transport through a clean bed as described in CFT. The discrepancies from experimental observation and numerical simulation have been addressed by the modification of CFT in various approaches to improve the

prediction of the colloid/NP transport. Tong et al. (2005) demonstrated that colloid transport in porous media could be better described by taking into account a spatial variation in deposition rates. Tufenkji and Elimelech (2004) proposed a dual-deposition mode model that also suggested different deposition rates for colloid retention and successfully described transport of fluorescent polystyrene latex colloids in glass beads. This model considers the coupled effects of "slow" (deposition in a primary energy minimum) and "fast" (deposition due to a deep secondary minimum and surface charge heterogeneity) deposition rates. Frequently, to account for the decreasing and increasing deposition rates as time, a blocking term (Deshpande and Shonnard 1999) or filter ripening (Simunek et al. 2005) is introduced into the filtration model, respectively. For example, a ψ was proposed to describe the increasing or decreasing retention rate as time as (2.9) and (2.10), respectively:

$$\psi = 1 - \frac{S}{S_{max}} \tag{2.9}$$

$$\psi = \max\left(1, S^{S_{max}}\right) \tag{2.10}$$

where S is particle concentration in the solid phase and S_{max} is the maximum solid phase concentration [$N_c M^{-1}$]. The term of S_{max} that reflects the maximum capacity of porous media for colloid/NP retention is frequently included in modified CFT to improve the accurate description of the transport behavior (Johnson and Elimelech 1995; Bradford et al. 2006; Li et al. 2008; Wang et al. 2008). The fitted S_{max} has been observed to vary with experimental conditions such as solution chemistry, collector size, particle size and flow velocity. The introduction of ψ is able to better describe the trends in BTCs but not sufficient to fit RPs in the shapes of hyper-exponential, uniform, and non-monotonic. It has been confirmed that dual-permeability model is able to describe the RPs with a non-uniform shape in homogeneous porous media (Bradford et al. 2011a; Yuan and Shapiro 2011). However, this model involves coupled parameters needed further reliable measurements. To overcome this limitation, Bradford et al. (2011a) proposed an improved mathematical description of colloid

transport in unfavorable deposition conditions. It was assumed that the transport of colloids occurred in two regions, in which particles are transported through the bulk aqueous phase by advection and dispersion (region 1) or interacting with the solid-water interface (region 2). A two species model was also proposed by Bradford et al. (2006) to account for production of an aggregated species that had a different deposition behavior from the monodispersed species. These model formulations are able to successfully capture the shapes of hyperexponential, exponential, uniform, and nonmonotonic retention profiles.

In the case of colloid/NP transport in the presence of stabilizing agent, numerical simulation is normally proceed with adjusting the attachment rate (k_1) in the consideration of surfactant/polymer-modified porous media or concerning the reversibility of NP retention to the collectors (Wei and Wu 2010; Wang et al. 2012). Wang et al. (2012) proposed a model that accounts for coupled effects of surfactant-NP interactions, surfactant adsorption-desorption dynamics, and particle attachment kinetics to describe the retention of fullerene NPs in the presence of stabilizing agent. The model formulation assumed that the surfactant could block the retention sites on collector surface or be adsorbed onto NP surface. The transport and retention of fullerene NPs were then coupled to the information of surfactant transport and sorption by adjusting the effective attachment rate (k) of NPs based on surfactant concentration as:

$$k = \begin{cases} 0, & C_s > C_t \\ k_{att}\left(1 - \frac{S}{s_{max}}\right)\left(1 - \frac{C_S}{C_O}\right) & C_s < C_t \end{cases} \tag{2.11}$$

where C_s is the concentration of surfactant in aqueous phase, C_t is a threshold concentration of surfactant in aqueous phase, k_{att} is the NP attachment rate, S is NP concentration in the solid phase, and S_{max} is maximum retention capacity.

2.4 Release of colloids/nanoparticles and colloid- facilitated transport

In contrast to the removal of colloidal particles achieved by capturing and retaining particles in the porous media, the release of retained particles from the collector may also occur and thus reduces the removal effect. However, the release of deposited particles from solid to aqueous phases has received only limited attention (Um and Papelis 2002; Bradford and Kim 2010). Existing data indicate that release may occur with an increase in the hydrodynamic force (Bergendahl and Grasso 2000) or a reduction in the adhesive force (Ryan and Elimelech 1996). In particular, decreasing the solution ionic strength (Tufenkji and Elimelech 2004; Jaisi et al. 2008) and/or replacement of divalent cations by monovalent cations (Roy and Dzombak 1996) can induce colloid/NP release by reducing the depth of the secondary energy minimum of the DLVO interaction energy curve and cation bridging, respectively. In the case of NPs deposited in the presence of divalent cation, these deposited NPs are commonly resistant to release under decreasing ionic strength (e.g., deionized water) due to strong interaction in a primary minimum and bridging interaction (Jaisi et al. 2008). Conversely, the retained NPs in the presence of monovalent ions (such as Na^+, K^+) are relatively easy to be released from the collectors during irrigation with a lower ionic strength solution by a reduction in the depth of the secondary energy minimum.

Further, recent investigations have demonstrated the release of colloids from porous media and the transport of contaminants associated with soil colloidal particles (Grolimund et al. 1996; Roy and Dzombak 1996; Kretzschmar et al. 1999; de Jonge et al. 2004; Grolimund and Borkovec 2006; Grolimund et al. 2007; Bradford and Kim 2010; Torkzaban et al. 2010). These soil colloids suspended in the pore water and/or released from the matrix in the natural porous media act as contaminant carriers and a transport pathway for pollutant transport. Generally, this transport process is described as “colloid facilitated transport” and commonly enhances the spread of contaminants in the environment (Grolimund et al. 2007). Figure 2.2 schematically depicts the colloid facilitated transport of pollutants and the reconstruction of the pore structure in porous media. In particular, the released colloids from the solid phase

co-transport the contaminants and thus enhance the contamination (Figure 2.2a). On the other hand, the released clay fraction and/or colloids may clog the pores by deposition or aggregation resulting in decreased transport potential of contaminants (Figure 2.2b). Chemical properties of the porous media may also be changed due to a loss of soil colloids, which account for a high specific surface area for potential interaction with contaminants (Figure 2.2c). The change of permeability in aquifers and soils by ion exchange and the facilitated-transport of contaminants have also been demonstrated by other studies (Grolimund et al. 1996; Rinck-Pfeiffer et al. 2000; de Jonge et al. 2004; Suarez et al. 2006). All of this information indicates a potential for NP co-transport with natural soil colloids.

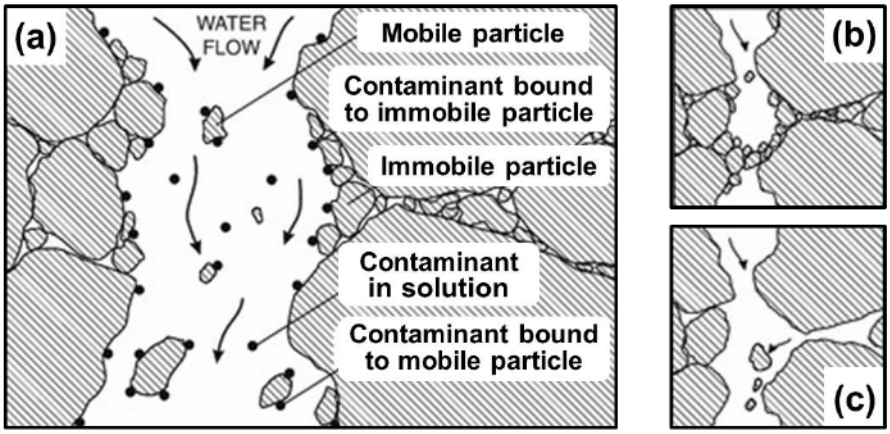

Figure 2.2. Contaminant transport influenced by the released colloids in a porous medium. (a) Colloid facilitated transport. Contaminants (black dots) are either in the aqueous phase, or adsorbed on the solid phase that is assumed to be immobile, while colloids can be released from the matrix and act as contaminant carriers. (b) Change of the pore structure. Clogging of pores by deposition of mobile colloids or filtration of suspended aggregates. (c) Change of chemical property of the matrix. Release of colloids with a high specific surface area results in a reduction in chemical reactivity of the stationary phase. Reprinted from Grolimund et al. (2007).

3 Objectives of the thesis

This study aims to provide a better understanding of the transport behavior of AgNPs under environmentally relevant conditions. The main focus of this study is the systematic investigation of the influence of physicochemical factors on AgNP transport in simplified (quartz sand) and natural porous media with small-(undisturbed soil column) and large-scale (lysimeter) experiments. The information on the retention profiles and the remobilization of AgNPs from undisturbed soil is essential to assess the long-term transport potential, the fate of NPs in the environment, and the potential risk of groundwater contamination. However, these crucial aspects have not been reported in the literature so far. The specific objectives of this study therefore include:

Transport of AgNPs in model systems – In order to investigate the sensitivity of the transport and retention of stabilized AgNPs to physicochemical factors, water-saturated sand column experiments were conducted under a variety of ionic strengths, grain sizes, NP concentrations, and flow velocities. XDLVO interaction energies of AgNP-sand and AgNP-AgNP were calculated to interpret the transport behavior of AgNPs in quartz sands. Besides the breakthrough curves, information on retention profiles was also provided in this study. To deduce the influence of surfactants, transport experiments were conducted in quartz sand in the presence of surfactant that was added to the AgNP dispersion before pulse application in the column or used to pre-coat the surface of quartz sand. In general, the collected data provide valuable insights into the transport behavior of particles (NPs, colloids, and microorganisms) in porous media.

Transport and remobilization of AgNPs in undisturbed soil – Another objective is to improve the understanding of the retention and remobilization behavior of stabilized AgNPs in undisturbed soil. Specifically, undisturbed soil column experiments were conducted under different solution chemical conditions, input AgNP concentrations, and flow velocities to investigate AgNP transport under environmentally relevant condition. Around 90% water

saturation was employed to represent the maximum transport potential in the vadose zone. The interaction of retained AgNPs with the natural matrix (soil) is much more complex than with the idealized medium (pure quartz sand). Therefore, the observation of AgNP transport in undisturbed soil represents a more realistic investigation to predict the transport of AgNPs in the environment. Following AgNP transport and retention, release experiments were performed by systematically changing the ionic strength and cation type of the eluting solution to better understand the effect of naturally occurring chemical heterogeneity and cation exchange on NP transport in natural soil. The association of AgNPs and natural soil colloids was analyzed by means of transmission electron microscopy and energy-dispersive X-ray spectroscopy. A larger scale and long-term experiment in a lysimeter was performed to better assess the transport potential of AgNPs in a more realistic environment.

Mathematical modeling – Numerical simulation was applied to quantitatively assess the influences of physicochemical factors on the transport and retention of AgNPs and to deduce the potential mechanisms. A mathematical model that accounts for time/concentration- and depth-dependent retention was used to simultaneously describe both the breakthrough curves and retention profiles from transport experiments with quartz sand and soil. The results of numerical simulations are crucial for predicting NP transport behavior in the environment.

4 Materials and methods*

4.1 Silver nanoparticles

AgNP suspensions (10.16 % w/w) were produced by chemical precipitation of silver nitrate using an aqueous reduction method (AgPURE™, rent a scientist ® GmbH, Germany). The AgNPs were modified using a mixture of two stabilizers, 4% w/w each of polyoxyethylene glycerol trioleate and polyoxyethylene (20) sorbitan mono-laurate (Tween 20) (Figure 4.1). This product corresponds to the OECD reference material NM-300 Silver currently being used for nanomaterial research. Both of the surfactants are non-ionic and form steric repulsion barriers between AgNPs that help to stabilize the suspension and minimize aggregation. The total unbounded/free surfactant in the original concentrated AgNP suspension measured after ultracentrifugation was around 5%. Silver ion fractions in the influent and effluent determined after ultracentrifugation were less than 2%, which is similar to other studies with the NM-300 product (Kaegi et al. 2011; Klein et al. 2011)

The size and morphology of dry AgNPs were measured using a scanning electron microscope (SEM, Gemini 1550 VP, Carl Zeiss, Jena, Germany) and a transmission electron microscope (TEM, Philips CM 20 FEG) combined with an energy-dispersive X-ray spectroscopy (EDAX, Genesis). When prepared TEM samples, one drop of effluent was pipetted on standard holey carbon film grids and dried quickly. A Nano-Zetasizer apparatus (Malvern ZetaSizer 4) was used to analyze the size of AgNPs in dispersion. The suspension for each experiment was freshly prepared (to minimize the dissolution of AgNPs) by dilution of the

* Contains parts from Liang, Y.; Bradford, S. A.; Simunek, J.; Vereecken, H.; Klumpp, E., Sensitivity of the transport and retention of stabilized silver nanoparticles to physicochemical factors, Water Research 2013, 47 (7) 2572-2582 and Liang, Y.; Bradford, S. A.; Simunek, J.; Heggen, M.; Vereecken, H.; Klumpp, E., Retention and Remobilization of Stabilized Silver Nanoparticles in an Undisturbed Loamy Sand Soil. Environmental Science & Technology, 2013, 47 (21), 12229-12237 with permissions from Elsevier and American Chemical Society, respectively.

concentrated stock suspension of stabilized AgNPs into selected electrolyte solutions to achieve approximate concentrations of 10, 5, and 1 mg L^{-1} and then solicited for 15 min in a sonication bath. The final amount of surfactant in the suspension was less than 1×10^{-3} % (w/w) and was proportional to the AgNPs concentration. The Nano-Zetasizer apparatus was also used to determine the size distribution as a function of time and the electrophoretic mobility (EPM) of the AgNPs in different KNO_3 or $Ca(NO_3)_2$ solutions.

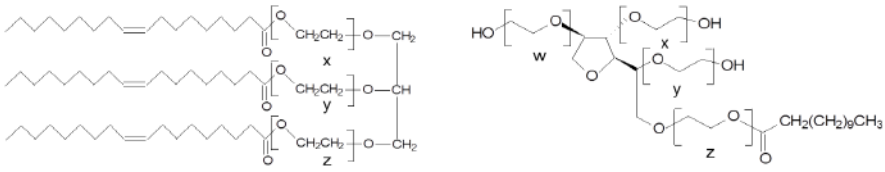

Figure 4.1. Structure of polyoxyethylene glycerol trioleate (a) (Hensel et al. 1997) and polyoxyethylene (20) sorbitan mono-laurate (Tween 20) (b) (Carnero Ruiz et al. 2003)

4.2 Electrolyte solutions and porous media

4.2.1 Electrolyte solutions

Electrolyte solutions were made using Milli-Q water and KNO_3 or $Ca(NO_3)_2$. Three solution ionic strengths (IS) were considered for water saturated column, namely: 1, 2.5, and 5 mM KNO_3. In the case of unsaturated system, IS of 1, 5, 10, and 100 mM KNO_3 and $Ca(NO_3)_2$ were considered. These electrolyte solutions were unbuffered, and the pH of influent and effluent ranged from 6 to 7 during the course of the column transport experiments.

4.2.2 Quartz sand

Three sizes of quartz sands were employed in the column experiments. The median grain size of these sands are 240, 350 (Quarzwerke GmbH, Germany) and 607 µm (Teco-Sil, CE

Minerals Greenville, USA). The sands are reported to consist of at least 99.7% SiO_2 (quartz) and trace amounts of metal oxides. Additional purification procedures were applied to control the metal oxide content and organic impurities in the sands, which can limit or enhance NP transport (Lin et al. 2011; Thio et al. 2012). First, the quartz sand was immersed in deionized water for 24 h, boiled at 100°C in deionized water, and then soaked in 65% HNO_3 for 2 h. A glass filter was used to remove the sand from the HNO_3, and then the sand was washed with deionized water until the pH-value of the leachate was around 5. In the next step, 10% H_2O_2 solution was added to the sand and boiled for 2 h. Finally, the sand was washed with deionized water, and then dried at 50°C in an oven.

The surface charge characteristics of the clean sand were determined using the Nano-ZetaSizer after it had been crushed to powder and placed in a selected electrolyte solution. The specific surface area was analyzed by nitrogen sorption with an AUTOSORB^r-1 (Quantachrome) apparatus and calculated by the multipoint Brunauer-Emmett-Teller (BET) method.

4.2.3 Soil

Undisturbed soil used to fill polyvinyl chloride columns (8 cm in inner diameter and 10 cm in length) was taken from the upper 30 cm of an agricultural field (Kaldenkirchen, Northrhine-Westphalia, Germany). Soil samples were analyzed for specific properties. The soil was classified as a loamy sand, with 4.9% clay (<0.002 mm), 26.7% silt (0.002-0.064 mm), and 68.5% sand (0.064-2.000 mm) (Unold et al. 2009). This soil had a total organic matter content of 1.1% (Unold et al. 2009) and a cationic exchange capacity of 7.8 $cmol_c kg^{-1}$(Förster et al. 2008). The surface charge characteristics of the soil in a selected electrolyte solution were determined using the Nano-Zetasizer and the specific surface area of soil was analyzed by BET method. The clay minerals were analyzed by X-ray diffraction (XRD) after the clay fraction was isolated from soil.

4.3 Water saturated column experiment with quartz sand

Figure 4.2 shows the schematic overview of the saturated column experiment. Briefly, the AgNP dispersion was introduced into the sand column and rinsed by NP-free solution. The effluent was analyzed to obtain breakthrough curves (BTCs) and the amount of deposited AgNP in the sand column was measured to obtain retention profiles (RPs). In particular, water saturated transport experiments were performed in stainless steel columns (3 cm inner diameter, 12 cm length) that were wet-packed with quartz sand. A hydrophilic nylon membrane, which was supported by a steel plate, was used as a capillary barrier and filter at the bottom and the top of the column. During packing, the column was vibrated to minimize air entrapment and to ensure homogenous packing. A peristaltic pump was used to inject solutions at a steady Darcy velocity (q=0.03-0.7 cm min^{-1}) through the column in an upflow mode. A three-way valve was used to switch flow to the column between a D_2O tracer in electrolyte solution, AgNPs suspensions, and particle-free electrolyte solutions.

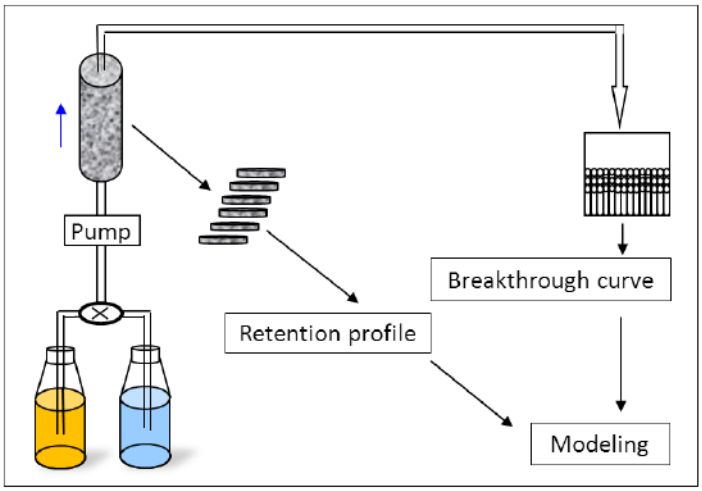

Figure 4.2. The schematic image of column experiments under water saturated condition. The NP suspension and particle-free solution were pumped into the column in an upflow mode separately. After completion of transport experiment, concentrations of AgNPs in the effluent and retained in different depths of the porous media were measured to obtain breakthrough curves and retention profiles, respectively.

Before initiating a transport experiment, the packed column was conditioned with around 50 pore volumes of KNO_3 solution. A nonreactive tracer experiment was then conducted by injecting 90 mL of D_2O into the column. The same electrolyte solution and injection velocity were used in D_2O and NP transport experiments in a given column. Column effluent samples (2 mL each) were collected continuously in ultra-high performance plastic centrifuge tubes (VWR International GmbH, Germany) using a fraction collector. Concentrations of tracer D_2O were quantified by high-performance liquid chromatography (D-7000 HPLC, High-Technologies Corporation, Japan) with a refractive detector (RI, L-2490). D_2O concentrations were evaluated using a calibration curve between the peak area of the RI signal and standard solutions (correlation coefficients were greater than 0.999). The column pore water velocity and dispersivity were obtained by fitting D_2O BTCs to the one-dimensional form of the advective-dispersive transport equation using the CXTFIT code (Toride et al. 1999). Table 1 provides a summary of the column transport properties for all experiments. After the tracer experiment, a 90 mL pulse of AgNP suspension was injected into the column, followed by flushing with several pore volumes of particle-free electrolyte solution. The electrolyte concentration and flow rate were kept constant during a given experiment. Effluent concentrations of AgNPs were determined from Ag concentrations that were determined by inductively coupled plasma mass spectrometry (ICP-MS, Agilent 7500ce). In brief, AgNPs were treated by 15% HNO_3 to dissolve the particles and to diminish sorption onto the sampling tubes. Solutions were diluted when needed before analysis by ICP-MS. Each sample was measured three times and the average value was taken for analysis. After completion of the transport experiments (the normalized concentration in BTC less than 0.5%), the porous medium was carefully excavated in 1 cm increments (12 layers). The sand was freeze dried and then digested by HNO_3. The Ag concentration in the HNO_3 digest was again determined by ICP-MS. The AgNP RPs were subsequently determined from this information and the measured dry mass of sand in each increment.

4.4 Column experiments by adding surfactant

To investigate the AgNP transport in the presence of free surfactant molecules, water-saturated sand column experiments were conducted by adding different surfactant concentrations into the AgNP suspension or to pre-cover porous media. The surfactants used were the same as the original surface coating, a mixture of polyoxyethylene glycerol trioleate and Tween 20 at equal concentrations. Experiments were conducted under two conditions: (1) adding additional surfactant in AgNP suspension, named simultaneous transport experiments; (2) injecting the same amount of surfactant into columns before introduction of AgNPs, named transport in modified media. These experiments followed a similar approach described in the previous section of the quartz sand column.

Simultaneous transport experiments. Surfactants at the final concentrations of 10 and 30 mg L^{-1} were introduced into 90 mL AgNP suspensions (around 3 pore volumes) before the suspensions were injected into the columns after a tracer experiment. A concentration of 10 mg L^{-1} AgNPs, IS of 5 mM KNO_3, and flow velocity of 0.7 cm min^{-1} were employed for all the experiments.

Transport in modified media. After completion of tracer transport experiment, a pulse injection of 90 mL surfactant at 10, 30, or 500 mg L^{-1} was applied into columns to pre-coat porous media and immediately followed by pulse injection of AgNP. The AgNP input concentration, IS and flow velocity were the same as in simultaneous transport experiments.

4.5 Undisturbed soil column

Polyvinyl chloride columns (8 cm in inner diameter and 10 cm in length) were filled with undisturbed soil from the upper 30 cm of the field. The undisturbed soil samples were collected using a metal adaptor with a sharp front attached to the column bottom to minimize any disturbance of the soil structure (Unold et al. 2009). A water balance was used to vertically insert the soil into the column. Before use, the undisturbed soil columns were stored at 4 °C. The column bottom was fitted with a fiber filter with 2 μm pores supported by a nylon plate with 2 mm openings. The soil column was then slowly saturated from the bottom with selected KNO_3 solutions for 3 to 4 days before running the transport experiments.

All column experiments were run with a software-controlled system to achieve homogeneous water-saturation and steady-state flow conditions in the soil columns (Unold et al. 2009). Setup of the unsaturated system is shown in Figure 4.3. In brief, the background solution, tracer and AgNPs in storage bottles were separately introduced using a peristaltic pump through an irrigation device with needles placed on the top of the column. A constant irrigation rate was controlled and measured by recording the weight of storage bottles of the irrigation solution with a balance linked to a computer. The suction at the column bottom was controlled with an air pump and a pressure regulation. The matrix potential inside the column was measured using two tensiometers installed 2.5 and 7.5 cm below the column surface. Effluent samples (15 mL for each sample) controlled by an electric circuit with two water level sensors were collected over the course of the experiment using a fraction collector. Important parameters such as electrical conductivity (related to electrolyte concentration), irrigation rate, weight from the balance, and time were recorded automatically for each sample. The columns were irrigated with at least 30 pore volumes of background solution at a selected flow rate until unit gradient (a constant matrix potential), steady state flow, and constant electrical conductivity (a baseline conductivity) conditions were achieved. The anions such as chloride were washed out and replaced by nitrate in this equilibrium process to avoid precipitation of silver chloride that can affect AgNP stability (Sagee et al. 2012) and the subsequent Ag

concentration measurements. After this conditioning procedure, KNO_3 solution at a 2 to 5-fold concentration of the background solution was used as a non-reactive tracer and the BTC was determined from conductivity measurement of effluent samples.

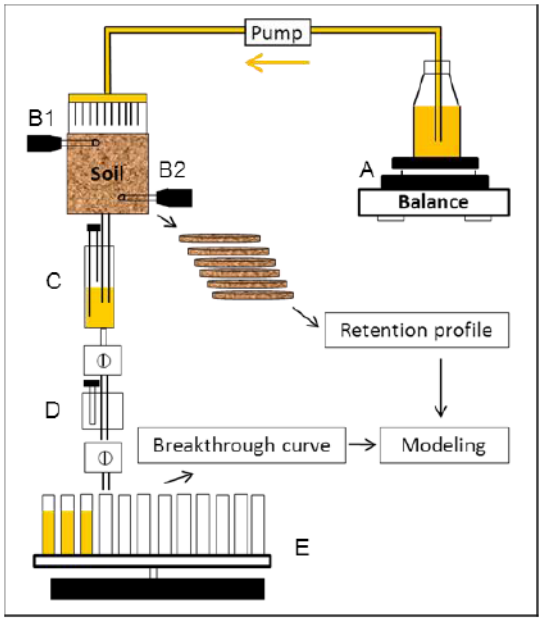

Figure 4.3. The schematic image of column experiments for water-unsaturated conditions. An arrow below the pump shows the flow direction. A is a magnetic stirring apparatus on a balance, B1 and B2 are tensiometers, C is the vessel with two water level sensors that form an electric circuit to control the volume for each sample, D is the vessel with a sensor that measures the electrical conductivity (related to electrolyte concentration), and E is the fraction collector. The irrigation rate, weight from the balance, and time were recorded automatically for each sample. After completion of transport experiment, concentrations of AgNPs in the effluent and retained in different depths of the porous media were measured to obtain breakthrough curves and retention profiles, respectively.

AgNP transport experiments were conducted at different IS (1, 5 and 10 mM), input concentration values (C_o, 1 and 10 mg L^{-1}), and Darcy water velocities (q, 0.02 and 0.006 cm min^{-1}) by injecting a pulse (around 2 pore volumes) of AgNP suspension into the columns. An approximately 90% water-saturation was employed in these experiments to reflect the influence of entrapped air on water flow in the vadose zone. The AgNP suspension was continuously mixed with a magnetic stirrer, and the AgNP suspension was stable in size during the transport experiment; e.g., no noticeable difference in the AgNP size was observed between influent and effluent samples. The electrolyte concentration and flow rate were kept constant during a given experiment. After recovery of the AgNP BTC (the C/C_o value less than 0.5%), the soil in the column was carefully excavated in approximately 1 cm increments, and then freeze dried. BTCs and RPs for AgNPs were obtained from concentrations of Ag in the effluent and soil samples, respectively. The liquid samples were treated by 15% HNO_3, while the solid samples were digested in 65% boiling HNO_3 for 2h and then removed the residual by filtration. The treated samples were diluted as needed before analysis by ICP-MS. Each sample was measured three times and the average value was taken for analysis. The dissolution of AgNPs was determined to be negligible in this study. Consequently, Ag concentrations were directly related to the number of AgNPs in the sample.

4.6 Release of retained silver nanoparticles

A series of experiments was performed to deduce the effects of cation type and concentration, IS reduction, and cation exchange on the release of AgNPs. The setup of release experiments were the same as undisturbed soil column experiment (Figure 4.3). The input concentration of AgNPs was 10 mg L^{-1} and the Darcy velocity was 0.02 cm min^{-1} for all the release experiments. Four different solution chemistry conditions were considered for the initial AgNP deposition and elution with AgNP free solution (step A), namely: 0.333 mM $Ca(NO_3)_2$ (experiment I), 1.65 mM $Ca(NO_3)_2$ (experiment II), 3.33 mM $Ca(NO_3)_2$ (experiment III), and 10 mM KNO_3 (experiment IV). Similar to the AgNP transport experiments described in the preceding section, the IS was 1, 5, 10, and 10 mM for experiments I, II, III, and IV, respectively. The release experiments I-III were subsequently conducted using the following elution solution chemistry sequence: Milli-Q water (step B); KNO_3 at the same IS as in step A (step C); Milli-Q water (step D); 100 mM KNO_3 (step E); and Milli-Q water (step F). Experiment IV consisted of only steps A and B. Concentrations of Ag, K, Ca, Fe, and Al in select effluent samples were measured using inductively coupled plasma mass spectrometry/optical emission spectrometry (ICP-MS/OES). Concentrations of K and Ca demonstrate the process of cation exchange. Concentrations of Fe and Al reflect the amount of released soil colloids in the effluent. Additional analysis of selected effluent samples was conducted, including: zeta potential, TEM, and energy-dispersive X-ray spectroscopy (EDX) (EDAX, Genesis).

4.7 Extended DLVO calculations for the interactions of AgNP-AgNP and AgNP-sand

Due to the presence of surfactant coating on AgNP surface, DLVO theory should be extended to take into account steric repulsion for total interaction energies of NP-NP and NP-sand. Steric interaction is the sum of osmotic and elastic repulsive energies due to the overlapping of surfactant segments on two approaching particles (Vincent et al. 1986) and the deformation of attached surfactant chains (Fritz et al. 2002), respectively. Extended DLVO (XDLVO) theory was therefore used to better interpret AgNP deposition in porous media, including the DLVO interaction energy (sum of electrostatic and van der Waals interactions) and two additional repulsive potentials arising from osmotic (V_{osm}) and elastic (V_{elas}) interactions.

The electrostatic and van der Waals interactions were calculated by eqs. (2.1) - (2.4). To obtain the value of A_{123}, a value of 5.3×10^{-20} J was employed (Bhattacharya et al. 2008) for the calculation of A_{11} (the Hamaker constant for stabilized AgNPs), and 6.5×10^{-20} J was used for the calculation of A_{22} (the Hamaker constant for quartz sand). Soft particle theory (Ohshima 1994; Ohshima 2005) was employed to determine the core surface potential (ψ_1) and electrophoretic softness (l^{-1}) for surfactant stabilized AgNPs using the following equations:

$$\psi_1 = \frac{k_b T_k}{z_e e}\left(\ln\left[\frac{\sigma}{2z_e e n^{\infty}} + \left\{\left(\frac{\sigma}{2z_e e n^{\infty}}\right)^2 + 1\right\}^{1/2}\right] + \frac{2z_e e n^{\infty}}{\sigma}\left[1 - \left\{\left(\frac{\sigma}{2z_e e n^{\infty}}\right)^2 + 1\right\}^{1/2}\right]\right) \quad (4.1)$$

$$\psi_{\mathrm{DON}} = \frac{k_b T_k}{z_e e}\left(\ln\left[\frac{\sigma}{2z_e e n^{\infty}} + \left\{\left(\frac{\sigma}{2z_e e n^{\infty}}\right)^2 + 1\right\}^{1/2}\right]\right) \quad (4.2)$$

$$\kappa_{\mathrm{m}} = \kappa\left[1 + \left(\frac{\sigma}{2z_e e n^{\infty}}\right)^2\right]^{1/4} \quad (4.3)$$

$$\mu = \frac{\varepsilon_r \varepsilon_o}{\eta}\frac{(\psi_o/\kappa_{\mathrm{m}}) + (\psi_{\mathrm{DON}}/l)}{(1/\kappa_{\mathrm{m}}) + (1/l)} + \frac{\sigma}{\eta l^2} \quad (4.4)$$

where σ is the volumetric fixed charge density, η is the dynamic viscosity of water, ψ_{DON} is the Donnan potential in the coating layer, κ_m is the Debye-Hückel parameter of the coating layer, n^{∞} is the bulk number concentration of the electrolyte, and μ is the electrophoretic mobility. Other parameters (z_e, ε_r, ε_o, k_b, T_k, e) are the same as in eqs. (2.3) and (2.4). Parameter values of l and σ in eqs. (4.1) - (4.4) were determined by the nonlinear least squares optimization to measure μ at different solution IS. The value of ψ_1 was subsequently determined using eq. (4.1), and employed in the calculation of the electrostatic interaction energy given by eq. (2.3).

Osmotic and elastic repulsive energies between two coated-AgNPs are estimated from the following expressions as (Vincent et al. 1986; Fritz et al. 2002; Phenrat et al. 2008):

$$\frac{V_{osm}}{K_b T_k} = 0 \qquad 2d \le h \qquad (4.5)$$

$$\frac{V_{osm}}{K_b T_k} = \frac{4\pi r_1}{v}\Phi^2\left(\frac{1}{2}-\chi\right)\left(d-\frac{h}{2}\right)^2 \qquad d \le h \le 2d \qquad (4.6)$$

$$\frac{V_{osm}}{K_b T_k} = \frac{4\pi r_1}{v}\Phi^2\left(\frac{1}{2}-\chi\right)\left[\frac{h}{2d}-\frac{1}{4}-\ln\left(\frac{h}{d}\right)\right] \qquad h \le d \qquad (4.7)$$

$$\frac{V_{eles}}{K_b T_k} = 0 \qquad d \le h \qquad (4.8)$$

$$\frac{V_{eles}}{K_b T_k} = \left(\frac{2\pi r_1}{M_w}\Phi^2 d^2 \rho\right)\left\{\frac{h}{d}\ln\left[\frac{h}{d}\left(\frac{3}{2}-\frac{h}{2d}\right)^2\right]-6\ln\left(\frac{3}{2}-\frac{h}{2d}\right)+3\left(1+\frac{h}{d}\right)^2\right\} \qquad d > h \qquad (4.9)$$

$$\Phi = \frac{3\Gamma_{max} r_1^2}{\rho[(d+r_1)^3 - r^3]} \qquad (4.10)$$

where Φ is the volume fraction of coating within the brush layer (d) (a value of 10 nm for d was taken for calculation according to size measurement and spatial structure of the surfactants), Γ_{max} is the maximum attained surface excess concentration, which was calculated from the w/w

(weight/weight) of surfactant and AgNPs (a value of 2.10 mg m^{-2} can be taken for calculation in this study), χ is the Flory-Huggins solvency parameter (a value of 0.45 was taken for calculation), M_w is the molecular weight of the surfactant (1532.5 g mol^{-1}), ρ is the density of adsorbed surfactant layer (1.1 g cm^{-3}), and v is the volume of a solvent molecule (0.03 nm^3) (Wang et al. 2012). The estimation of osmotic and elastic repulsive potentials (defined in the range of $d \geq h > 0$) between coated-AgNPs and an uncoated flat surface is given as the following expression as (Song et al. 2011):

$$\frac{V_{\mathrm{osm}}}{K_{\mathrm{b}}T_{\mathrm{k}}} = \frac{2\pi r_1}{v}\Phi^2\left(\frac{1}{2}-\chi\right)\left(d-\frac{h}{2}\right)^2 \tag{4.11}$$

$$\frac{V_{\mathrm{eles}}}{K_{\mathrm{b}}T_{\mathrm{k}}} = \left(\frac{2\pi r_1}{M_{\mathrm{w}}}\Phi d^2\rho\right)\left[\frac{2}{3}-\frac{1}{6}\left(\frac{h}{d}\right)^3-\frac{h}{2d}+\left(\frac{h}{d}\right)\ln\left(\frac{h}{d}\right)\right] \tag{4.12}$$

The total XDLVO interaction energy (V_T) then is:

$$V_{\mathrm{T}} = V_{\mathrm{vdW}} + V_{\mathrm{ed}} + V_{\mathrm{osm}} + V_{\mathrm{elas}} \tag{4.13}$$

4.8 Lysimeter experiment

A larger scale, long-term outdoor experiment was performed for better understanding of the AgNP transport in a more realistic condition. The main features of lysimeter setup and the station, and the schematic image are shown in Figures 4.4 and 4.5, respectively. A stainless steel lysimeter with a surface area of 0.5 m^2 and a depth of 1.1 m was filled by an undisturbed soil monolith removed from a test site in Kaldenkirchen-Hülst, Germany. A stainless steel plate was used to cover the lysimeter in order to prevent rain, evaporation, sunshine, and plant growth. Artificial irrigation was applied using a hand-operated sprayer. A designed irrigation rate of around 1400 mm y^{-1} was achieved by an irrigation of 5 L of tap water twice in each 5 days. Two time-domain reflectrometry (TDR) probes were installed horizontally at depths of 5 and 30 cm, respectively, to continuously observe the water content in time intervals of 30 min. The information on volumetric water content was obtained by the analysis of the TDR wave forms (Topp et al. 1980). The lysimeter was firstly equilibrated with the same irrigation rate for two months, and then a pulse of 15 g KBr in 1 L solution was applied as a conservative tracer that was homogeneously introduced into the lysimeter by dropping KBr solution onto soil surface with a pipette. After two months, 25 g AgNPs in 5 L tap water was then uniformly applied to the lysimeter. The leachate accumulated in a stainless steel pan at the bottom of the lysimeter was pumped out at around each 10 days. The bromide concentration in the effluent was determined using an ion chromatography (IC, Dionex ICS 3000), and the AgNP concentration was determined by ICP-MS after digested in 30 % HNO_3. After 12 months irrigation, soil samples were taken by a stainless steel soil corer (diameter of 22 mm and maximum drilling depth of 1 m) at three different points. The soil at different depths was then determined to obtain the RP for AgNPs with a similar approach as the small undisturbed soil columns described in section 4.5.

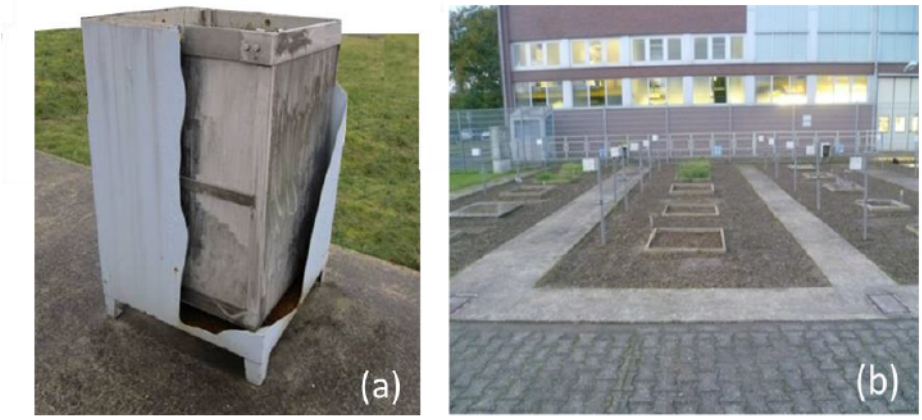

Figure 4.4. Setup of lysimeter (a) and the lysimeter station (b) at Agrosphere Institute (IBG-3), Forschungszentrum Jülich GmbH, Germany.

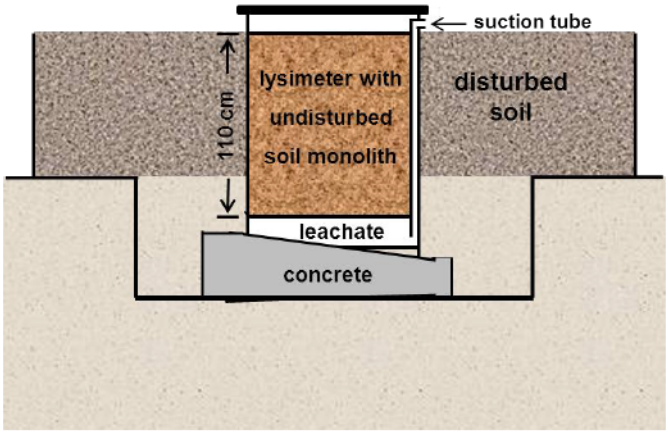

Figure 4.5. The schematic presentation of lysimeter facility at Agrosphere Institute (IBG-3), Forschungszentrum Jülich GmbH, Germany. Modified from Burauel and Führ (2000).

4.9 Mathematical modeling of particle transport

Version 4.14 of the HYDRUS-1D computer code (Šimůnek et al. 2008) was used to simulate the transport and retention of stabilized AgNPs in column experiments conducted under various physicochemical conditions. The aqueous and solid phase mass balance equations (a modified form of ADE, eqs. 2.5 and 2.6) for AgNPs are given in this model as:

$$\frac{\partial(\theta_{\mathrm{w}}C)}{\partial t} = \frac{\partial}{\partial z}\left(\theta_{\mathrm{w}}D\frac{\partial C}{\partial z}\right) - \frac{\partial(qC)}{\partial z} - \theta_{\mathrm{w}}\psi k_1 C \tag{4.14}$$

$$\frac{\partial(\rho_{\mathrm{b}}S)}{\partial t} = \theta_{\mathrm{w}}\psi k_1 C \tag{4.15}$$

where θ_w [–] is the volumetric water content, C [M L^{-3}, M and L denote units of mass and length, respectively] is the aqueous phase AgNP concentration, t is time [T, T denotes time units], z [L] is the distance from the column inlet, D [L^2T^{-1}] is the hydrodynamic dispersion coefficient, q [L T^{-1}] is the Darcy water flux, ψ [-] is a dimensionless function to account for time- and depth-dependent blocking, k_1 [T^{-1}] is the first-order retention coefficient, ρ_b [M L^{-3}, M denote units of mass] is the soil bulk density, and S [M M^{-1}] is the AgNP concentration on the solid phase. The first and second terms on the right hand side of eq. (4.14) account for dispersive and advective transport of AgNPs, whereas the third term is used to describe NP retention on the solid phase. The pore water velocity and dispersivity values in the AgNP transport simulations were based on values determined from the conservative tracer experiments.

When ψ=1, an exponential distribution of retained AgNPs is predicted with depth. Conversely, ψ can be less than 1 when it is given as (Bradford et al. 2006):

$$\psi = \left(1 - \frac{S}{S_{\max}}\right)\left(\frac{d_{50} + z}{d_{50}}\right)^{-\beta} \tag{4.16}$$

where d_{50} [L] is the median grain size of the porous medium, β [–] is an empirical parameter

controlling the shape of the spatial distribution of retained NPs (i.e., the depth dependence of the retention coefficient), and S_{max} [M M^{-1}] is the maximum solid phase concentration of deposited AgNPs. The first term on the right side of eq. (4.16) accounts for time-dependent blocking/filling of retention sites using a Langmuirian approach (Deshpande and Shonnard 1999). This blocking term implies that retention decreases with time and that the retention profile becomes uniform with depth as S approaches S_{max}. The second term on the right side of eq. (4.16) describes depth-dependent retention (e.g., a decreasing retention rate with depth). When β=0, this term equals 1 and an exponential distribution of retained AgNPs is predicted with depth similar to conventional filtration theory. Conversely, when β>0 is employed, then the retention profile of AgNPs exhibits a uniform or hyperexponential shape (e.g., a higher deposition rate close to the column inlet). For the simulation of AgNP transport in sand, a value of β=0.432 was employed based on information presented in the literature (Bradford et al. 2003), while β=1.532 was chosen in the case of soil.

The model parameters (k_1 and S_{max}) were determined by simultaneously inverse fitting to experimental BTC and RP data using the Levenberg-Marquardt nonlinear least squares optimization algorithm (Marquardt 1963) in HYDRUS-1D. It should be mentioned that eqs. (4.14) - (4.16) cannot account for nonmonotonic retention profiles (a peak in retention down gradient from the column inlet) that have sometimes been reported (Li and Johnson 2005; Tong et al. 2005; Bradford et al. 2006).

5 Results and discussion*

5.1 Colloid-chemical characterization of silver nanoparticles, sand, and soil

Figure 5.1 presents SEM and TEM images of the stabilized AgNPs. These images indicate that the AgNPs used were spherical in shape and had a very narrow size distribution with around 99% of the diameters in the size range of 15-20 nm. In the size characterization of AgNPs corresponding to the solution chemistry employed for water-saturated column experiments, the hydrodynamic diameter (d_p) of the AgNPs measured by DLS ranged from 45.1 ± 4.5 to 60.7 ± 14.9 nm when the ionic strength (IS) was 1-5 mM and the particle concentration was 10 mg L^{-1}. Measurements of d_p taken over a 24 h period demonstrated that the AgNP suspensions were very stable. Similar size results have been reported in the literature (Klein et al. 2011). The core surface potentials of the AgNPs in 1, 2.5, and 5 mM KNO_3 solutions that were predicted by soft particle theory (Ohshima 2005) and the measured electrophoretic mobilities are summarized in Table 3. Core surface potentials of AgNPs and clean sand were always negative and did not vary much over the considered range of IS, pH, and C_o (Table 3). The zeta potential of the clean sands was much more negatively charged than that for the AgNPs.

* Contains parts from Liang, Y.; Bradford, S. A.; Simunek, J.; Vereecken, H.; Klumpp, E., Sensitivity of the transport and retention of stabilized silver nanoparticles to physicochemical factors, Water Research 2013, 47 (7) 2572-2582 and Liang, Y.; Bradford, S. A.; Simunek, J.; Heggen, M.; Vereecken, H.; Klumpp, E., Retention and Remobilization of Stabilized Silver Nanoparticles in an Undisturbed Loamy Sand Soil. Environmental Science & Technology, 2013, 47 (21), 12229-12237 with permissions from Elsevier and American Chemical Society, respectively.

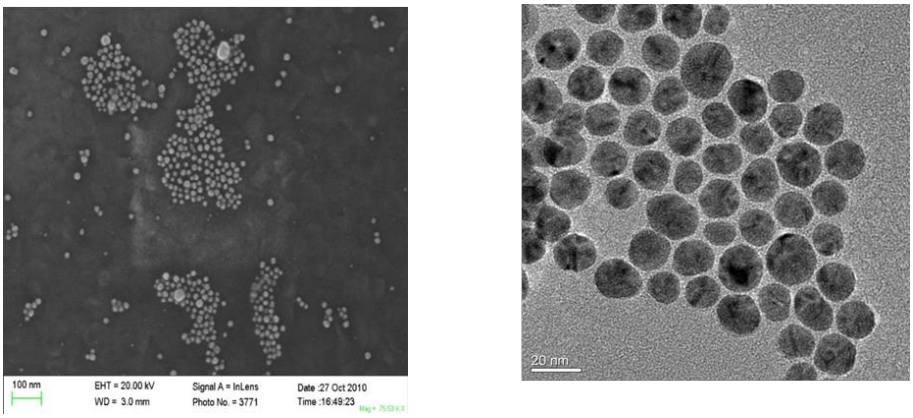

Figure 5.1. Scanning electron micrograph and transmission electron micrograph of AgNPs

AgNP - sand and AgNP - AgNP interactions. Measured and predicted surface potential information given in Table 3 were used to determine the AgNP-sand and AgNP-AgNP interaction energies based on XDLVO theory. The maximum of van der Waals and electrostatic double layer interaction energy, $(V_{vdW} + V_{ed})_{max}$, predicted for AgNP-sand and AgNP-AgNP slightly decreased with increasing IS (Table 3). A shallow secondary minimum was predicted for both AgNP-sand and AgNP-AgNP interactions. These energies were very weak compared to steric repulsion formed by the adsorbed surfactant layer. Steric interactions arising from the surfactants on the AgNPs contributed significantly to the total energy barriers. Consequently, unfavorable conditions were predicted for AgNP retention and aggregation. However, it should be mentioned that these calculations only considered mean properties of the AgNPs and sand, and did not account for the roles of physical or chemical heterogeneity and grain-grain contacts on AgNP retention. Furthermore, the surfactant coating on AgNPs can also attach to collector surfaces (Lin et al. 2012).

AgNP - soil characteristics. Characterizations of AgNPs and soil were also conducted under the same solution chemistry as for column experiments, including retention and remobilization experiments. The zeta potentials of the AgNPs and soil in IS between 1-100 mM with KNO_3 and $Ca(NO_3)_2$ are presented in Figure 5.2. The zeta potentials of the soil

exhibited much more negative charges than the AgNPs. The AgNPs have proven to be stable in the tested IS range for experiments. When measured by Nano-Zetasizer, the sizes of 10 mg L^{-1} AgNPs under IS of 1, 5, 10, 50, and 100 mM in the presence of K^+ and Ca^{2+} ranged from 45 to 78 nm without a systematic tendency, e.g., particles size increasing with IS in this range was not observed. The size determined by dynamic light scattering (DLS) is normally larger than other techniques such as TEM because DLS measures a hydrodynamic size and is biased toward a larger size fraction (Diegoli et al. 2008). In addition, the thickness of the surfactant coating may also influence the size of AgNPs determined by DLS. XRD analysis shows that the clay fraction contains the clay minerals illite, montmorillonite, and kaolinite.

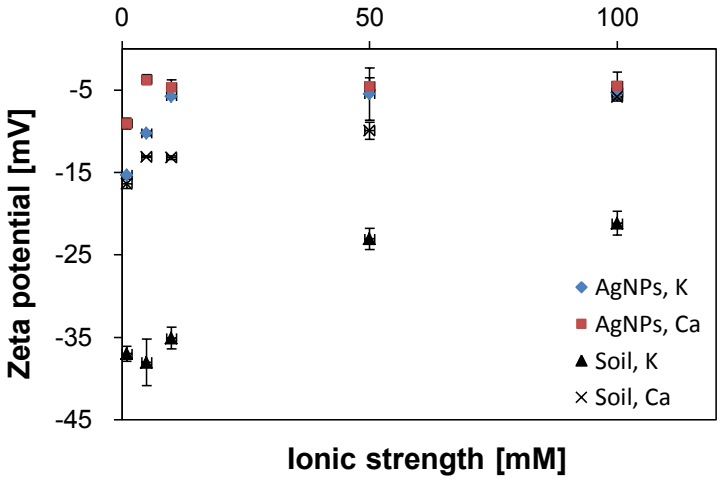

Figure 5.2. Zeta potentials of AgNPs and milled soil grains as a function of the ionic strength in KNO_3 and $Ca(NO_3)_2$ electrolyte solutions.

5.2 Transport and retention of silver nanoparticles in water-saturated quartz sand

A series of column transport experiments was carried out to investigate the transport and deposition behavior of AgNPs under water-saturated conditions. Experimental conditions and the corresponding mass balance information for breakthrough curve (BTC), retention profile (RP), and total column are presented in Table 1. Specifically, the influences of grain size (d_{50}), AgNP input concentration (C_o), ionic strength (IS), and flow velocity (q) were systematically investigated under water saturated conditions. The total column mass balance was > 88% and this provides a high degree of confidence in the experimental procedures and protocols (Table 1). The BTCs are plotted as the normalized effluent concentrations (C/C_o) versus pore volumes. The RPs are plotted as the normalized solid phase concentration (S/C_o) as a function of distance from the column inlet. Observed and simulated results indicated that the model simulation successfully captured the main features for both BTC and RP. A BTC of tracer D_2O is presented in Figure 5.3.

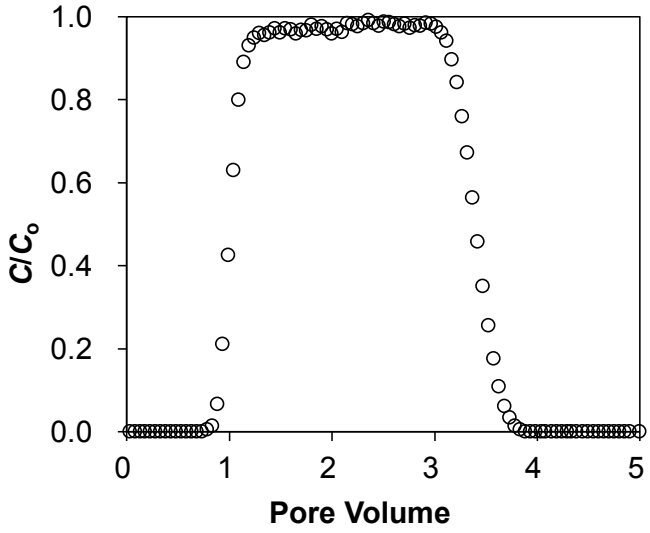

Figure 5.3. Observed breakthrough curve of tracer D_2O from a water-saturated quartz sand column experiment.

Table 1. Experimental Parameters and the Mass Recovery for Water Saturated Column Experiments of Surfactant Stabilized AgNPs in Quartz Sand.

	d_{50}	C_o	IS	q	λ	φ	Recovery, %		
	μm	mg L^{-1}	mM	cm min^{-1}	cm		M_{eff}	M_{sand}	M_{total}
Figure 5.4	240	10	1	0.7	0.055	0.353	13.9	115.8	129.7
	350	10	1	0.7	0.049	0.403	41.5	52.0	93.5
	607	10	1	0.7	0.056	0.418	45.6	54.1	99.7
Figure 5.5	607	10	1	0.7	0.056	0.418	45.6	54.1	99.7
	607	5	1	0.7	0.077	0.429	43.1	44.8	87.9
	607	1	1	0.7	0.089	0.396	17.4	92.5	109.9
Figure 5.6	607	10	5	0.7	0.097	0.403	4.6	103.5	108.1
	607	10	2.5	0.7	0.064	0.388	21.8	75.6	97.4
	607	10	1	0.7	0.056	0.418	45.6	54.1	99.7
Figure 5.7	350	10	5	0.7	0.038	0.369	5.6	101.4	107
	350	10	2.5	0.7	0.044	0.388	11.1	81.0	92.1
	350	10	1	0.7	0.049	0.403	41.5	52.0	93.5
Figure 5.9	607	10	1	0.03	0.110	0.427	24.9	73.2	98.1
	607	10	1	0.14	0.045	0.393	27.0	73.2	100.2
	607	10	1	0.35	0.08	0.415	40.1	64.0	104.1
	607	10	1	0.7	0.056	0.418	45.6	54.1	99.7

Figure 5.4: grain size effect; Figure 5.5: concentration effect; Figures 5.6 and 5.7: ionic strength effect; Figure 5.9: flow rate effect. $d_{50,}$ grain size; C_o, AgNP input concentration; IS, ionic strength; q, Darcy velocity; λ, dispersivity; φ, porosity; M_{eff}, M_{sand}, and M_{total} are mass percentages recovered from effluent, sand, and total, respectively. The value of λ was obtained by fitting tracer BTC, φ was determined gravimetrically.

Table 2. Fitted Values (k_1 and S_{max}/C_o) of Surfactant Stabilized AgNP Transport and Retention in Quartz Sand under Various Experimental Conditions.

	d_{50} μm	C_o mg L^{-1}	IS mM	q cm min^{-1}	k_1 min^{-1}	Standard error of k_1	S_{max}/C_o cm^3 g^{-1}	Standard error of S_{max}/C_o	R^2
Figure 5.4	240	10	1	0.7	3.417	0.191	5.320	1.266	0.979
	350	10	1	0.7	1.182	0.020	0.754	0.023	0.969
	607	10	1	0.7	0.855	0.029	0.732	0.027	0.963
Figure 5.5	607	10	1	0.7	0.855	0.029	0.732	0.027	0.963
	607	5	1	0.7	1.018	0.047	1.679	0.219	0.975
	607	1	1	0.7	1.683	0.087	6.949	2.524	0.979
Figure 5.6.	607	10	5	0.7	3.038	0.095	4.439	0.816	0.969
	607	10	2.5	0.7	1.422	0.033	3.593	0.749	0.962
	607	10	1	0.7	0.855	0.029	0.732	0.027	0.963
Figure 5.7.	350	10	5	0.7	3.378	0.222	23.012	6.456	0.982
	350	10	2.5	0.7	2.859	0.102	3.482	0.751	0.970
	350	10	1	0.7	1.182	0.020	0.754	0.023	0.969
Figure 5.9	607	10	1	0.03	0.058	0.001	1.532	0.067	0.952
	607	10	1	0.14	0.356	0.013	1.095	0.048	0.970
	607	10	1	0.35	0.39	0.021	2.017	0.411	0.956
	607	10	1	0.7	0.855	0.029	0.732	0.027	0.963

Figure 5.4: grain size effect; Figure 5.5: concentration effect; Figures 5.6 and 5.7: ionic strength effect; Figure 5.9: flow rate effect. $d_{50,}$ grain size; C_o, AgNP input concentration; IS, ionic strength; q, Darcy velocity; $k_{1,}$ the first-order retention coefficient; $S_{max}/C_{o,}$ normalized maximum solid phase concentration of deposited NPs; R^2, Pearson's correlation coefficient.

5.2.1 Effect of grain size

In order to investigate the influence of grain size on AgNP mobility, column experiments were conducted in 607, 350, and 240 μm sands when IS=1 mM, q=0.7 cm min^{-1}, and C_o=10 mg L^{-1}. Observed and simulated BTCs and RPs are shown in Figure 5.4. The model simulation successfully captured the gradual ascent trend of the BTCs and the shape of RPs.

Lower values of C/C_o occur in the BTCs with decreasing sand size (Figure 5.4a), especially between the 350 and 240 μm sands. The amount of AgNP retention shown in the RPs (Figure 5.4b) was inversely related to their BTCs. Consistent with these observations, fitted values of k_1 increased with decreasing grain size (Table 2). Filtration theory (described in section 2.3) provides an explanation because it predicts that the mass transfer rate to the grain surface increases with decreasing grain size. However, the shape of the BTCs and RPs was also sensitive to the grain size. This can be explained in part by time-dependent retention processes associated with blocking. Fitted values of S_{max}/C_o increased with decreasing grain size (Table 2) because of its larger surface area. The retention rate declines as retention sites are increasingly occupied by AgNPs (eq. 4.16). Consequently, smaller values of S_{max}/C_o in the coarser sands (350 and 607 μm) produce more asymmetric BTCs (Figure 5.4a) and more uniform RPs (Figure 5.4b) because of stronger blocking (Bradford et al. 2006). The smallest 240 μm sand produced a hyperexponential RP when blocking is less important. In this case, straining is unlikely because the extremely small ratio of d_p/d_{50} is much lower than the reported threshold for straining (Bradford et al. 2002; Li et al. 2004). Alternatively, variations in the pore-scale velocity can provide a viable explanation for this behavior (Bradford et al. 2011a; Bradford et al. 2011b). Specifically, hyperexponential RPs occur when the flux adjacent to the solid surface at the column inlet is the dominant mass transfer mechanism of NPs to the grain surface (Bradford et al. 2011a). Pore-scale water flow simulations demonstrate that this flux increases as the grain size decreases (Bradford et al. 2011a).

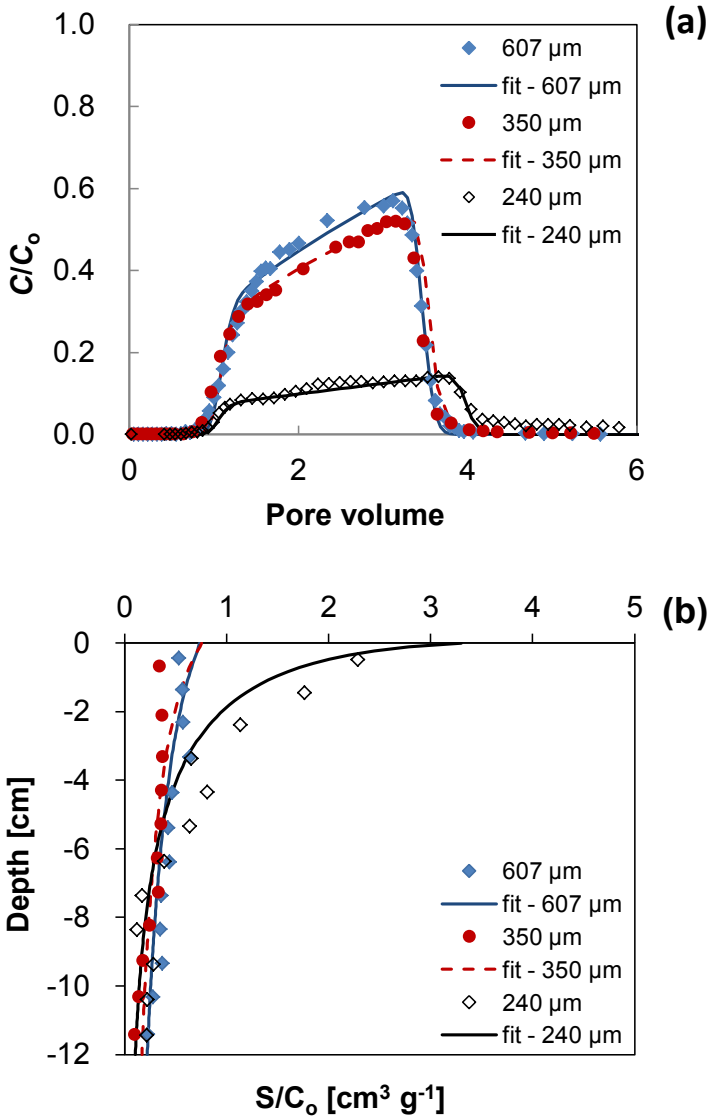

Figure 5.4. Effect of grain size on the transport and retention of AgNPs in water-saturated quartz sand: observed and fitted breakthrough curves (a) and retention profiles (b) of AgNPs in 240, 350 and 607 µm sands, respectively. Other experimental conditions were the same: electrolyte, 1 mM KNO_3; input concentration, 10 mg/L AgNPs; Darcy velocity, 0.7 cm/min.

5.2.2 Effect of input concentration

Additional transport experiments were conducted to demonstrate the influence of time-dependent retention on AgNP BTCs and RPs. Figure 5.5 presents observed and simulated BTCs and RPs for AgNPs in 607 μm sand when the IS=1 mM KNO_3, q=0.7 cm min^{-1}, and C_o=1, 5, and 10 mg L^{-1}. The normalized BTCs were sensitive to the value of C_o. Higher C_o produced greater recovery of AgNPs in the effluent and more asymmetric BTCs. The amount of AgNPs in the RPs was inversely related to the BTCs, and the shape of the RPs systematically varied with C_o. In particular, the RP was hyperexponential when C_o=1 mg L^{-1}, was nonmonotonic when C_o=5 mg L^{-1}, and approached a uniform distribution when C_o=10 mg L^{-1}.

The model used was able to simulate well the BTCs and most of the RPs in Figure 5.5 (R^2>0.96). The value of k_1 increased with decreasing C_o (Table 2). Consequently, this observation suggests that repulsive AgNP-AgNP interactions between mobile and retained NPs hampered AgNP retention on the grain surface at higher values of C_o. Note that the number of AgNP-AgNP collisions is expected to be proportional to C_o. The hyperexponential RP shape at lower values of C_o=1 mg L^{-1} is attributed to pore-scale hydrodynamic at the column inlet as discussed in the previous section. Observed differences in BTCs and RPs with C_o indicate that time-dependent blocking diminished retention with time (Bradford et al. 2009). Furthermore, values of S_{max}/C_o also increased with decreasing C_o (Table 2). In particular, the BTCs were more asymmetric (Figure 5.5a) and the RPs were more uniform (Figure 5.5b) at a higher C_o because S_{max} was filled more rapidly. The observed transition in RP shape from hyperexponential, to nonmonotonic, and to uniform with increases in C_o indicates that blocking contributed to the development of nonmonotonic RPs. However, the model did not capture the nonmonotonic RP shape for the C_o=5 mg L^{-1} data. Consequently, other factors were also involved in the development of the nonmonotonic RP shape. Potential explanations for these observations will be explored below.

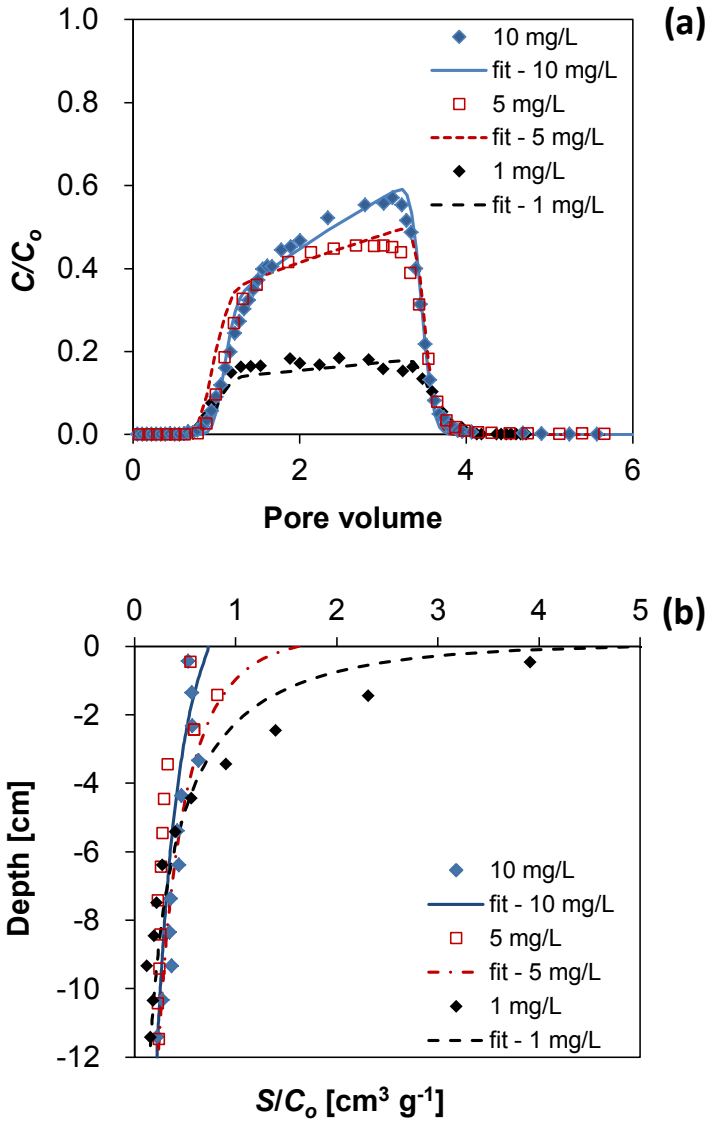

Figure 5.5. Effect of AgNP input concentration on the transport and retention of AgNPs in water-saturated quartz sand: observed and fitted breakthrough curves (a) and retention profiles (b) of AgNPs under input concentrations of 1, 5, and 10 mg/L AgNPs, respectively. Other experimental conditions were the same: grain size, 607 µm; electrolyte, 1 mM KNO_3; Darcy velocity, 0.7 cm/min.

5.2.3 Effect of ionic strength

Transport experiments were conducted at several IS to better understand the nature of the adhesive interaction influencing AgNP retention. Figure 5.6 presents observed and simulated BTCs and RPs of AgNPs in 607 μm quartz sand when q=0.7 cm min^{-1}, C_o=10 mg L^{-1}, and IS=1, 2.5, and 5 mM KNO_3. Figure 5.7 provides similar information but in 350 μm quartz sand. For a given sand size, increases in IS produced a significant decline of AgNPs transport and a corresponding increase in retention. This observed trend is consistent with compression of the electrostatic double layer surrounding the collectors at higher IS as reported in previous studies (Jaisi et al. 2008; Lin et al. 2011). The BTCs were well described using the model (R^2>0.96), whereas the nonmonotonic RP was not accurately simulated.

The sensitivity of BTCs and RPs to IS provides further insight on AgNP retention. BTCs were more asymmetric at the lowest IS=1 mM and RPs were nonmonotonic when the IS equaled 2.5 or 5 mM. The increase of IS from 1 to 5 mM resulted in an increase of nearly 4-fold on k_1 and around 6-fold on S_{max} (Table 2). Consequently, BTCs were asymmetric and RPs were uniform with depth when IS=1 mM because the smaller S_{max} was filled rapidly. Conversely, when the IS=2.5 and 5 mM, values of S_{max} were larger, and the RPs were nonmonotonic because it took longer to fill these regions of the solid surface. Similar behavior occurred at higher IS and in the finer textured 350 μm sand, but in this case the value of S_{max} and the filling times were even larger. The nonmonotonic RPs were therefore more pronounced in the finer sand and at higher IS (2.5 and 5 mM) conditions.

XDLVO calculations predict a shallow secondary minima and significant energy barriers to attachment under these IS conditions (Table 3). An additional experiment at IS=5 mM was conducted to verify the role of the secondary minima. After application of AgNPs and rinsing with background particle-free electrolyte solution (around 8 pore volumes in total), the column was flushed with several pore volumes of Milli-Q water to expand the double layer thickness and to eliminate the secondary minimum (Figure 5.8). A pulse of AgNPs was released into the

effluent (C/C_o was approximately 0.4) when the secondary minimum was eliminated. However, integration of this pulse indicated that it only accounted for around 7% of the retained mass. This observation suggests that most of the retained AgNP mass was interacting in a primary minimum as a result of physical and/or chemical heterogeneity. Values of k_1 and S_{max} mainly determine the amount of AgNP retention, and both these parameters were lowest at IS of 1 mM. The effect of microscopic heterogeneity on k_1 and S_{max} has been reported to increase with IS because of a smaller zone of electrostatic influence when the double layer is compressed (Torkzaban et al. 2008). Consequently, increasing values of k_1 and S_{max} with IS (Table 2) are therefore expected to largely reflect the effects of microscopic heterogeneity.

Table 3. Extended DLVO Parameters of Stabilized AgNPs and Quartz Sand.

IS mM	d_p nm	ζ^a mV	ζ^b mV	$(V_{vdw}+V_{ed})_{max}$ NP-sand, kT	$(V_{vdw}+V_{ed})_{max}$ NP-NP, kT	V_{Tmax} NP-NP, kT	V_{Tmax} NP-sand, kT
1	45.1	-16.9	-55	6.31	1.07	1.71×10^4	2.16×10^3
2.5	48.2	-7.5	-55.4	1.4	< 0	1.84×10^4	2.29×10^3
5	60.7	-3.2	-55.3	0.31	< 0	2.30×10^4	2.89×10^3

IS, ionic strength; d_p, diameter of AgNPs; ζ^a, predicted core surface potential of AgNPs; ζ^b, measured zeta potential of quartz sand; $(V_{vdw}+ V_{ed})_{max}$, maximum energy of van der Waals (V_{vdW}) and electrostatic double layer interaction (V_{ed}); V_{Tmax}, maximum of the total XDLVO energy. NP-NP and NP-sand, the interaction between two nanoparticles and between nanoparticle and grain surface, respectively.

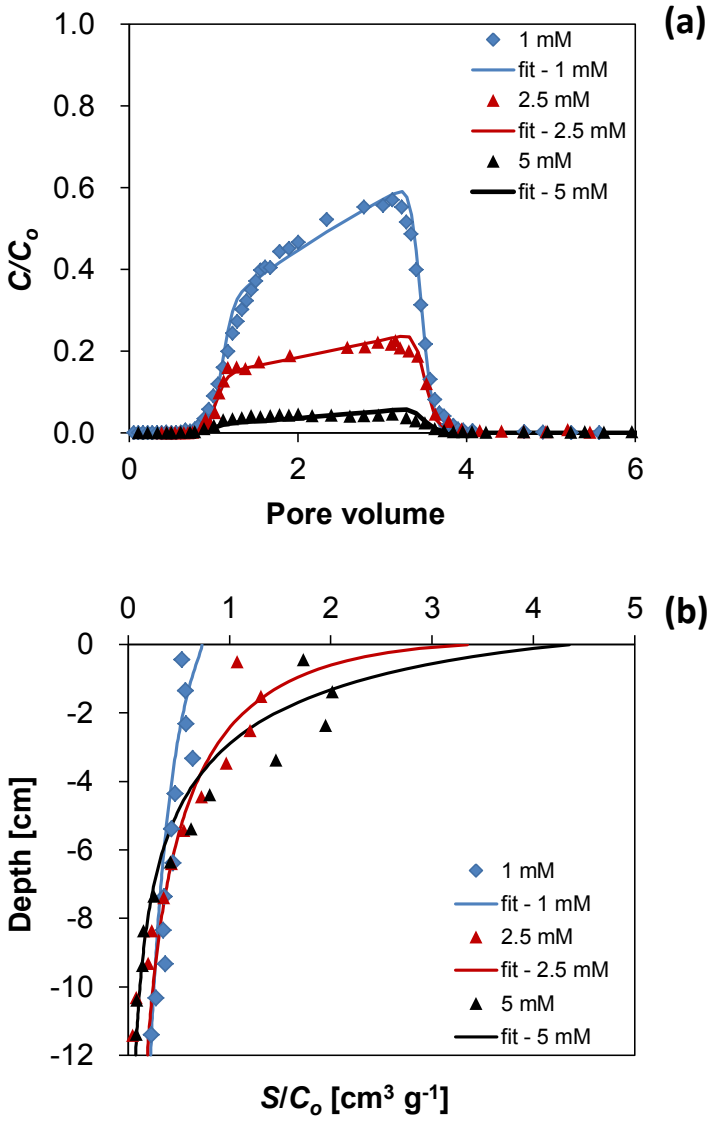

Figure 5.6. Effect of ionic strength on the transport and retention of AgNPs in water-saturated quartz sand: observed and fitted breakthrough curves (a) and retention profiles (b) of AgNPs under 1, 2.5 and 5 mM KNO_3, respectively. Other experimental conditions were the same: grain size, 607 µm; input concentration, 10 mg/L AgNPs; Darcy velocity, 0.7 cm/min

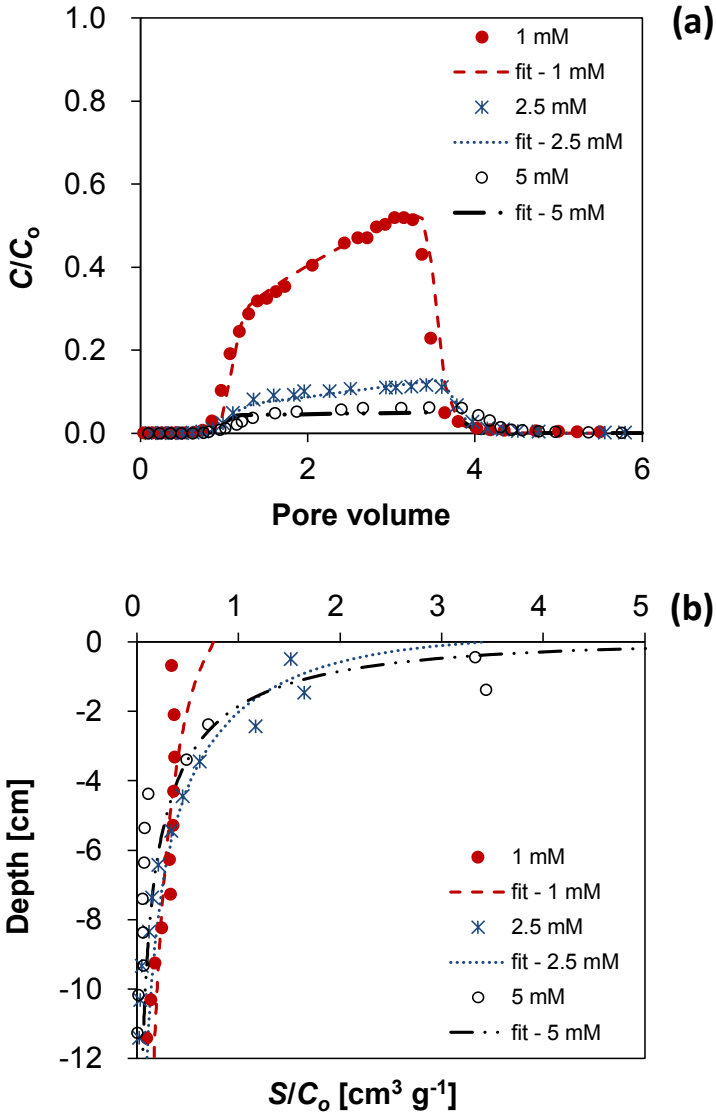

Figure 5.7. Effect of ionic strength on the transport and retention of AgNPs in water-saturated quartz sand: observed and fitted breakthrough curves (a) and retention profiles (b) of AgNPs under 1, 2.5 and 5 mM KNO_3, respectively. Other experimental conditions were the same: grain size, 350 µm; input concentration, 10 mg/L AgNPs; Darcy velocity, 0.7 cm/min.

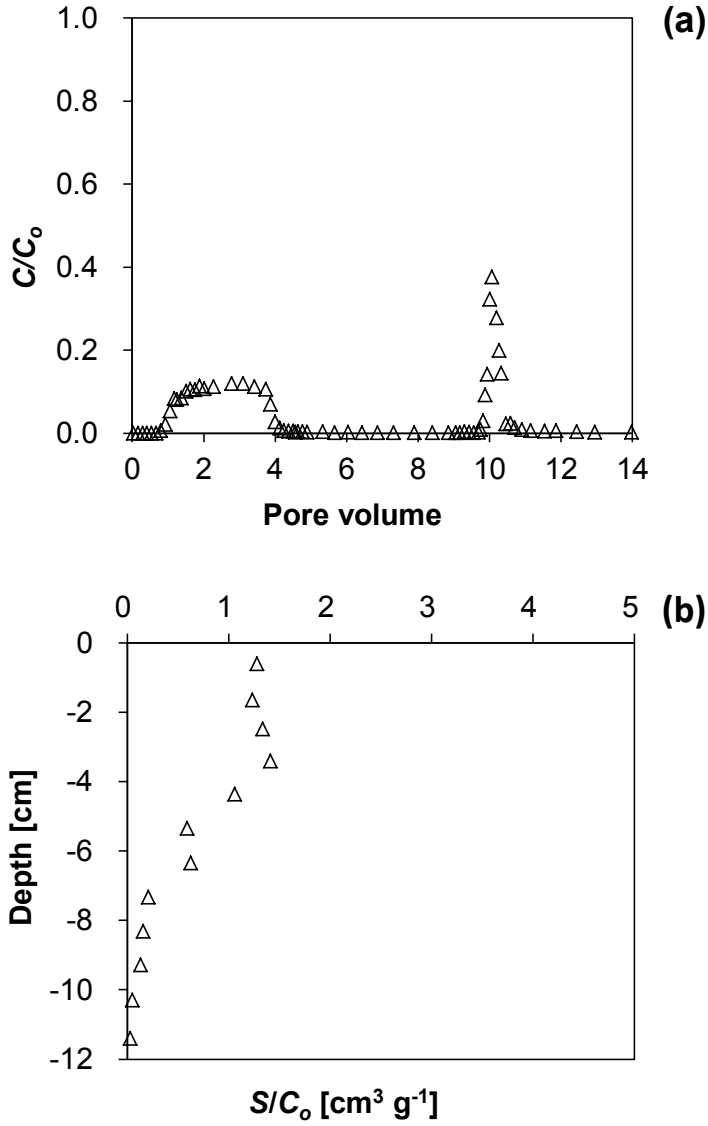

Figure 5.8. Observed breakthrough curves (a) and retention profiles (b) of AgNPs under 5 mM KNO_3, rinsing by Milli-Q water after particle retention. Grain size: 607 μm; input concentration: 10 mg/L AgNPs; Darcy velocity: 0.7 cm/min.

5.2.4 Effect of flow velocity

A series of experiments was performed under various flow velocities in 607 μm sand at an IS=1 mM KNO_3 to further investigate the influence of system hydrodynamics on AgNP fate. The results demonstrated an increased mass removal of AgNPs with decreasing flow rate (Figure 5.9). Higher effluent concentrations and significantly less retention occurred when the flow velocity increased from 0.03 to 0.7 cm min^{-1}. The RPs were nonmonotonic when Darcy velocities were 0.03, 0.14, and 0.35 cm min^{-1}.

Hydrodynamics may affect AgNPs transport and retention in 3 ways by influencing: (i) the rate of mass transfer from the bulk phase to the solid phase (Yao et al. 1971); (ii) the value of S_{max} that is associated with a secondary minimum (Li et al. 2005; Torkzaban et al. 2008); and (iii) the migration rate of particles adjacent to the solid phase (Ko and Elimelech 2000; Bradford et al. 2011a; Bradford et al. 2011b). Each of these factors will be briefly discussed below. In filtration theory, physicochemical interactions are assumed to control the rate of AgNP mass transfer to the solid surface. The values of k_1 obtained from the model all increased with increasing velocity (Table 2), consistent with expected trends for the bulk mass transfer rate predicted by filtration theory (Yao et al. 1971; Logan et al. 1995). Conversely, a systematic decrease in S_{max} with increasing velocity was not observed (S_{max}/C_o ranged from 0.732 to 2.017 $cm^3\ g^{-1}$) as would be predicted from torque balance considerations for AgNPs interacting by a secondary minimum. However, S_{max} was found to be lowest at the highest velocity. These observations highlight the relatively insignificant role of secondary minimum interactions for AgNPs and the importance of primary minimum interactions as a result of physical and/or chemical heterogeneity. Furthermore, systematic trends in the RP shape with velocity were not very apparent in Figure 5.9b as would be expected if solid phase AgNP migration occurred over long distances. Consequently, the amount of retention in the RPs was primarily determined by differences in the bulk phase mass transfer rate, and the shape of the RPs was mainly influenced by blocking of S_{max} arising from microscopic heterogeneities.

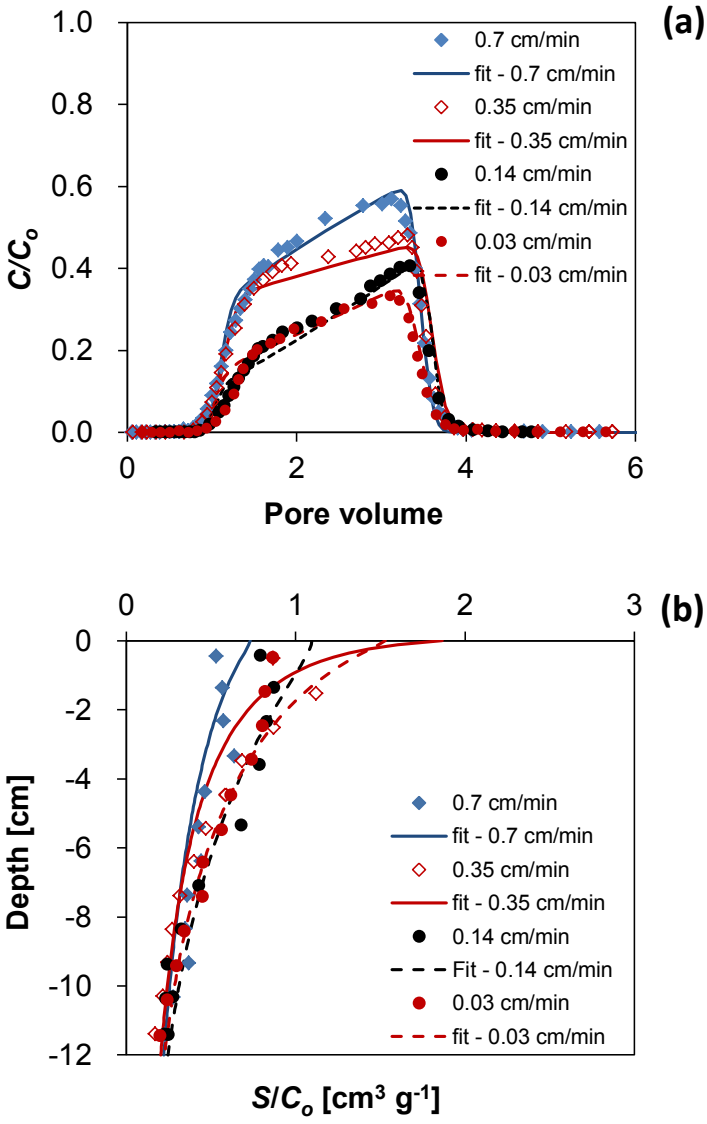

Figure 5.9. Effect of flow rate on the transport and retention of AgNPs in water-saturated quartz sand: observed and fitted breakthrough curves (a) and retention profiles (b) of AgNPs under Darcy velocities of 0.03, 0.14, 0.35, and 0.7 cm/min, respectively. Other conditions were the same: grain size, 607 µm; electrolyte, 1 mM KNO_3; input concentration, 10 mg/L AgNPs.

5.2.5 Nonmonotonic retention profiles

Nonmonotonic RPs were frequently observed for AgNP retention in water saturated-sand column. It has been suggested that nonmonotonic RPs may occur as a result of straining by aggregates and the reversibility of the particle retention influenced by factors such as grain size, hydrodynamic shearing forces, and electrostatic repulsion of deposited colloids (Bradford et al. 2006). The peak values of RPs are therefore varied from the different physicochemical conditions employed. Several model formulations have also been proposed in the literature to account for nonmonotonic RPs, such as an aggregated species that accounts for the reversible deposition of aggregates captured in straining sites (Bradford et al. 2006), an additional region that accounts for colloid interaction with the solid-water-interface (Bradford et al. 2011a), and re-entrainment of colloids (Li and Johnson 2005).

In this study, the experimental and modeling results discussed above indicated that the nonmonotonic RPs were strongly linked to blocking behavior. One potential explanation is due to the free surfactants (previously exist or desorption from the stabilized AgNPs) that subsequently adsorbed onto porous media. The RP shape may be altered by surfactant and NP competition for attachment sites that diminishes S_{max} (Lin et al. 2012; Wang et al. 2012). The role of surfactant on AgNP retention will be discussed below.

5.2.6 The influence of surfactant on silver nanoparticle transport and retention

The results of AgNP transport in quartz sand have indicated the significance of surfactant on the shape of RPs, which predict the mobility potential of NPs in the subsurface environment. The retention sites can be occupied by surfactant molecules and thus affect the retention of AgNPs. Column experiments with quartz sand were therefore conducted in an attempt to deduce the role of surfactant on AgNP transport and retention regarding the simultaneous transport of NPs and surfactant molecules, and the NP transport in surfactant- modified porous media.

Simultaneous transport experiments were performed with adding 10, 30 mg L^{-1} surfactant in the AgNP suspension before it was injected into columns after tracer experiments (Figure 5.10). To test the influence of surfactant-modified collector on NP transport behavior, another series of experiments was conducted by a pulse injection of 90 mL (around 3 pore volumes) surfactant solution at 10, 30, or 500 mg L^{-1} into columns to pre-coat porous media and immediately followed by a pulse injection of AgNP (Figure 5.11). All column experiments were carried out with a concentration of 10 mg L^{-1} AgNP, IS of 5 mM KNO_3, and flow velocity of 0.7 cm min^{-1}. Experimental conditions are provided in Table 4.

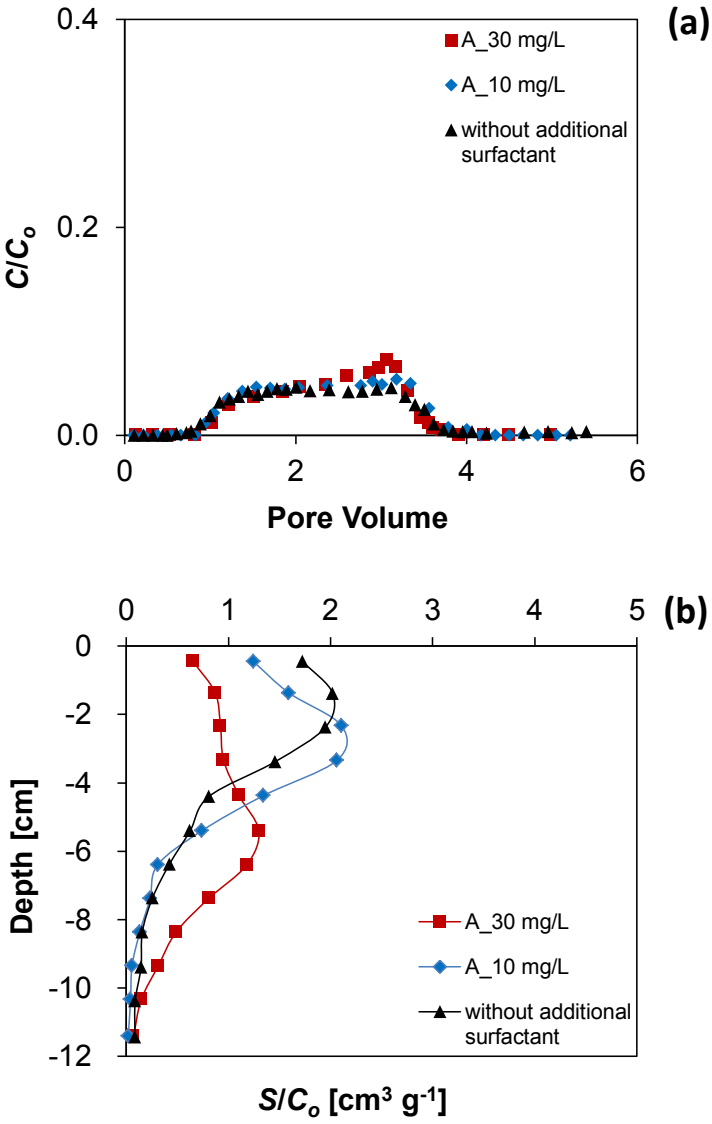

Figure 5.10. Observed breakthrough curves (a) and retention profiles (b) of AgNPs without additional surfactant and with adding 10 or 30 mg/L surfactant. A: AgNPs simultaneously transported with surfactant introduced during pulse injection of AgNPs. Other experimental conditions were the same: grain size, 607 μm; electrolyte, 5 mM KNO_3; input concentration, 10 mg/L AgNPs; Darcy velocity, 0.7 cm/min.

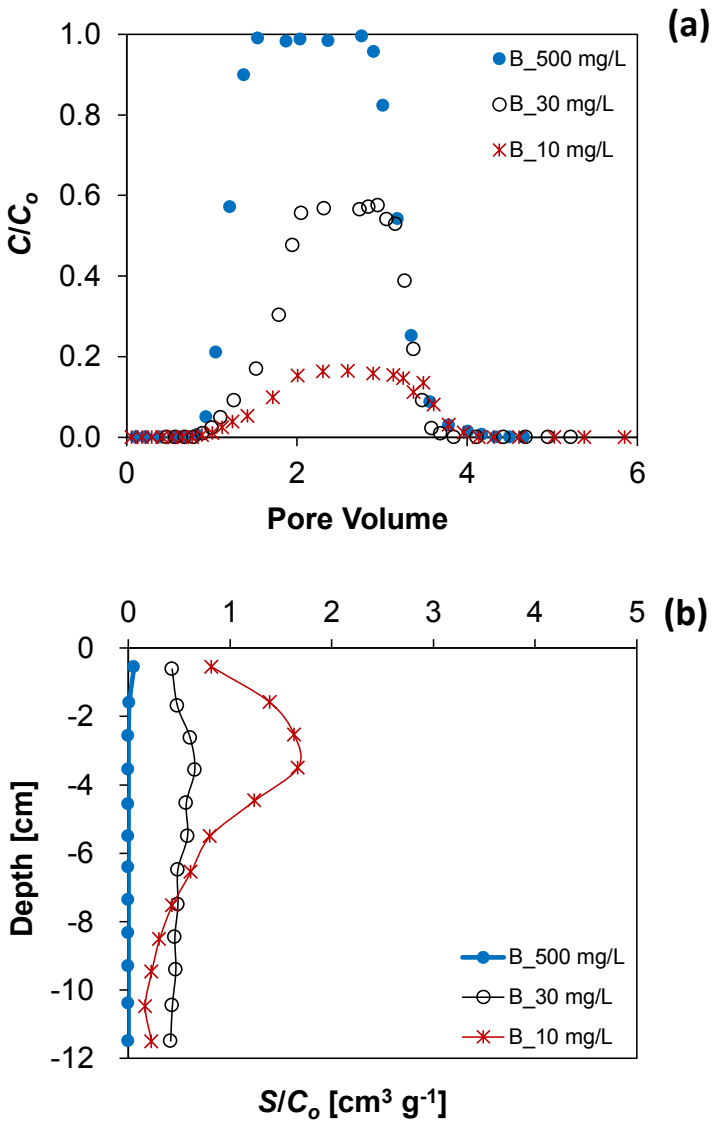

Figure 5.11. Observed breakthrough curves (a) and retention profiles (b) of AgNPs in surfactant pre-coated porous media. B: 90 mL (around 3 pore volumes) surfactant solution at 10, 30, or 500 mg/L was applied to pre-coat porous media and immediately followed by pulse injection of AgNPs. Other experimental conditions were the same: grain size, 607 μm; electrolyte, 5 mM KNO_3; input concentration, 10 mg/L AgNPs; Darcy velocity, 0.7 cm/min.

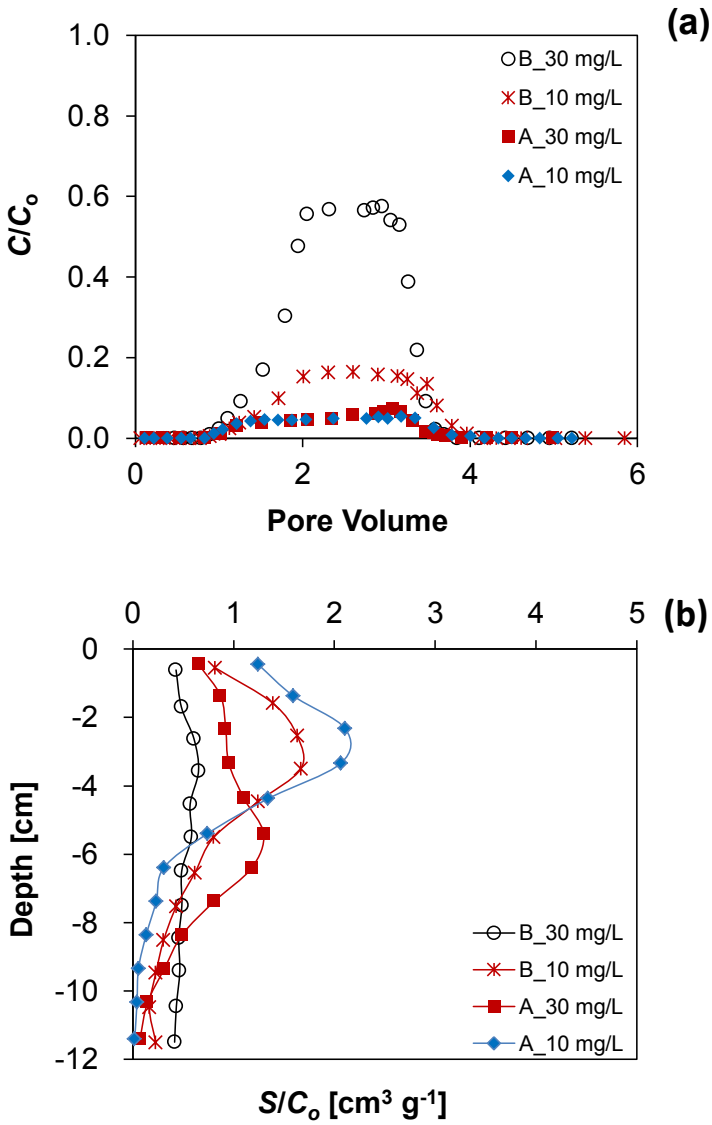

Figure 5.12. Observed breakthrough curves (a) and retention profiles (b) of AgNPs that simultaneously transported with surfactant and transported in surfactant-modified porous media, respectively (data from Figures 5.10 and 5.11). A: AgNPs simultaneously transported with surfactant. B: AgNP transported in modified porous media. Other experimental conditions were the same: grain size, 607 μm; electrolyte, 5 mM KNO_3; input concentration, 10 mg/L AgNPs; Darcy velocity, 0.7 cm/min.

Figures 5.10-5.12 present the results from simultaneous transport experiments, transport in modified media, and the comparison for the both cases, respectively. Note that in the simultaneous transport experiments, an increase of surfactant concentration from 10 to 30 mg L^{-1} had a relatively minor influence on the BTCs and produced nearly the same recoveries from effluent (Table 4), but a large effect on the nonmonotonic RPs was observed (Figure 5.10). In particular, higher surfactant concentrations were associated with nonmonotonic RPs having peak concentrations at greater distances. The decreasing amount of AgNP retained near the column inlet with increasing surfactant concentration is therefore likely a result of surfactant adsorption onto the grains that fills the retention sites and then decreases S_{max} at this location. It should be mentioned that a portion of surfactant is not bounded on the particle surface during synthesis and that the presence of adsorbed surfactant onto the sand surface can also increase the reversibility of particle retention. C/C_o in the BTCs increased significantly when the concentration of surfactant used for pre-coating the collector surface increased from 10 to 30 mg L^{-1} (Figure 5.11a), and the corresponding mass recoveries from the solid phase decreased from 90.3% to 58.4% (Table 4). Furthermore, the peak value of C/C_o in the case of 500 mg L^{-1} surfactant was even as high as 1 and almost all AgNPs were recovered in the effluent. The shapes of RPs became more uniform as the surfactant filled more retention sites at a higher concentration (Figure 5.11b). Figure 5.12 clearly indicates that using the surfactant to pre-coat the porous media was much effective to increase NP mobility compared with simultaneously injecting the same amount of surfactant during pulse application of AgNPs into the column. Retardation of NP breakthrough was also observed (the center of mass of the AgNP breakthrough front occurred after 1 pore volume) in Figure 5.11a. These findings indicate the gradual occupation of retention sites and that the retention of AgNPs was likely reversible. The retention of AgNPs close to the column inlet was much less in the case of transport in modified porous media. Consequently, the nonmonotonic RPs were governed by the combined influence of time-and depth-dependent retention (described by k_1 and S_{max}), and the effect of surfactant adsorption on S_{max}. The surfactant effect also provides a good explanation for the RPs showed in Figure 5.5b (effect of input concentration). The amount of surfactant in the solution is

expected to be proportional to C_o, so the effects of surfactant on AgNP retention are expected to increase with C_o because the blocking effect is more pronounced at a higher input concentration. In the case of nonmonotonic RPs in Figures 5.6b and 5.7b (effect of ionic strength), the competitive retention of AgNPs and surfactants is also likely an important effect. It should be mentioned that the surfactant molecules pre-coated on sand surface could also be desorbed during the subsequent rinse step. Therefore, the inverse simulation of AgNP transport in the presence of surfactant should take into account the information on surfactant interacting with collector such as surfactant sorption isotherm (batch experiment) and its transport behavior (column experiment).

Table 4. Experimental Parameters and the Mass Recovery for Column Experiments of Surfactant Stabilized AgNPs with and without Adding Surfactant as well as in Surfactant Pre-coated Sand.

	Series name	Surfactant con. mg L^{-1}	Recovery, %		
			M_{eff}	M_{sand}	M_{total}
Figure 5.10	without adding surfactant	/	4.6	103.5	108.1
	A_10 mg/L	10	4.5	91.6	96.1
	A_30 mg/L	30	5.2	96.8	102
Figure 5.11	B_10 mg/L	10	11.6	90.3	101.9
	B_30 mg/L	30	40.1	58.4	98.5
	B_500 mg/L	500	102.7	0.7	103.4
Figure 5.12	A_10 mg/L	10	4.5	91.6	96.1
	B_10 mg/L	10	11.6	90.3	101.9
	A_30 mg/L	30	5.2	96.8	102
	B_30 mg/L	30	40.1	58.4	98.5

Figure 5.10: AgNPs transported with and without adding surfactant. AgNPs simultaneously transported with surfactant introduced during pulse injection of AgNPs; Figure 5.11: AgNP transported in surfactant-modified porous media. Surfactant was applied to pre-coat collector before AgNP injection. Figure 5.12: data from Figures 5.10 and 5.11. A: AgNPs simultaneously transported with surfactant. B: AgNP transported in modified porous media. Other experimental conditions were the same: grain size, 607 μm; electrolyte, 5 mM KNO_3; input concentration, 10 mg/L AgNPs; Darcy velocity, 0.7 cm/min.

5.2.7 Conclusions of silver nanoparticle transport in water-saturated sand columns

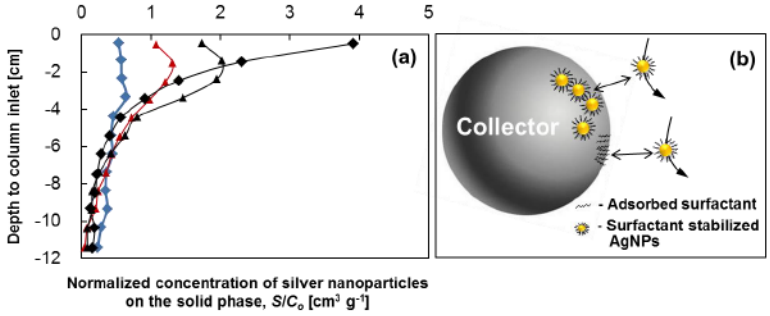

Figure 5.13. The diagram (a) shows the transition of RP shapes depending on particle concentration and ionic strength. The schematic presentation (b) depicts blocking effect and the reduced attachment of AgNPs due to surfactant coating and retained AgNPs.

Recoveries of AgNPs from effluent and sand in water-saturated sand column experiments clearly displayed the transport potential of AgNPs under the examined experimental conditions. Stronger mobility of AgNPs was observed at greater grain size, higher input concentration, lower IS, and higher flow velocity. Results of experiments and numerical simulation, and XDLVO calculations indicated that AgNPs mainly interacted in irreversible primary minimum and partially in a weak reversible secondary minimum at higher IS. The RPs exhibited hyperexponential, nonmonotonic, and uniform shapes (Figure 5.13a) controlled by the coupled effects of hydrodynamics near the column inlet and the competition of AgNPs and surfactant on the retention sites. The filling of retention sites reduced the retention capacity of the porous media (Figure 5.13b). This mechanism was supported by the introduction of surfactant with different concentrations and application ways (adding surfactant in the NP dispersion or pre-cover the sand grain surface by surfactant before AgNP injection). In fact, the retention capacity for AgNP was reduced to a higher degree in the case of surfactant-modified porous media. Nevertheless, the highly idealized system (pure quartz sand and monovalent electrolyte solutions) employed in this transport study cannot fully reflect the complex natural system.

5.3 Transport and retention of silver nanoparticles in an undisturbed soil

5.3.1 Influence of physicochemical factors

Figures 5.15-5.17 show the observed and simulated BTCs and RPs for AgNPs in the undisturbed soil for various IS (Figure 5.15), input concentrations (Figure 5.16), and flow velocities (Figure 5.17). Mass balance information for the BTCs, RPs, and total columns are provided in Table 5. The water saturation ranged from 85%-95%. The total column mass balance (92% - 111%) was very good. Table 6 summarizes the fitted model parameters, the 95% confidence intervals for the fitted parameters, and the Pearson's correlation coefficient (R^2) between observed and simulated data. Overall, the simulated curves were able to capture the main features of AgNP transport and retention (R^2>0.959).

The BTCs for AgNPs were retarded in comparison with the tracer (an example for the tracer is shown in Figure 5.14). This retardation is evident in Figures 5.15-5.17. In particular, the center of mass of the AgNP breakthrough front frequently occurred after 1 pore volume. These retarded breakthrough curves can be quantified with the fitted parameters k_1 and S_{max}/C_o in eqs. (4.14) - (4.16) which are related to the retention rate and capacity of AgNPs on the porous media, respectively. A high value of k_1 produces complete retention until S_{max}/C_o is filled. Consequently, more retarded BTCs are expected for higher k_1 and larger S_{max}/C_o. However, if k_1 is too low then breakthrough will occur (no retardation) and the BTC will slowly increase with time as the favorable retention locations are gradually filled.

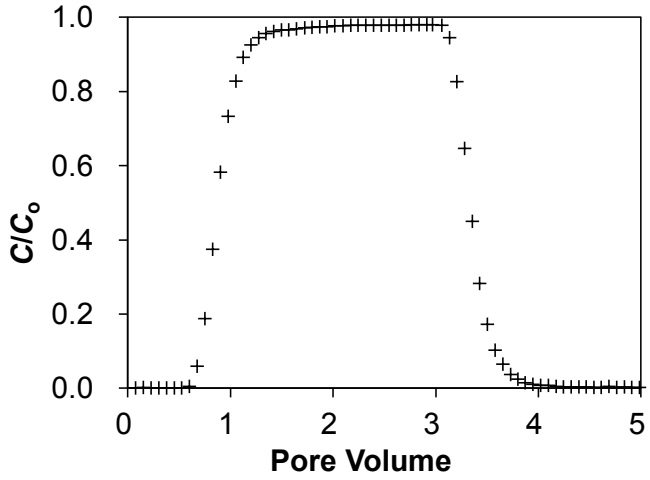

Figure 5.14. Observed breakthrough curve of tracer from an undisturbed and unsaturated (90%) soil column experiment

More retarded BTCs, lower effluent concentrations, and greater retention occurs at higher IS in Figure 5.15. This can be explained by an increase in k_1 and S_{max}/C_o with IS (Table 6) that occurs due to compression of the electrical double layer thickness that produces a shallow secondary minimum and enhances the effects of nanoscale heterogeneities (Bradford and Torkzaban 2013). Higher values of C_o (input concentration) produced less retardation, higher effluent concentrations, and less retention in Figure 5.16. One potential explanation is due to blocking which increases the rate of filling of S_{max} with a larger C_o (Bradford et al. 2009). In addition, the retained AgNPs could hinder further retention due to the repulsive AgNP-AgNP interactions especially when more particles were retained at higher C_o as discussed for effect of AgNP input concentration in quartz sand in previous section. An observed decrease in k_1 and S_{max}/C_o with larger C_o supports this hypothesis (Table 6). Higher effluent concentrations and less retention were observed in Figure 5.17 for higher q (flow velocity). Similar to experimental observations, filtration theory predicts that k_1 is proportional to q to the 1/3 power (Schijven and Hassanizadeh 2000). However, the overall rate of advection is proportional to q, so a decrease in retention is expected with an increase in q. Experimental values of S_{max}/C_o also decrease with higher q similar to predicted trends when conducting a balance of applied hydrodynamic and

resisting adhesive torques to determine the fraction of the solid surface that contributes to colloid immobilization (Bradford and Torkzaban 2013).

The above results indicate that AgNP transport and retention in soil are highly dependent on blocking, which has also been demonstrated to play an important role in homogeneous quartz sand as shown in previous sections. Similar to Figures 5.15-5.17, BTCs for AgNPs in quartz sand (Figures 5.5-5.7, 5.9) were observed to decrease with IS, and to increase with C_o and q. In contrast to Figures 5.15-5.17, retardation was not observed to play a significant role in the quartz sands. Furthermore, the RPs in the loamy sand (Figures 5.15-5.17) were always hyperexponential in shape and a significant fraction of the retained AgNPs (approximately 70 %) was in the top 0-3 cm. In contrast, blocking caused the RP shapes to transit from hyperexponential, to nonmonotonic, and to uniform in the quartz sand (Figures 5.4b-5.7b). These differences can partially be ascribed to the higher values of S_{max}/C_o in the current work (>1.94 $cm^3\ g^{-1}$). In comparison, values of S_{max}/C_o were frequently as low as 0.732 $cm^3\ g^{-1}$ in the quartz sand. In addition, as confirmed by the BET surface area analysis, the interacting surface area in the loamy sand (1.7 $m^2\ g^{-1}$) is much greater than in the quartz sand (less than 0.2 $m^2\ g^{-1}$). Both of these factors tend to diminish the relative importance of blocking in loamy sand in comparison to quartz sand, e.g., it takes more AgNPs to fill a larger value of S_{max}/C_o (Tufenkji and Elimelech 2005; Tong and Johnson 2006).

Several explanations have been proposed in the literature for hyperexponential RPs, including: aggregation (Bradford et al. 2006), straining (Li et al. 2004), chemical heterogeneity on the particle (Tufenkji and Elimelech 2005) and system hydrodynamics (Bradford et al. 2011a). These hypotheses will be briefly examined below. TEM images taken from the column effluent (Figure 5.18) demonstrated that the AgNPs were still well dispersed. Furthermore, the BTCs did not exhibit ripening behavior (increasing retention rate with time). This information suggests that AgNP aggregation was insignificant during the transport experiments. Straining was neglected because of the small ratio of the AgNP diameter to the soil grain size (Li et al. 2004). Charge heterogeneity on the AgNP surface was an unlikely explanation because the zeta

potentials for AgNPs in influent and effluent solutions were very similar. Alternatively, variations in the pore-scale velocity can provide a viable explanation for the hyperexponential RPs when the flux adjacent to the solid surface near the column inlet is the dominant mass transfer mechanism to the solid-water interface (Bradford et al. 2011a). This effect is reported to be more pronounced in finer textured porous media (Bradford et al. 2011a), which is consistent with the higher value of β in eq. (4.16) for AgNP transport in loamy sand (β=1.532) than quartz sand (β=0.432). A higher value of β indicates a stronger depth dependence of the retention coefficient (k_1).

AgNPs attached to quartz sand in a weak secondary minimum and a strong primary minimum has been discussed in previous sections. Similar interactions are expected for AgNPs in the loamy sand. Secondary minimum interactions are very shallow for AgNPs under low IS conditions. Consequently, the kinetic energy of diffusing AgNPs is expected to be sufficiently large to overcome most of the shallow secondary minimum interactions (Shen et al. 2007). Conversely, primary minimum interactions may be significant for nanoparticles as a result of nanoscale chemical and physical heterogeneity on the soil surface (Bradford and Torkzaban 2013). Nanoscale heterogeneity is well-known to be significant for soils due to roughness and adsorbed clays, natural organic matter (NOM), metal oxides, ions, and variations in mineralogy (Cornelis et al. 2012). The nanoscale heterogeneity on the soil surface may produce primary minimum interactions for AgNPs depending on the cross-sectional area of the heterogeneity and the solution IS (Bradford and Torkzaban 2013). However, charge heterogeneity on the soil surface will tend to be masked by NOM (Lecoanet et al. 2004; Badawy ; Pan and Xing 2012) present in the loamy sand (1.1%) (Unold et al. 2009) or free surfactant in the AgNP suspension (Unold et al. 2009). Furthermore, the effect of nanoscale heterogeneity on AgNP retention is expected to be diminished under low IS conditions (Bradford and Torkzaban 2013). Both of these factors can help to explain the high mobility of AgNPs in the loamy sand when the IS was 1 mM (Figure 5.15). Higher mobility of AgNP was observed from a water-saturated column packed with disturbed soil under comparable conditions as the sand columns (Figure 5.19).

Collectively, these results suggest that AgNP transport in the loamy sand soil was mainly controlled by primary minimum interactions from soil heterogeneities that were diminished by NOM, especially under low IS conditions.

Table 5. Experimental Parameters and the Mass Recovery for Transport Experiments of Surfactant Stabilized AgNPs in an Undisturbed Soil

	C_o	q	IS	φ	θ_w	S_w	Recovery, %		
	mg L^{-1}	cm min^{-1}	mM				M_{eff}	M_{sand}	M_{total}
Figure 5.15	10	0.006	1	0.431	0.407	0.944	37.9	70.5	108.4
	10	0.006	5	0.453	0.429	0.947	13.9	78.7	92.6
	10	0.006	10	0.452	0.407	0.900	3.40	88.6	92.0
Figure 5.16	10	0.006	1	0.431	0.407	0.944	37.9	70.5	108.4
	1	0.006	1	0.462	0.438	0.949	14.4	96.2	110.6
Figure 5.17	10	0.02	1	0.467	0.397	0.851	64.3	40.0	104.3
	10	0.006	1	0.431	0.407	0.944	37.9	70.5	108.4

Figure 5.15. ionic strength effect; Figure 5.16: concentration effect; Figure 5.17: flow rate effect. C_o, AgNP input concentration; q, Darcy velocity; IS, ionic strength; φ, porosity; θ_w: water content; S_w, water saturation; M_{eff}, M_{sand}, and M_{total} are mass percentages recovered from effluent, sand, and total, respectively.

Table 6. Fitted Values (k_1 and S_{max}/C_o) of Surfactant Stabilized AgNP Transport and Retention Parameters in an Undisturbed Soil.

	C_o	q	IS	k_1	Standard	S_{max}/C_o	Standard error	R^2
	mg L^{-1}	cm min^{-1}	mM	min^{-1}	error, k_1	$cm^3\ g^{-1}$	S_{max}/C_o	
Figure 5.15	10	0.006	1	0.488	0.039	2.097	0.03	0.989
	10	0.006	5	1.305	0.089	3.184	0.025	0.966
	10	0.006	10	3.581	0.400	3.535	0.035	0.959
Figure 5.16	10	0.006	1	0.488	0.039	2.097	0.030	0.989
	1	0.006	1	0.606	0.056	3.185	0.021	0.981
Figure 5.17	10	0.02	1	0.667	0.058	1.940	0.147	0.976
	10	0.006	1	0.488	0.039	2.097	0.030	0.989

Figure 5.15: ionic strength effect; Figure 5.16: concentration effect; Figure 5.17: flow rate effect. C_o, AgNP input concentration; q, Darcy velocity; IS, ionic strength; k_1, the first-order retention coefficient; S_{max}/C_o, normalized maximum solid phase concentration of deposited NPs; R^2, Pearson's correlation coefficient.

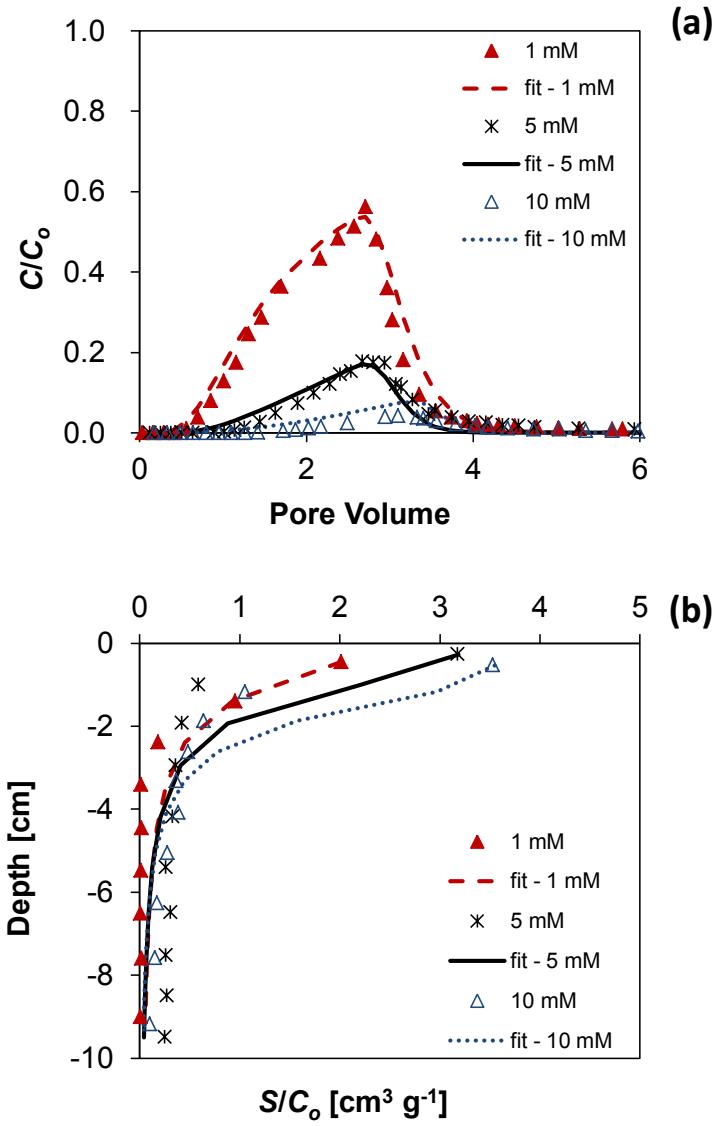

Figure 5.15. Effect of ionic strength on the transport and retention of AgNPs in an undisturbed loamy sand soil: observed and fitted breakthrough curves (a) and retention profiles (b) of AgNPs under 1, 5, and 10 mM KNO_3, respectively. Other experimental conditions were the same: input concentration, 10 mg/L AgNPs; Darcy velocity, 0.006 cm/min.

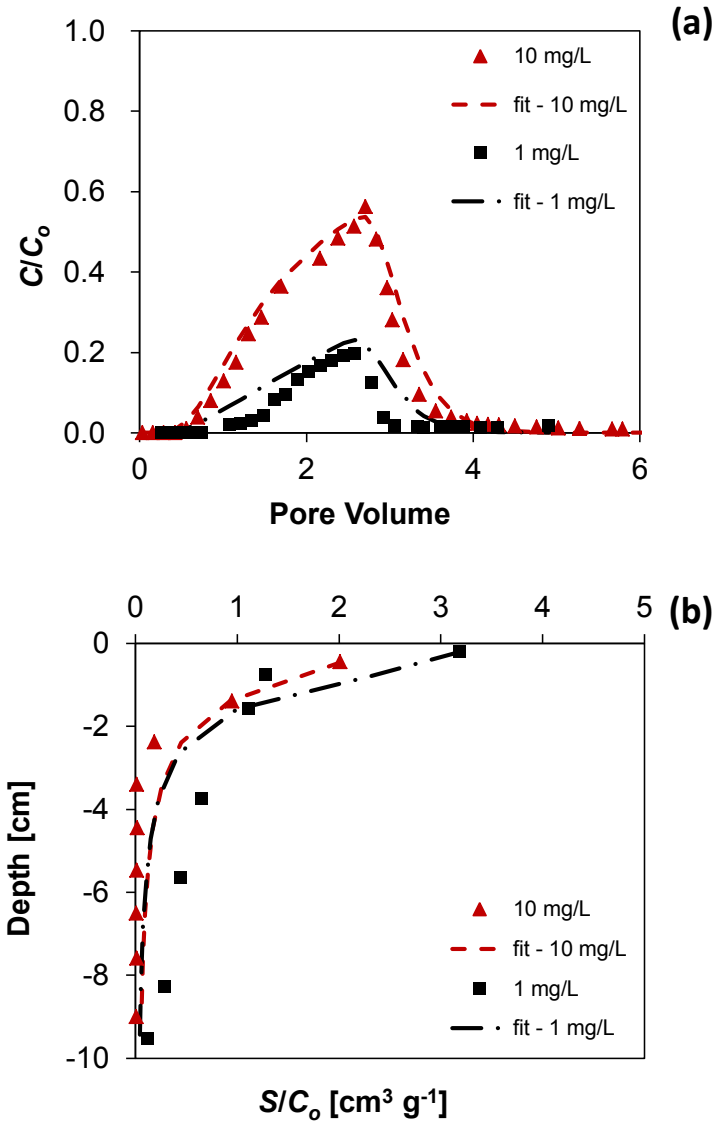

Figure 5.16. Effect of AgNP concentration on the transport and retention of AgNPs in an undisturbed loamy sand soil: observed and fitted breakthrough curves (a) and retention profiles (b) of AgNPs under AgNP input concentrations of 1 and 10 mg/L, respectively. Other experimental conditions were the same: electrolyte, 1mM KNO_3; Darcy velocity, 0.006 cm/min.

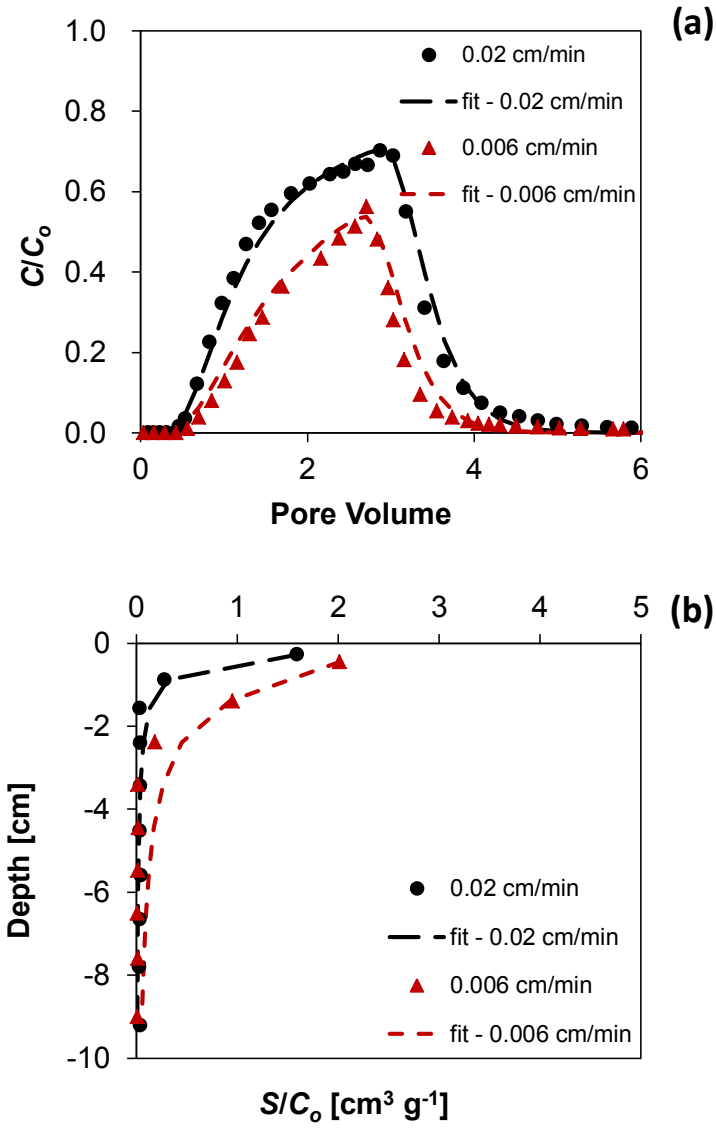

Figure 5.17. Effect of flow rate on the transport and retention of AgNPs in an undisturbed loamy sand soil: observed and fitted breakthrough curves (a) and retention profiles (b) of AgNPs under Darcy velocity of 0.006 and 0.02 cm/min, respectively. Other experimental conditions were the same: electrolyte, 1 mM KNO_3; input concentration, 10 mg/L AgNPs.

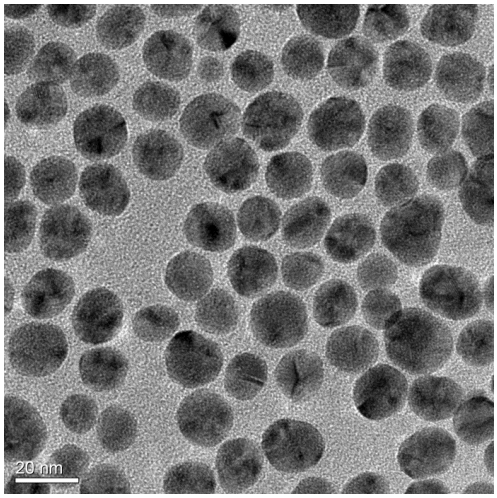

Figure 5.18. Transmission electron micrograph of AgNPs in an effluent sample from a transport experiment with undisturbed soil

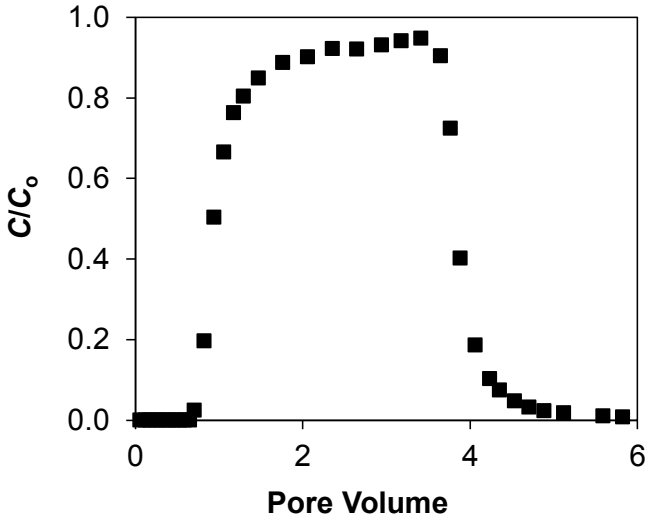

Figure 5.19. Transport of AgNPs in a water-saturated repacked soil column experiment. Experimental conditions were: electrolyte, 1 mM KNO_3; input concentration, 10 mg/L AgNPs; flow velocity: 0.7 cm/min.

5.3.2 Remobilization of silver nanoparticles in an unsaturated - undisturbed soil

Experiments I-IV were conducted to better understand the effect of cation type, IS reduction, and cation exchange on the release of AgNPs in soil. Figure 5.20 presents BTCs when AgNPs were deposited and eluted (step A) in the presence of KNO_3 or $Ca(NO_3)_2$ at an IS of 10 mM, and then release of AgNPs was initiated in step B by a reduction in IS (Milli-Q water). Retention of AgNPs in step A was more pronounced in the presence of $Ca(NO_3)_2$ than KNO_3, even though the IS was the same. This can be explained by bridging complexation between soil grains and functionalized nanoparticles in the presence of Ca^{2+} (Torkzaban et al. 2012). Natural mineral surfaces such as clays are known to show a stronger affinity for divalent than monovalent cations (Roy and Dzombak 1996). Release of AgNPs by IS reduction (step B) was more pronounced when the AgNPs were retained (step A) in the presence of monovalent cation. Mass balance information indicates that the recovery in step B was 31.7% for KNO_3 solution and only 16% for $Ca(NO_3)_2$ (Table 7). This behavior indicates that some of the AgNPs were interacting in a reversible minimum that was eliminated by a reduction in the IS. However, the resistance to AgNP release with IS reduction was apparently greater in the presence of $Ca(NO_3)_2$ than KNO_3, suggesting that cation bridging created stronger primary minimum interactions (Jaisi et al. 2008). The experimental results also indicate that these primary minimum interactions were not diminished by long elution at reduced IS.

Table 7. Experimental Parameters and the Mass Recovery for Release Experiments of Surfactant Stabilized AgNPs in an Undisturbed Soil

	Experiment	IS_A mM	M_A	M_B H_2O	IS_C mM	M_C	M_D H_2O	IS_E mM	M_E	M_F H_2O
Figure 5.20	III	10, Ca^{2+}	< 1%	16						
	IV	10, K^+	9.1	31.7						
Figure 5.21a	I	1, Ca^{2+}	3.9	3.8	1, K^+	< 1%	1.5	100, K^+	5	9.4
	II	5, Ca^{2+}	< 1%	4.6	5, K^+	< 1%	10.8	100, K^+	< 1%	7.7
	III	10, Ca^{2+}	< 1%	16	10, K^+	< 1%	16.7	100, K^+	< 1%	4.2

Figure 5.20: release of AgNPs by ionic strength reduction; Figure 5.21a: release of AgNPs by cation exchange and ionic strength reduction; IS, ionic strength; M_A-M_F are the mass percentages recovered from steps A-F in release experiments. The Darcy velocity (q) was 0.02 cm/min and the input AgNP concentration (C_o) was 10 mg/L.

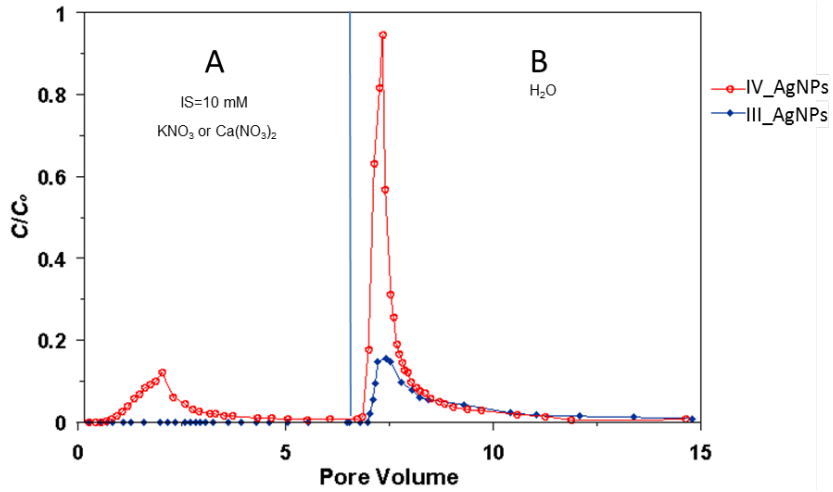

Figure 5.20. Breakthrough and release behavior of AgNPs in an undisturbed loamy sand soil. Deposition (step A) occurred at an IS=10 mM using $Ca(NO_3)_2$ (experiment III) or KNO_3 (experiment IV), whereas release (step B) was initiated by eluting with Milli-Q water as summarized in Table 7. The Darcy velocity (q) was 0.02 cm/min and the input AgNP concentration (C_o) was 10 mg/L.

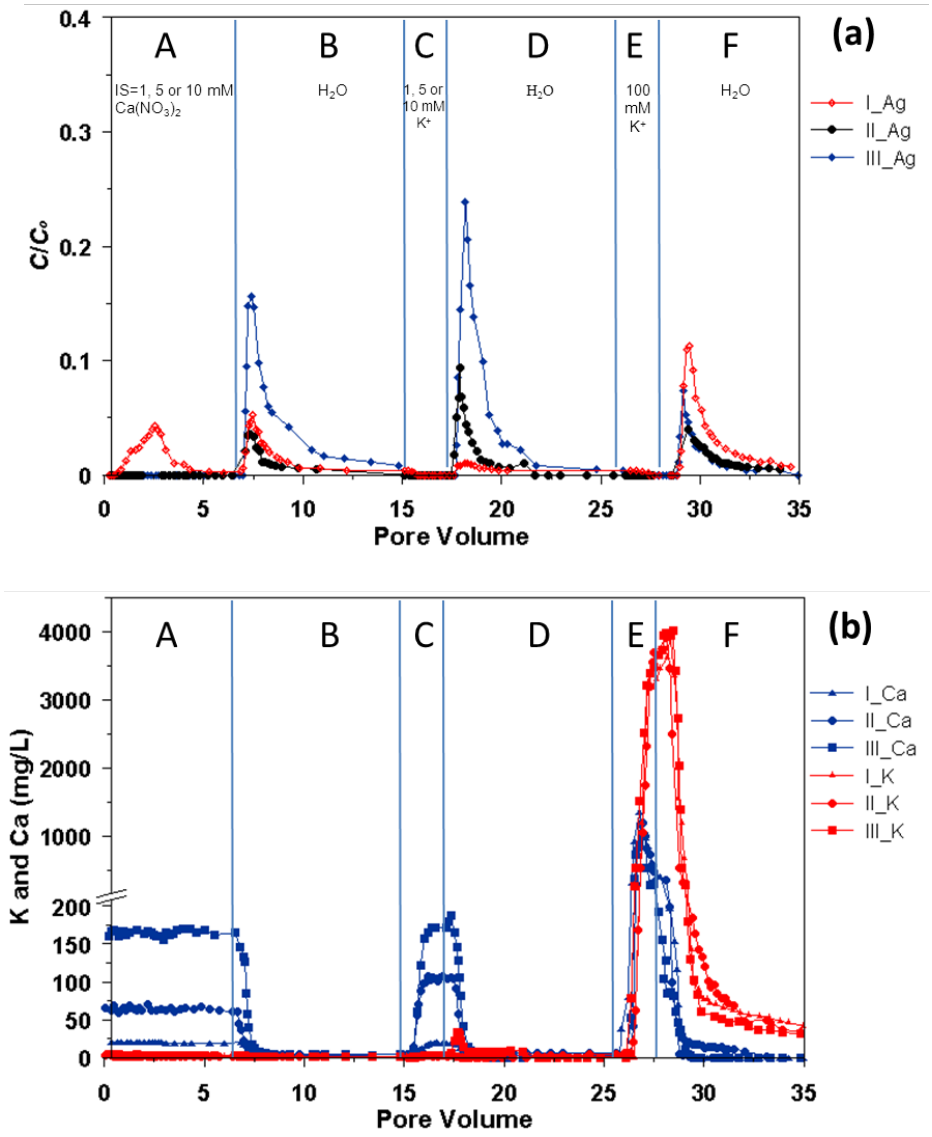

Figure 5.21. (a) Breakthrough and release behavior of AgNPs in an undisturbed loamy sand soil. Deposition (step A) occurred at an IS=1, 5, and 10 mM using $Ca(NO_3)_2$ for experiment I, II, and III, respectively, whereas release was initiated by eluting with Milli-Q water (steps B, D, and F) and cation exchange (steps C and E) as summarized in Table 7. (b): Effluent concentrations of K and Ca during steps A-F. The Darcy velocity (q) was 0.02 cm/min and the input AgNP concentration (C_o) was 10 mg/L.

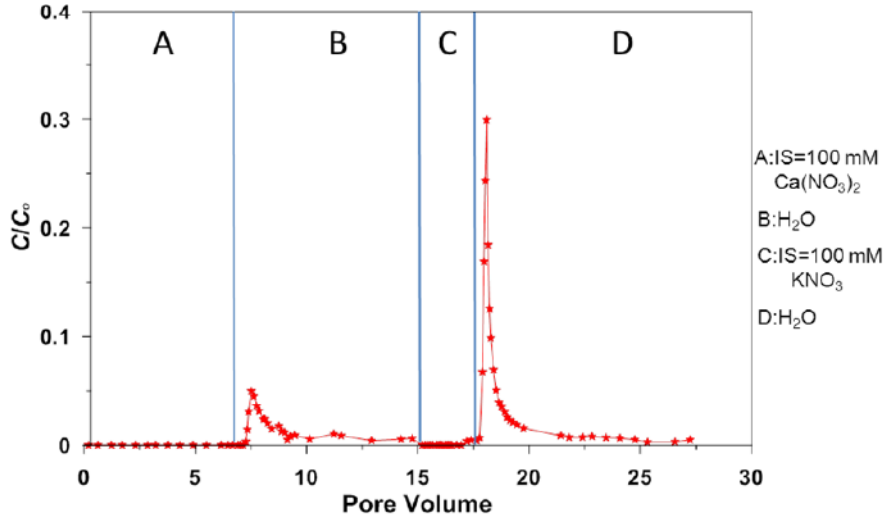

Figure 5.22. Breakthrough and release behavior of AgNPs in an undisturbed loamy sand soil. Deposition (step A) occurred at an IS=100 mM using $Ca(NO_3)_2$, whereas release was initiated by eluting with Milli-Q water (steps B and D) and cation exchange (steps C). The Darcy velocity (q) was 0.02 cm/min and the input AgNP concentration (C_o) was 10 mg/L.

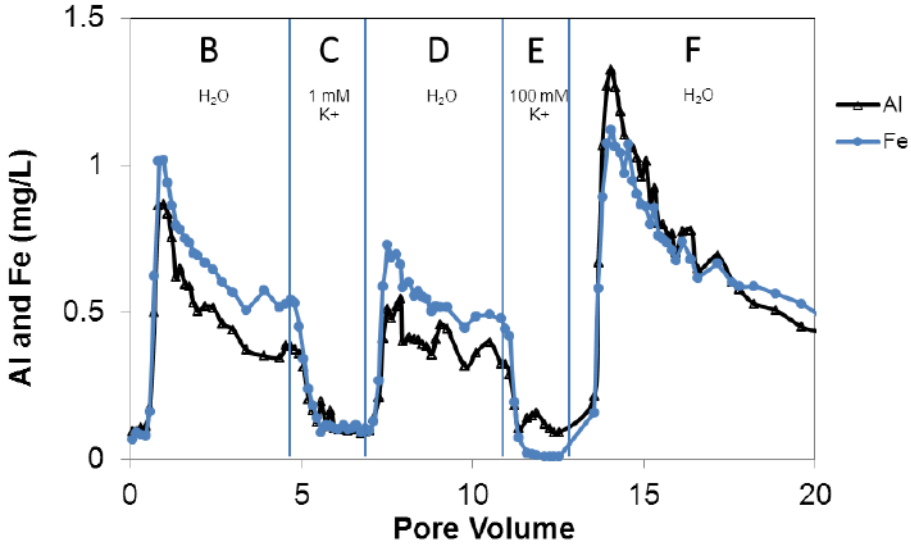

Figure 5.23. Release behavior of Al and Fe that are associated with natural soil colloids from an undisturbed column during steps B-F (without AgNPs injection). Release was initiated by eluting with Milli-Q water (steps B, D, and F) and cation exchange (steps C and E). The Darcy velocity (q) was 0.02 cm/min and the input AgNP concentration (C_o) was 10 mg/L.

Figure 5.21a shows the AgNP BTCs from experiments I-III in the presence of $Ca(NO_3)_2$ when the IS in step A was 1, 5, and 10 mM, respectively. The subsequent release procedures were Milli-Q water (step B), KNO_3 at the same IS as in step A (step C), Milli-Q water (step D), 100 mM KNO_3 (step E), and Milli-Q water (step F). A small amount (3.9%) of the injected AgNPs was transported through the undisturbed soil column during step A in experiment I. In contrast, the AgNP concentrations in the effluent from step A were under the detection limit in experiments II and III. The recoveries of AgNPs in step B (Milli-Q water) were 3.8%, 4.6%, and 16.0% for experiment I, II, and III respectively. Similar to Figure 5.15, these observations suggests that a greater amount of AgNPs were reversibly retained in a secondary minimum with the higher IS in step A.

When KNO_3 was introduced in step C at the same IS as in step A and at a much larger IS of 100 mM in step E, further AgNP remobilization occurred by IS reduction in steps D and F. The continued release of AgNPs as IS reduced during steps D and F was initiated by the cation exchange during steps C and E, respectively. Figure 5.21b shows plots of K^+ and Ca^{2+} concentrations in the column effluent for experiments I-III. Around 95% of the injected K^+ mass in step C was retained in the column even after flushing with Milli-Q water during step D. Conversely, less than 20% of the injected K^+ (100 mM) in step E was adsorbed to the soil and high release peaks for Ca^{2+} were observed. This clearly indicates that excess amounts of K^+ in step E produced substantial release of Ca^{2+} as a result of cation exchange. However, very little AgNP release occurred during cation exchange (C and E), while rather significant release of AgNPs occurred during IS reduction (D and F) immediately following cation exchange. Exchange of K^+ for Ca^{2+} will decrease the potential for bridging complexation, whereas IS reduction will expand the double layer thickness and eliminate the secondary minimum. These observations suggest that both cation exchange and IS reduction were needed to release the AgNPs that were interacting with the soil grains in the presence of divalent cation.

The amount of AgNPs that were released in step D followed a similar trend to that shown in step B (Table 7 and Figure 5.21a); e.g., increasing with IS of KNO_3 in step C. In addition,

Figure 5.22 demonstrates a stronger release of AgNPs in step D after cation exchange and IS reduction when the NPs were retained under an IS of 100 mM with $Ca(NO_3)_2$ in step A. This observation suggests that IS reduction was the dominant cause of release in this case. Conversely, greater amounts of AgNP release occurred in step F for soils exposed to lower concentrations of $Ca(NO_3)_2$ during step A (Table 7). Consequently, a larger amount of AgNPs was released when the cation exchange was more pronounced followed by IS reduction. Bradford and Kim (Bradford and Kim 2010) observed significant amounts of kaolinite clay release following similar processes of cation exchange (Na^+ for Ca^{2+}) and IS reduction. Similarly, the effluent was very turbid during steps B, D, and F. This phenomenon implied the release of natural soil colloids from the loamy sand soil. The remobilization of soil colloids from an AgNP-free soil column was confirmed by measuring effluent concentrations of Al and Fe shown in Figure 5.23. Notice that the release of Al and Fe in soil showed a very similar trend as the release of AgNPs (Figure 5.21a), suggesting the potential for AgNP association with soil colloids. Additionally, in order to make a comparison between the natural soil and simplified systems regarding the presence and absence of soil colloids/clays, respectively, another experiment series was performed under the same procedure as release experiments for soil columns, but with pure quartz sand (no clay). Additional release experiments were carried out in the same system as transport experiments with quartz sand columns using purified quartz sand at a mean size of 607 μm and a flow velocity of 0.7 cm min^{-1}. AgNP input concentration and IS were the same as in undisturbed soil columns. Note that the release of AgNPs from sand columns accounted for less than 2% recovery in step B (Figure 5.24), and the released AgNPs after cation exchange and IS reduction were below the detection limit. These observations further implied the potential of co-transport of released AgNPs and clays in steps D and F in soil columns. Additional evidence for the role of soil colloids on AgNP release is provided below.

To further confirm the potential for soil colloids to facilitate the release of AgNPs, Figure 5.25 presents plots of Ag, Al, and Fe concentration for steps A-F. In this case, AgNP deposition and elution during step A occurred in the presence of $Ca(NO_3)_2$ at an IS of 5 mM when C_o was

10 mg L^{-1} and q was 0.7 cm min^{-1}. In contrast to other experiments, a repacked soil column was employed under saturated conditions. Similar to Figure 5.23, the release of AgNPs was highly correlated with Fe and Al concentrations of soil colloids. The association of AgNPs with soil colloids was further confirmed by TEM investigation. Figure 5.25 (b and c) presents representative TEM images of soil colloids in the effluent. The black dots on these colloids were confirmed by EDX to be AgNPs (Figure 5.25d and e). A rigorous determination of the colloid-associated fraction of AgNPs was not attempted because of TEM limitations in sample preparation and inspection, and the transient solution chemistry conditions. Nevertheless, the TEM images (Figure 5.25 b and c) and EDX analysis (Figure 5.25d and e), correlations between Ag, Fe, and Al (Figure 5.25 a), and available literature (Cornelis et al. 2012; Zhou et al. 2012) do support the interaction between soil colloids and some fraction of the released AgNPs. It is to mention here that additional research is needed to fully resolve the role of soil colloids (such as clay minerals, iron oxide-hydroxide and their complexes) in facilitating the release and transport of AgNPs during transient solution chemistry conditions.

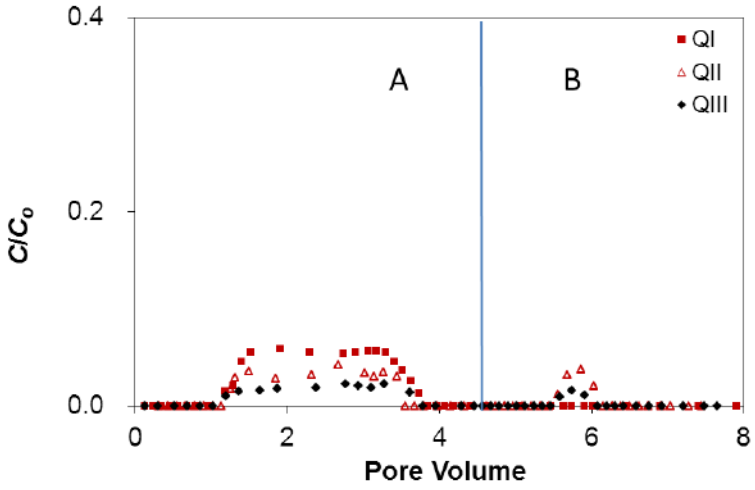

Figure 5.24. Breakthrough and release behavior of AgNPs in quartz sand. Deposition (step A) occurred at an IS=1, 5, and 10 mM using $Ca(NO_3)_2$ for experiment QI, QII, and QIII, respectively. In step B, the columns were irrigated by Milli-Q water. Grain size, 607 µm; input AgNP concentration (C_o), 10 mg/L; flow rate, 0.7 cm/min.

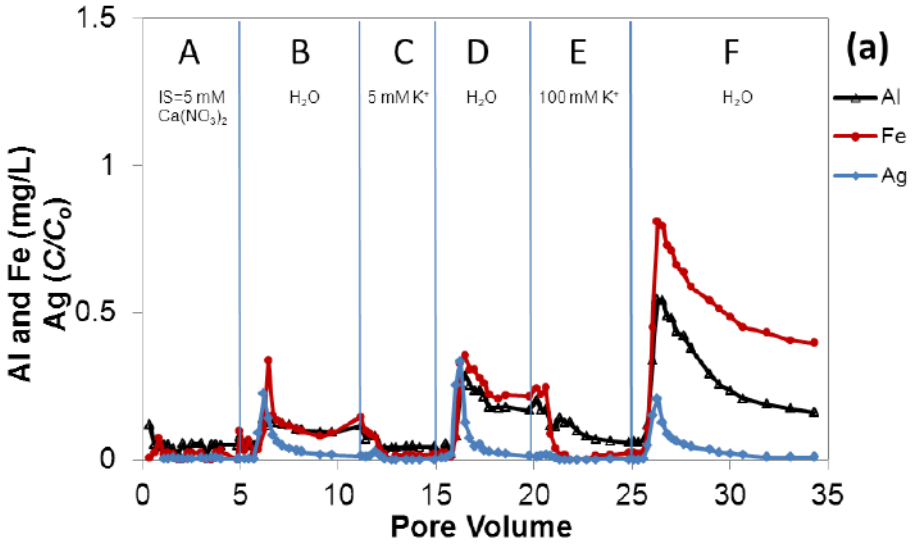
A
IS=5 mM Ca(NO3)2
B
H2O
C
5 mM K+
D
H2O
E
100 mM K+
F
H2O
(a)
Al
Fe
Ag
Al and Fe (mg/L)
Ag (C/C0)
Pore Volume
0
0.5
1
1.5
0
5
10
15
20
25
30
35

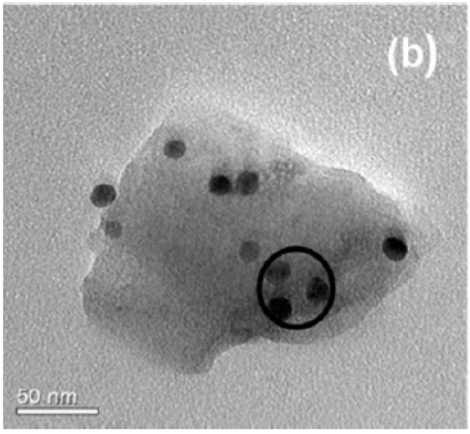
(b)
50 nm

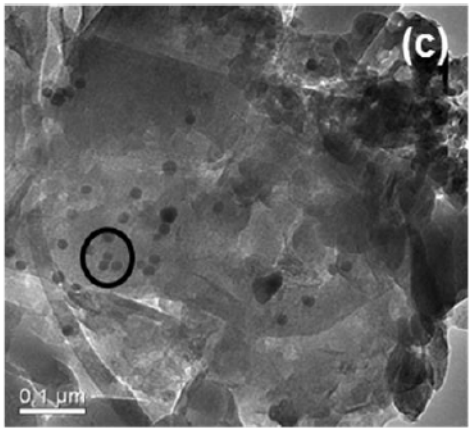
(c)
0.1 µm

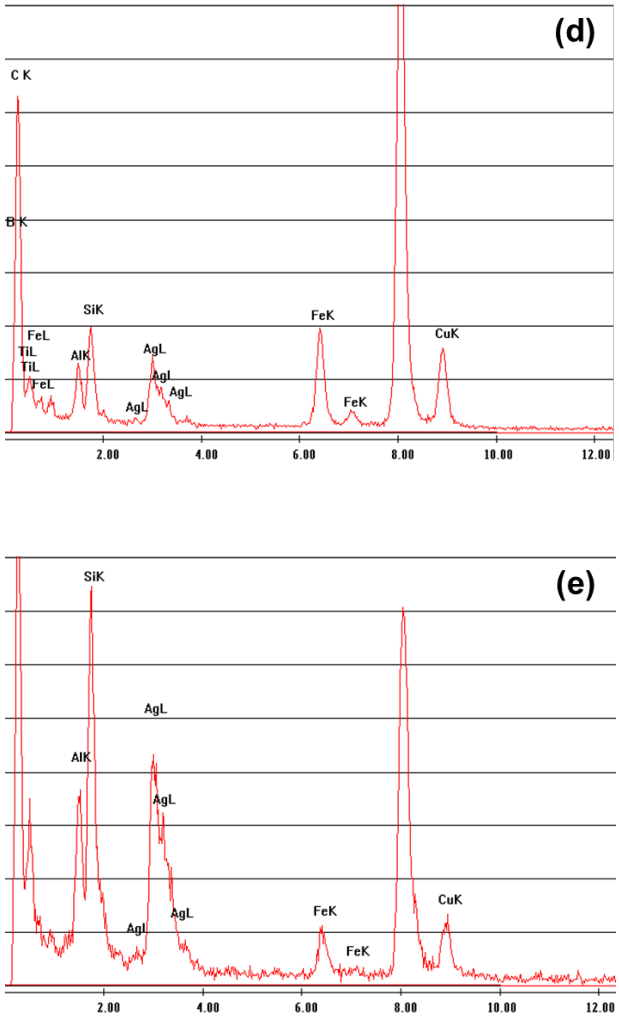

Figure 5.25. (a): Release of AgNPs and naturally occurring minerals by cation exchange (steps C and E) and ionic strength reduction (steps B, D, and F) in a saturated, repacked soil column. The Darcy velocity was 0.7 cm/min and the input AgNP concentration (C_o) was 10 mg/L. (b)-(e): Transmission electron microscopy (b and c) and energy-dispersive X-ray spectroscopy (EDX) (d and e) measurements of AgNPs in the effluent sampled from release experiment after cation exchange (AgNPs co-transported through soil column with released naturally occurring colloids/clay). The marked points in (b) and (c) were selected for EDX analysis as shown in (d) and (e), respectively.

5.3.3 Transport and retention of silver nanoparticles in lysimeter

The bromide tracer was recovered in the leachate after around 120 days irrigation (Figure 5.26a), while only a very low concentration of AgNPs was detected in the effluent during 12 months irrigation and no apparent trend was observed for the breakthrough of AgNPs (results not shown). The analyzed volumetric water contents at the depths of 5 and 30 cm during the long-term irrigation were 0.14 ± 0.05 and 0.17 ± 0.08, respectively, which were much lower than in small soil columns (Table 5). Similar to the results shown for small undisturbed soil columns (Figures 5.15-5.17), a hyperexponential RP for AgNPs was observed in the 1.1 m soil monolith (Figure 5.26b). The retention profile of AgNPs indicates that most of the injected AgNPs were retained in the upper 20 cm of soil. The retention of AgNPs in lysimeter was much higher than in small soil columns. This observation was likely due to the longer transport distance, much lower water content, and the intermittent irrigation applied in lysimeter, while 90% water saturation and constant irrigation were employed for small soil columns. This result also indicated that the AgNPs were mainly retained in a primary minimum and the interaction was strong enough to overcome the influence by a flow interruption, especially at a low water saturation degree. The experimental findings implied that most of the AgNP removal occurred in the subsurface after exposure to the environment. However, very low concentrations of AgNPs were found in some effluent samples. The contamination risk of AgNPs to groundwater cannot be fully excluded, particularly at flood events. Nevertheless, the influence of other important factors in the environment such as preferential flow paths, oversaturation in the case of flood event, and the interaction with plants or organisms should also be considered to access the risk of AgNPs to the terrestrial environment.

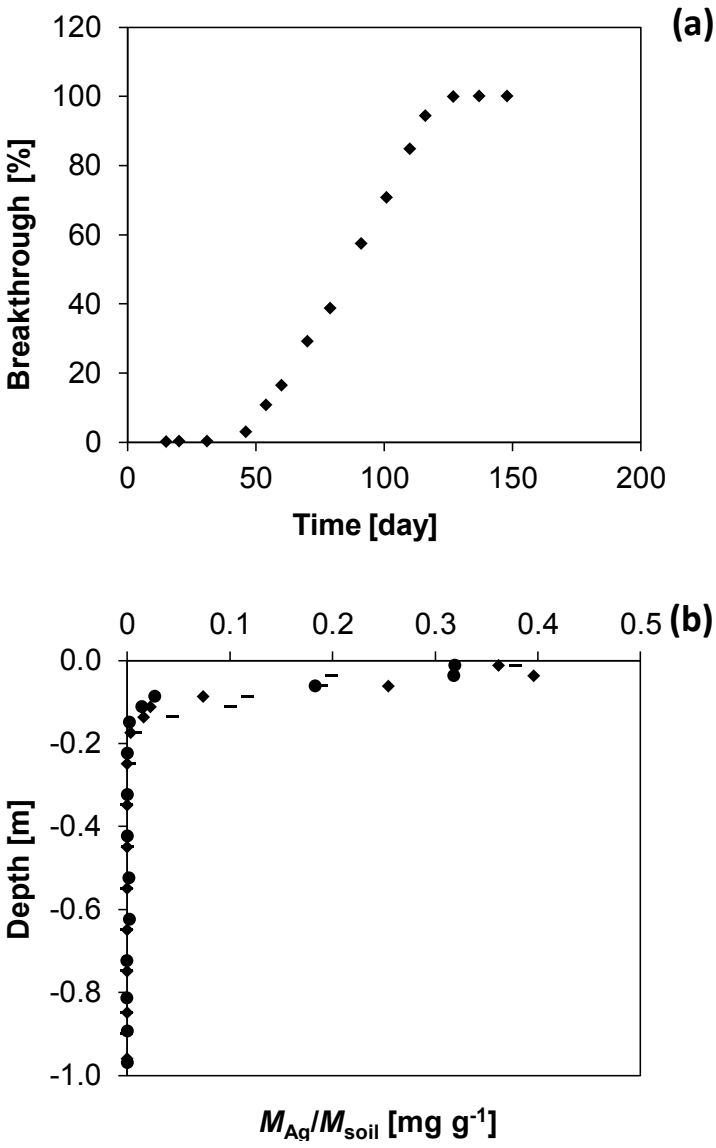

Figure 5.26. Observed cumulative breakthrough of tracer (a) and retention profile of AgNPs from the lysimeter experiment (b). The lysimeter was filled with an undisturbed loamy sand soil. M_{Ag}/M_{soil} represents the solid phase concentration of AgNPs, the mass of AgNP in 1 g soil. Three curves represent three different positions for sampling by a stainless steel soil corer after 12 months irrigation.

5.3.4 Conclusions of silver nanoparticle transport and release in an undisturbed soil

Transport experiments in undisturbed soil columns with around 90% water saturation demonstrated similar trends of AgNP mobility as in quartz sand columns by the influences of physicochemical factors. The retention of AgNPs in soil columns increased with increasing IS, smaller input concentration and lower flow velocity. However, strong NP retardation and hyperexponential RPs were observed for almost all the examined conditions with soil column, while only the deposition with the smallest grain size (Figure 5.4b) and/or with the lowest input concentration (Figure 5.5b) displayed hyperexponential RPs in quartz sand columns. The main fraction of deposited AgNPs was located in the top layers of the soil column because of the larger retention capacity for AgNP in the soil. In addition, the BET surface area analysis indicated a much greater interacting surface area in the loamy sand soil than the quartz sand used. The blocking effect was therefore less important in soil in comparison to quartz sand because the higher availability of retention sites in the soil has a larger capacity for interacting with AgNPs. Similarly, results of lysimeter showed a hyperexponential RP for AgNPs supporting the hypothesis that the AgNPs retained in a primary minimum were resistant to transport into a deeper layer by intermittent irrigation at a low water content.

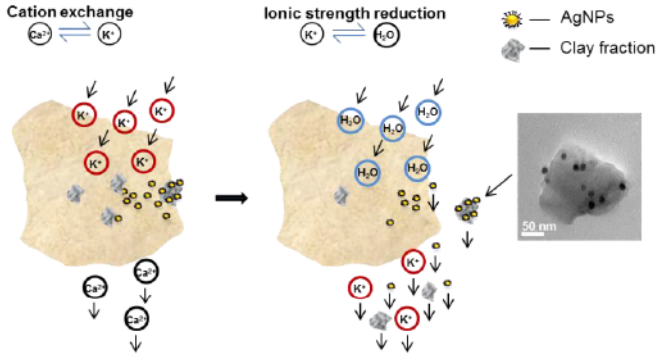

Figure 5.27. Schematic representation of the release of retained AgNPs, clay fraction, and the AgNPs co-transported by released clay from the soil after cation exchange and ionic strength reduction.

Release experiments for deposited AgNPs demonstrated that the release of AgNPs retained in K^+ containing electrolyte at the IS of 10 mM was easier than in Ca^{2+}. Further release of AgNPs retained in the presence of Ca^{2+} was observed when the column was irrigated with deionized water after cation exchange. This release process is schematically presented in Figure 5.27: a portion of retained AgNPs are interacting with soil clay fraction; exchange of monovalent cation (K^+) for divalent cation (Ca^{2+}) reduces the potential of cation bridging; the introduction of deionized water instead of K^+ expands the electrical double layer thickness thus promotes the release of clay fraction and AgNPs weakly interacting with soil matrix; the association of AgNPs and clays also takes place, which is demonstrated by TEM image. Both cation exchange and IS reduction are necessary for the remobilization of AgNPs retained in the presence of Ca^{2+}. Nevertheless, the soil clays largely account for the chemical heterogeneity of the soil surface, the quantification of the association of AgNPs and the soil colloids therefore would be needed to better understand the role of clay fraction on NP transport behavior.

6 Summary, conclusions and outlook

An understanding of the effect of physicochemical factors on the transport and retention of stabilized AgNPs in subsurface environments is needed for risk assessment. Model (quartz sand) and natural porous media (undisturbed soil) were employed to deduce the role of grain size, AgNP input concentration, ionic strength, and flow velocity on AgNP transport and retention. The remobilization of retained AgNPs, which is a crucial process that affects the fate of NPs in the environment and the risk of groundwater contamination, was also considered by changing the cation types and ionic strength to explore the influence of the transition of chemical conditions on retained AgNPs. In addition, a long-term lysimeter experiment was performed to study the AgNP transport behavior with artificial irrigation. Specifically, the spatial distribution of deposited AgNPs in the porous media (retention profile) was determined. Previous research on NP transport has frequently not considered retention profiles that provide important information on their predicted long-term transport potential. A mathematical model that accounts for time- and depth-dependent retention successfully captured the main features for both breakthrough curves and retention profiles.

In the water-saturated packed sand system, the transport of AgNPs was enhanced with an increase in water velocity, grain size, and AgNP input concentration, and a decrease in solution ionic strength. AgNPs were found to mainly interact with the matrix in an irreversible primary minimum as a result of microscopic heterogeneity and partially in a reversible secondary minimum at higher IS. Consequently, the effects of flow velocity on AgNP retention were primarily controlled by the rate of mass transfer to the solid surface. Significantly, the retention profiles were found to transit from hyperexponential to nonmonotonic and then to uniform with depth due to the combined effects of hydrodynamics near the column inlet and time-dependent blocking of S_{max} (maximum retained concentration on the solid phase) that was influenced by the amounts of surfactants. These findings provide valuable information for interpreting the evolution of retention profiles in porous media. The low-concentration surfactant that was

simultaneously transported with AgNPs or that pre-coated the porous media before the injection of AgNPs significantly enhanced particle mobility when compared to those particles without the addition of surfactant. In particular, the high sensitivity of AgNP retention to the stabilizing agent indicates that artificial stabilizers or naturally occurring organic matter will likely facilitate NP transport deeper into the subsurface environment and increase the potential risk of groundwater contamination. Both the breakthrough curves and retention profiles provide essential information for understanding transport behavior.

Similar to column studies conducted with repacked quartz sand, the mobility of the AgNPs in undisturbed soil columns under near water-saturated conditions (90%) exhibited high mobility under low IS (1 mM). The transport behavior in soil columns was highly dependent on the physicochemical conditions and displayed similar trends under these conditions as in quartz sand. In contrast, the breakthrough curves for AgNPs in the undisturbed soil exhibited significant amounts of retardation and the shape of the retention profiles was hyperexponential. The amount of retardation was dependent on physicochemical properties that influenced the retention rate and/or capacity. Results from a lysimeter experiment (a larger-scale) showed a limited transport of AgNPs and the main AgNP removal took place with the top layer of subsurface, but potential contamination of the groundwater with AgNPs cannot be excluded especially in the case of heavy precipitation events.

Release experiments showed that AgNP retention in the presence of the divalent cation (Ca^{2+}) was more pronounced than that with the monovalent cation K^{+} because of cation bridging. The remobilization of AgNPs was promoted by a reduction in IS and by a replacement of Ca^{2+} by K^{+}. In addition, further remobilization of AgNPs was observed when the column was irrigated with Milli-Q water (deionized water) after cation exchange. The AgNP release was therefore dependent on the coupled effects of cation exchange and expansion of the double layer thickness. An association between the fraction of the released AgNPs and soil colloids was also observed. Collectively, these findings demonstrate that the release processes can produce significant amounts of AgNP migration that pose a potential risk for

groundwater contamination during rain and irrigation events that produce transient changes in solution chemistry.

To better understand the fate of AgNPs and their interaction with the natural matrix, the influence of other important factors in the environment such as preferential flow paths, oversaturation in the case of flood events, and processes such as dissolution, transformation, and aging should also be considered. The morphological and colloid-chemical characterization of AgNPs attached to natural soil colloids would be of importance to assess the fate of AgNPs. This can be performed by means of scanning electron microscopy and transmission electron microscopy combined with energy dispersive X-ray spectroscopy. Furthermore, the interaction with plants or microorganisms that ubiquitously exist in the subsurface environment may also play an important role. For example, the network constructed by fungi hyphae may potentially facilitate AgNP mobility in porous media, or on the other hand, it may hinder particle transport by clogging pore structures, which will lead to a stronger retention.

References

Adamczyk, Z., B. Siwek and L. Szyk, 1995. Flow-Induced Surface Blocking Effects in Adsorption of Colloid Particles. Journal of Colloid and Interface Science 174(1), 130-141.

Baalousha, M., 2009. Aggregation and disaggregation of iron oxide nanoparticles: Influence of particle concentration, pH and natural organic matter. Science of the Total Environment 407(6), 2093-2101.

Badawy, A. E., 2011. Assessment of the Fate and Transport of Silver Nanoparticles in Porous Media. Ph.D. Dissertation, University of Cincinnati, USA.

Badawy, A. M. E., T. P. Luxton, R. G. Silva, K. G. Scheckel, M. T. Suidan and T. M. Tolaymat, 2010. Impact of Environmental Conditions (pH, Ionic Strength, and Electrolyte Type) on the Surface Charge and Aggregation of Silver Nanoparticles Suspensions. Environmental Science and Technology 44(4), 1260-1266.

Benn, T., B. Cavanagh, K. Hristovski, J. D. Posner and P. Westerhoff, 2010. The Release of Nanosilver from Consumer Products Used in the Home. Journal of Environmental Quality 39(6), 1875-1882.

Benn, T. M. and P. Westerhoff, 2008. Nanoparticle Silver Released into Water from Commercially Available Sock Fabrics. Environmental Science & Technology 42(11), 4133-4139.

Bergendahl, J. and D. Grasso, 2000. Prediction of colloid detachment in a model porous media: hydrodynamics. Chemical Engineering Science 55(9), 1523-1532.

Bhattacharya, S. N., M. R. Kamal and R. K. Gupta, 2008. Polymeric Nanocomposites - Theory and Practice, Hanser Publishers.

Blaser, S. A., M. Scheringer, M. MacLeod and K. Hungerbühler, 2008. Estimation of cumulative aquatic exposure and risk due to silver: Contribution of nano-functionalized plastics and textiles. Science of The Total Environment 390(2-3), 396-409.

Bradford, S. A., S. R. Yates, M. Bettahar and J. Simunek, 2002. Physical factors affecting the transport and fate of colloids in saturated porous media. Water Resour. Res. 38(12), 1327.

Bradford, S. A., J. Simunek, M. Bettahar, M. T. van Genuchten and S. R. Yates, 2003. Modeling Colloid Attachment, Straining, and Exclusion in Saturated Porous Media. Environmental Science & Technology 37(10), 2242-2250.

Bradford, S. A., J. Simunek and S. L. Walker, 2006. Transport and straining of *E. coli* O157:H7 in saturated porous media. Water Resour. Res. 42(12), W12S12.

Bradford, S. A. and S. Torkzaban, 2008. Colloid Transport And Retention In Unsaturated Porous Media: A Review Of Interface-, Collector-, And Pore-scale Processes And Models. Vadose Zone J. 7(2), 667-681.

Bradford, S. A., H. N. Kim, B. Z. Haznedaroglu, S. Torkzaban and S. L. Walker, 2009. Coupled Factors Influencing Concentration-Dependent Colloid Transport and Retention in Saturated Porous Media. Environmental Science & Technology 43(18), 6996-7002.

Bradford, S. A. and H. Kim, 2010. Implications of Cation Exchange on Clay Release and Colloid-Facilitated Transport in Porous Media. J. Environ. Qual. 39(6), 2040-2046.

Bradford, S. A., S. Torkzaban and J. Simunek, 2011a. Modeling colloid transport and retention in saturated porous media under unfavorable attachment conditions. Water Resour. Res. 47(10), W10503.

Bradford, S. A., S. Torkzaban and A. Wiegmann, 2011b. Pore-Scale Simulations to Determine the Applied Hydrodynamic Torque and Colloid Immobilization. Vadose Zone Journal 10(1), 252-261.

Bradford, S. A. and S. Torkzaban, 2013. Colloid Interaction Energies for Physically and Chemically Heterogeneous Porous Media. Langmuir 29(11), 3668-3676.

Burauel, P. and F. Führ, 2000. Formation and long-term fate of non-extractable residues in outdoor lysimeter studies. Environmental Pollution 108(1), 45-52.

Camesano, T. A., K. M. Unice and B. E. Logan, 1999. Blocking and ripening of colloids in porous media and their implications for bacterial transport. Colloids and Surfaces A: Physicochemical and Engineering Aspects 160(3), 291-307.

Carnero Ruiz, C. C. R., J. M.-B. Molina-Bolívar, J. A. Aguiar, G. M. MacIsaac, S. M. Moroze and R. P. Palepu, 2003. Effect of ethylene glycol on the thermodynamic and micellar properties of Tween 20. Colloid & Polymer Science 281(6), 531-541.

Chen, K. L. and M. Elimelech, 2006. Aggregation and Deposition Kinetics of Fullerene (C_{60}) Nanoparticles. Langmuir 22(26), 10994-11001.

Choi, J. Y., G. Ramachandran and M. Kandlikar, 2009. The Impact of Toxicity Testing Costs on Nanomaterial Regulation. Environmental Science & Technology 43(9), 3030-3034.

Choi, O., C.-P. Yu, G. Esteban Fernández and Z. Hu, 2010. Interactions of nanosilver with Escherichia coli cells in planktonic and biofilm cultures. Water Research 44(20), 6095-6103.

Chowdhury, I., Y. Hong, R. J. Honda and S. L. Walker, 2011. Mechanisms of TiO_2 nanoparticle transport in porous media: Role of solution chemistry, nanoparticle concentration, and flowrate. Journal of Colloid and Interface Science 360(2), 548-555.

Christian, P., F. Von der Kammer, M. Baalousha and T. Hofmann, 2008. Nanoparticles: structure, properties, preparation and behaviour in environmental media. Ecotoxicology 17(5), 326-343.

Cornelis, G., C. DooletteMadeleine Thomas, M. J. McLaughlin, J. K. Kirby, D. G. Beak and D. Chittleborough, 2012. Retention and Dissolution of Engineered Silver Nanoparticles in Natural Soils. Soil Sci. Soc. Am. J. 76(3), 891-902.

Coutris, C., E. J. Joner and D. H. Oughton, 2012. Aging and soil organic matter content affect the fate of silver nanoparticles in soil. Science of The Total Environment 420, 327-333.

Darlington, T. K., A. M. Neigh, M. T. Spencer, O. T. N. Guyen and S. J. Oldenburg, 2009. Nanoparticle characteristics affecting environmental fate and transport through soil. Environmental Toxicology and Chemistry 28(6), 1191-1199.

de Jonge, L. W., C. Kjaergaard and P. Moldrup, 2004. Colloids and Colloid-Facilitated Transport of Contaminants in Soils. Vadose Zone J. 3(2), 321-325.

Derjaguin, B. and L. Landau, 1993. Theory of the stability of strongly charged lyophobic sols and of the adhesion of strongly charged particles in solutions of electrolytes. Progress in Surface Science 43(1–4), 30-59.

Deshpande, P. A. and D. R. Shonnard, 1999. Modeling the effects of systematic variation in ionic strength on the attachment kinetics of Pseudomonas fluorescens UPER-1 in saturated sand columns. Water Resour. Res. 35(5), 1619-1627.

Diegoli, S., A. L. Manciulea, S. Begum, I. P. Jones, J. R. Lead and J. A. Preece, 2008. Interaction between manufactured gold nanoparticles and naturally occurring organic macromolecules. Science of the Total Environment 402(1), 51-61.

El Badawy, A. M., R. G. Silva, B. Morris, K. G. Scheckel, M. T. Suidan and T. M. Tolaymat, 2010. Surface Charge-Dependent Toxicity of Silver Nanoparticles. Environmental Science & Technology 45(1), 283-287.

Förster, M., V. Laabs, M. Lamshöft, T. Pütz and W. Amelung, 2008. Analysis of aged sulfadiazine residues in soils using microwave extraction and liquid chromatography tandem mass spectrometry. Analytical and Bioanalytical Chemistry 391(3), 1029-1038.

Fabrega, J., S. R. Fawcett, J. C. Renshaw and J. R. Lead, 2009. Silver Nanoparticle Impact on Bacterial Growth: Effect of pH, Concentration, and Organic Matter. Environmental Science & Technology 43(19), 7285-7290.

Fabrega, J., J. C. Renshaw and J. R. Lead, 2009. Interactions of Silver Nanoparticles with Pseudomonas putida Biofilms. Environmental Science & Technology 43(23), 9004-9009.

Foss Hansen, S., B. H. Larsen, S. I. Olsen and A. Baun, 2007. Categorization framework to aid hazard identification of nanomaterials. Nanotoxicology 1(3), 243-250.

Fritz, G., V. Schädler, N. Willenbacher and N. J. Wagner, 2002. Electrosteric Stabilization of Colloidal Dispersions. Langmuir 18(16), 6381-6390.

Gargiulo, G., S. Bradford, J. Simunek, P. Ustohal, H. Vereecken and E. Klumpp, 2007. Bacteria transport and deposition under unsaturated conditions: The role of the matrix grain size and the bacteria surface protein. Journal of Contaminant Hydrology 92(3-4), 255-273.

Geranio, L., M. Heuberger and B. Nowack, 2009. The Behavior of Silver Nanotextiles during Washing. Environmental Science & Technology 43(21), 8113-8118.

Godinez, I. G. and C. J. G. Darnault, 2011. Aggregation and transport of nano-TiO_2 in saturated porous media: Effects of pH, surfactants and flow velocity. Water Research 45(2), 839-851.

Gottschalk, F., T. Sonderer, R. W. Scholz and B. Nowack, 2009. Modeled Environmental Concentrations of Engineered Nanomaterials (TiO_2, ZnO, Ag, CNT, Fullerenes) for Different Regions. Environmental Science & Technology 43(24), 9216-9222.

Gottschalk, F., T. Sonderer, R. W. Scholz and B. Nowack, 2010. Possibilities and limitations of modeling environmental exposure to engineered nanomaterials by probabilistic: Material flow analysis. Environmental Toxicology and Chemistry 29(5), 1036-1048.

Grasso, D., K. Subramaniam, M. Butkus, K. Strevett and J. Bergendahl, 2002. A review of non-DLVO interactions in environmental colloidal systems. Reviews in Environmental Science and Biotechnology 1(1), 17-38.

Gregory, J., 1981. Approximate expressions for retarded van der waals interaction. Journal of Colloid and Interface Science 83(1), 138-145.

Grolimund, D., M. Borkovec, K. Barmettler and H. Sticher, 1996. Colloid-Facilitated Transport of Strongly Sorbing Contaminants in Natural Porous Media: A Laboratory Column Study. Environmental Science & Technology 30(10), 3118-3123.

Grolimund, D. and M. Borkovec, 2006. Release of colloidal particles in natural porous media by monovalent and divalent cations. Journal of Contaminant Hydrology 87(3–4), 155-175.

Grolimund, D., K. Barmettler and M. Borkovec, 2007. Colloid Facilitated Transport in Natural Porous Media: Fundamental Phenomena and Modelling. Colloidal Transport in Porous Media. F. Frimmel, F. Kammer and H.-C. Flemming, Springer Berlin Heidelberg: 3-27.

Henglein, A. and M. Giersig, 1999. Formation of Colloidal Silver Nanoparticles: Capping Action of Citrate. The Journal of Physical Chemistry B 103(44), 9533-9539.

Hensel, A., M. Rischer, D. Di Stefano, I. Behr and E. Wolf-Heuss, 1997. Full chromatographic characterization of nonionic surfactant polyoxyethylene glycerol trioleate. Pharmaceutica Acta Helvetiae 72(3), 185-189.

Hoek, E. M. V. and G. K. Agarwal, 2006. Extended DLVO interactions between spherical particles and rough surfaces. Journal of Colloid and Interface Science 298(1), 50-58.

Hogg, R., T. W. Healy and D. W. Fuerstenau, 1966. Mutual coagulation of colloidal dispersions. Transactions of the Faraday Society 62, 1638-1651.

Huynh, K. A. and K. L. Chen, 2011. Aggregation Kinetics of Citrate and Polyvinylpyrrolidone Coated Silver Nanoparticles in Monovalent and Divalent Electrolyte Solutions. Environmental Science & Technology 45(13), 5564-5571.

Jacobsen, O. H., P. Moldrup, C. Larsen, L. Konnerup and L. W. Petersen, 1997. Particle transport in macropores of undisturbed soil columns. Journal of Hydrology 196(1-4), 185-203.

Jaisi, D. P., N. B. Saleh, R. E. Blake and M. Elimelech, 2008. Transport of Single-Walled Carbon Nanotubes in Porous Media: Filtration Mechanisms and Reversibility. Environmental Science & Technology 42(22), 8317-8323.

Jaisi, D. P. and M. Elimelech, 2009. Single-Walled Carbon Nanotubes Exhibit Limited Transport in Soil Columns. Environmental Science & Technology 43(24), 9161-9166.

Jeong, S. W. and S. D. Kim, 2009. Aggregation and transport of copper oxide nanoparticles in porous media. Journal of Environmental Monitoring 11(9), 1595-1600.

Johnson, P. R. and M. Elimelech, 1995. Dynamics of Colloid Deposition in Porous Media: Blocking Based on Random Sequential Adsorption. Langmuir 11(3), 801-812.

Johnson, W. P., X. Li and S. Assemi, 2007. Deposition and re-entrainment dynamics of microbes and non-biological colloids during non-perturbed transport in porous media in the presence of an energy barrier to deposition. Advances in Water Resources 30(6–7), 1432-1454.

Kaegi, R., A. Voegelin, B. Sinnet, S. Zuleeg, H. Hagendorfer, M. Burkhardt and H. Siegrist, 2011. Behavior of Metallic Silver Nanoparticles in a Pilot Wastewater Treatment Plant. Environmental Science & Technology 45(9), 3902-3908.

Kanel, S. R. and H. Choi, 2007. Transport characteristics of surface-modified nanoscale zero-valent iron in porous media. Water Science and Technology 55(1-2), 157-162.

Kanel, S. R., D. Nepal, B. Manning and H. Choi, 2007. Transport of surface-modified iron nanoparticle in porous media and application to arsenic(III) remediation. Journal of Nanoparticle Research 9(5), 725-735.

Kang, K., D.-H. Lim, I.-H. Choi, T. Kang, K. Lee, E.-Y. Moon, Y. Yang, M.-S. Lee and J.-S. Lim, 2011. Vascular tube formation and angiogenesis induced by polyvinylpyrrolidone-coated silver nanoparticles. Toxicology Letters 205(3), 227-234.

Kasel, D., S. A. Bradford, J. Šimůnek, M. Heggen, H. Vereecken and E. Klumpp, 2013. Transport and retention of multi-walled carbon nanotubes in saturated porous media: Effects of input concentration and grain size. Water Research 47(2), 933-944.

Kennedy, A. J., M. S. Hull, A. J. Bednar, J. D. Goss, J. C. Gunter, J. L. Bouldin, P. J. Vikesland and J. A. Steevens, 2010. Fractionating Nanosilver: Importance for Determining Toxicity to Aquatic Test Organisms. Environmental Science & Technology 44(24), 9571-9577.

Kim, B., C.-S. Park, M. Murayama and M. F. Hochella, 2010. Discovery and Characterization of Silver Sulfide Nanoparticles in Final Sewage Sludge Products. Environmental Science & Technology 44(19), 7509-7514.

Kjaergaard, C., T. G. Poulsen, P. Moldrup and L. W. de Jonge, 2004. Colloid Mobilization and Transport in Undisturbed Soil Columns. I. Pore Structure Characterization and Tritium Transport. Vadose Zone J. 3(2), 413-423.

Klaine, S. J., P. J. J. Alvarez, G. E. Batley, T. F. Fernandes, R. D. Handy, D. Y. Lyon, S. Mahendra, M. J. McLaughlin and J. R. Lead, 2008. Nanomaterials in the environment: Behavior, fate, bioavailability, and effects. Environmental Toxicology and Chemistry 27(9), 1825-1851.

Klein, C. L., S. Comero, G. Locoro, B. M. Gawlik, B. Stahlmecke, J. Romazanov and T. A. J. Kuhlbusch, 2011. NM-Series of Representative Manufactured Nanomaterials NM-300 Silver Characterisation, Stability, Homogeneity. EUR 24693 EN– Joint Research Centre – Institute for Health and Consumer Protection.

Ko, C.-H. and M. Elimelech, 2000. The “Shadow Effect” in Colloid Transport and Deposition Dynamics in Granular Porous Media: Measurements and Mechanisms. Environmental Science & Technology 34(17), 3681-3689.

Kretzschmar, R., K. Barmettler, D. Grolimund, Y.-d. Yan, M. Borkovec and H. Sticher, 1997. Experimental determination of colloid deposition rates and collision efficiencies in natural porous media. Water Resour. Res. 33(5), 1129-1137.

Kretzschmar, R., M. Borkovec, D. Grolimund, M. Elimelech and L. S. Donald, 1999. Mobile Subsurface Colloids and Their Role in Contaminant Transport. Advances in Agronomy, Academic Press 66, 121-193.

Kvitek, L., A. Pancek, J. Soukupova, M. Kolar, R. Vecerova, R. Prucek, M. Holecova and R. Zboril, 2008. Effect of surfactants and polymers on stability and antibacterial activity of silver nanoparticles (NPs). Journal of Physical Chemistry C 112(15), 5825-5834.

Lecoanet, H. F., J.-Y. Bottero and M. R. Wiesner, 2004. Laboratory Assessment of the Mobility of Nanomaterials in Porous Media. Environmental Science & Technology 38(19), 5164-5169.

Lecoanet, H. F. and M. R. Wiesner, 2004. Velocity effects on fullerene and oxide nanoparticle deposition in porous media. Environmental Science & Technology 38(16), 4377-4382.

Lee, K. J., P. D. Nallathamby, L. M. Browning, C. J. Osgood and X.-H. N. Xu, 2007. In Vivo Imaging of Transport and Biocompatibility of Single Silver Nanoparticles in Early Development of Zebrafish Embryos. ACS Nano 1(2), 133-143.

Levard, C., E. M. Hotze, G. V. Lowry and G. E. Brown, 2012. Environmental Transformations of Silver Nanoparticles: Impact on Stability and Toxicity. Environmental Science & Technology 46(13), 6900-6914.

Li, X., T. D. Scheibe and W. P. Johnson, 2004. Apparent Decreases in Colloid Deposition Rate Coefficients with Distance of Transport under Unfavorable Deposition Conditions: A General Phenomenon. Environmental Science & Technology 38(21), 5616-5625.

Li, X. and W. P. Johnson, 2005. Nonmonotonic Variations in Deposition Rate Coefficients of Microspheres in Porous Media under Unfavorable Deposition Conditions. Environmental Science & Technology 39(6), 1658-1665.

Li, X., P. Zhang, C. L. Lin and W. P. Johnson, 2005. Role of Hydrodynamic Drag on Microsphere Deposition and Re-entrainment in Porous Media under Unfavorable Conditions. Environmental Science & Technology 39(11), 4012-4020.

Li, X., J. J. Lenhart and H. W. Walker, 2010. Dissolution-Accompanied Aggregation Kinetics of Silver Nanoparticles. Langmuir 26(22), 16690-16698.

Li, X. and J. J. Lenhart, 2012. Aggregation and Dissolution of Silver Nanoparticles in Natural Surface Water. Environmental Science & Technology 46(10), 5378-5386.

Li, Y., Y. Wang, K. D. Pennell and L. M. Abriola, 2008. Investigation of the Transport and Deposition of Fullerene (C_{60}) Nanoparticles in Quartz Sands under Varying Flow Conditions. Environmental Science & Technology 42(19), 7174-7180.

Liang, Z., A. Das and Z. Hu, 2010. Bacterial response to a shock load of nanosilver in an activated sludge treatment system. Water Research 44(18), 5432-5438.

Lin, D., X. Tian, F. Wu and B. Xing, 2010. Fate and Transport of Engineered Nanomaterials in the Environment. J. Environ. Qual. 39(6), 1896-1908.

Lin, S., Y. Cheng, Y. Bobcombe, K. L. Jones, J. Liu and M. R. Wiesner, 2011. Deposition of Silver Nanoparticles in Geochemically Heterogeneous Porous Media: Predicting Affinity from Surface Composition Analysis. Environmental Science & Technology 45(12), 5209-5215.

Lin, S., Y. Cheng, J. Liu and M. R. Wiesner, 2012. Polymeric Coatings on Silver Nanoparticles Hinder Autoaggregation but Enhance Attachment to Uncoated Surfaces. Langmuir 28(9), 4178-4186.

Liu, J. and R. H. Hurt, 2010. Ion Release Kinetics and Particle Persistence in Aqueous Nano-Silver Colloids. Environmental Science & Technology 44(6), 2169-2175.

Liu, X., D. M. O'Carroll, E. J. Petersen, Q. Huang and C. L. Anderson, 2009. Mobility of Multiwalled Carbon Nanotubes in Porous Media. Environmental Science & Technology 43(21), 8153-8158.

Logan, B., D. Jewett, R. Arnold, E. Bouwer and C. O'Melia, 1995. Clarification of Clean-Bed Filtration Models. Journal of Environmental Engineering 121(12), 869-873.

Lowry, G. V. and E. A. Casman, 2009. Nanomaterial Transport, Transformation, and Fate in the Environment a Risk-Based Perspective on Research Needs. Nanomaterials: Risks and Benefits, 125-137.

Marquardt, D. W., 1963. An Algorithm for Least-Squares Estimation of Nonlinear Parameters. Journal of the Society for Industrial and Applied Mathematics 11(2), 431-441.

Nowack, B. and T. D. Bucheli, 2007. Occurrence, behavior and effects of nanoparticles in the environment. Environmental Pollution 150(1), 5-22.

Nowack, B., 2010. Nanosilver Revisited Downstream. Science 330(6007), 1054-1055.

Nowack, B., H. F. Krug and M. Height, 2011. 120 Years of Nanosilver History: Implications for Policy Makers. Environmental Science & Technology 45(4), 1177-1183.

Oberdorster, G., 2005. Nanotoxicology : an emerging discipline evolving from studies of ultrafine particles. Environ. Health Perspect. 113, 823-839.

Ohshima, H., 1994. Electrophoretic Mobility of Soft Particles. Journal of Colloid and Interface Science 163(2), 474-483.

Ohshima, H., 2005. Approximate expression for the electrophoretic mobility of a spherical colloidal particle covered with an ion-penetrable uncharged polymer Layer. Colloid & Polymer Science 283(8), 819-825.

Pan, B. and B. Xing, 2012. Applications and implications of manufactured nanoparticles in soils: a review. European Journal of Soil Science 63(4), 437-456.

Phenrat, T., N. Saleh, K. Sirk, H.-J. Kim, R. Tilton and G. Lowry, 2008. Stabilization of aqueous nanoscale zerovalent iron dispersions by anionic polyelectrolytes: adsorbed anionic polyelectrolyte layer properties and their effect on aggregation and sedimentation. Journal of Nanoparticle Research 10(5), 795-814.

Phenrat, T., A. Cihan, H.-J. Kim, M. Mital, T. Illangasekare and G. V. Lowry, 2010. Transport and Deposition of Polymer-Modified Fe^0 Nanoparticles in 2-D Heterogeneous Porous Media: Effects of Particle Concentration, Fe^0 Content, and Coatings. Environmental Science & Technology 44(23), 9086-9093.

Phenrat, T., J. E. Song, C. M. Cisneros, D. P. Schoenfelder, R. D. Tilton and G. V. Lowry, 2010. Estimating Attachment of Nano- and Submicrometer-particles Coated with Organic Macromolecules in Porous Media: Development of an Empirical Model. Environmental Science & Technology 44(12), 4531-4538.

Rajagopalan, R. and C. Tien, 1976. Trajectory analysis of deep-bed filtration with the sphere-in-cell porous media model. AIChE Journal 22(3), 523-533.

Rinck-Pfeiffer, S., S. Ragusa, P. Sztajnbok and T. Vandevelde, 2000. Interrelationships between biological, chemical, and physical processes as an analog to clogging in aquifer storage and recovery (ASR) wells. Water Research 34(7), 2110-2118.

Roy, S. B. and D. A. Dzombak, 1996. Colloid release and transport processes in natural and model porous media. Colloids and Surfaces A: Physicochemical and Engineering Aspects 107, 245-262.

Ryan, J. N. and M. Elimelech, 1996. Colloid mobilization and transport in groundwater. Colloids and Surfaces A: Physicochemical and Engineering Aspects 107, 1-56.

Sagee, O., I. Dror and B. Berkowitz, 2012. Transport of silver nanoparticles (AgNPs) in soil. Chemosphere 88(5), 670-675.

Sarkar, A., S. Kapoor and T. Mukherjee, 2005. Preparation, characterization, and surface modification of silver nanoparticles in formamide. Journal of Physical Chemistry B 109(16), 7698-7704.

Schijven, J. F. and S. M. Hassanizadeh, 2000. Removal of Viruses by Soil Passage: Overview of Modeling, Processes, and Parameters. BEST 30(1), 49-127.

Shaw, B. J. and R. D. Handy, 2011. Physiological effects of nanoparticles on fish: A comparison of nanometals versus metal ions. Environment International 37(6), 1083-1097.

Shen, C., B. Li, Y. Huang and Y. Jin, 2007. Kinetics of Coupled Primary- and Secondary-Minimum Deposition of Colloids under Unfavorable Chemical Conditions. Environmental Science & Technology 41(20), 6976-6982.

Simunek, J., M. T. v. Genuchten and M. Sejna, 2005. The HYDRUS-1D software package for simulating the one-dimensional movement of water,heat, and multiple solutes in variably-saturated media, version 3.0. Dep. of Environ. Sci., Univ. of Calif., Riverside HYDRUS Software Ser. 1.

Šimůnek, J., M. T. v. Genuchten and M. Šejna, 2008. Development and applications of the HYDRUS and STANMOD software packages, and related codes. Vadose Zone Journal 7(2), 587-600.

Song, J. E., T. Phenrat, S. Marinakos, Y. Xiao, J. Liu, M. R. Wiesner, R. D. Tilton and G. V. Lowry, 2011. Hydrophobic Interactions Increase Attachment of Gum Arabic- and PVP-Coated Ag Nanoparticles to Hydrophobic Surfaces. Environmental Science & Technology 45(14), 5988-5995.

Suarez, D. L., J. D. Wood and S. M. Lesch, 2006. Effect of SAR on water infiltration under a sequential rain–irrigation management system. Agricultural Water Management 86(1–2), 150-164.

Thio, B. J. R., M. O. Montes, M. A. Mahmoud, D.-W. Lee, D. Zhou and A. A. Keller, 2012. Mobility of Capped Silver Nanoparticles under Environmentally Relevant Conditions. Environmental Science & Technology 46(13), 6985-6991.

Tian, Y. A., B. Gao, C. Silvera-Batista and K. J. Ziegler, 2010. Transport of engineered nanoparticles in saturated porous media. Journal of Nanoparticle Research 12(7), 2371-2380.

Tong, M., T. A. Camesano and W. P. Johnson, 2005. Spatial Variation in Deposition Rate Coefficients of an Adhesion-Deficient Bacterial Strain in Quartz Sand. Environmental Science & Technology 39(10), 3679-3687.

Tong, M., X. Li, C. N. Brow and W. P. Johnson, 2005. Detachment-Influenced Transport of an Adhesion-Deficient Bacterial Strain within Water-Reactive Porous Media. Environmental Science & Technology 39(8), 2500-2508.

Tong, M. and W. P. Johnson, 2006. Colloid Population Heterogeneity Drives Hyperexponential Deviation from Classic Filtration Theory. Environmental Science & Technology 41(2), 493-499.

Tong, M., H. Ma and W. P. Johnson, 2008. Funneling of Flow into Grain-to-grain Contacts Drives Colloid-Colloid Aggregation in the Presence of an Energy Barrier. Environmental Science & Technology 42(8), 2826-2832.

Tong, M. P., J. L. Ding, Y. Shen and P. T. Zhu, 2010. Influence of biofilm on the transport of fullerene (C_{60}) nanoparticles in porous media. Water Research 44(4), 1094-1103.

Topp, G. C., J. L. Davis and A. P. Annan, 1980. Electromagnetic determination of soil water content: Measurements in coaxial transmission lines. Water Resources Research 16(3), 574-582.

Toride, N., F. J. Leij and M. T. van Genuchten, 1999. The CXTFIT code for estimating transport parameters from laboratory or field tracer experiments.Version 2.1. U.S. Salinity Laboratory,USDA-ARS, Riverside, CA. Research Rep. 137.

Torkzaban, S., S. A. Bradford, M. T. van Genuchten and S. L. Walker, 2008. Colloid transport in unsaturated porous media: The role of water content and ionic strength on particle straining. Journal of Contaminant Hydrology 96(1-4), 113-127.

Torkzaban, S., S. S. Tazehkand, S. L. Walker and S. A. Bradford, 2008. Transport and fate of bacteria in porous media: Coupled effects of chemical conditions and pore space geometry. Water Resour. Res. 44(4), W04403.

Torkzaban, S., H. N. Kim, J. Simunek and S. A. Bradford, 2010. Hysteresis of Colloid Retention and Release in Saturated Porous Media During Transients in Solution Chemistry. Environmental Science & Technology 44(5), 1662-1669.

Torkzaban, S., J. Wan, T. K. Tokunaga and S. A. Bradford, 2012. Impacts of bridging complexation on the transport of surface-modified nanoparticles in saturated sand. Journal of Contaminant Hydrology 136-137, 86-95.

Tufenkji, N. and M. Elimelech, 2004. Deviation from the Classical Colloid Filtration Theory in the Presence of Repulsive DLVO Interactions. Langmuir 20(25), 10818-10828.

Tufenkji, N. and M. Elimelech, 2005. Breakdown of Colloid Filtration Theory: Role of the Secondary Energy Minimum and Surface Charge Heterogeneities. Langmuir 21(3), 841-852.

Tufenkji, N., 2007. Colloid and Microbe Migration in Granular Environments: A Discussion of Modelling Methods. Colloidal Transport in Porous Media. F. Frimmel, F. Kammer and H.-C. Flemming, Springer Berlin Heidelberg: 119-142.

Um, W. and C. Papelis, 2002. Geochemical effects on colloid-facilitated metal transport through zeolitized tuffs from the Nevada Test Site. Environmental Geology 43(1-2), 209-218.

Unold, M., J. Simunek, R. Kasteel, J. Groeneweg and H. Vereecken, 2009. Transport of Manure-Based Applied Sulfadiazine and Its Main Transformation Products in Soil Columns. Vadose Zone Journal 8(3), 677-689.

Verwey, E. J. W., 1947. Theory of the Stability of Lyophobic Colloids. The Journal of Physical and Colloid Chemistry 51(3), 631-636.

Vincent, B., J. Edwards, S. Emmett and A. Jones, 1986. Depletion flocculation in dispersions of sterically-stabilised particles ("soft spheres"). Colloids and Surfaces 18(2-4), 261-281.

Wang, D., M. Paradelo, S. A. Bradford, W. J. G. M. Peijnenburg, L. Chu and D. Zhou, 2011. Facilitated transport of Cu with hydroxyapatite nanoparticles in saturated sand: Effects of solution ionic strength and composition. Water Research 45(18), 5905-5915.

Wang, D., S. A. Bradford, R. W. Harvey, B. Gao, L. Cang and D. Zhou, 2012. Humic Acid Facilitates the Transport of ARS-Labeled Hydroxyapatite Nanoparticles in Iron Oxyhydroxide-Coated Sand. Environmental Science & Technology 46(5), 2738-2745.

Wang, Y., Y. Li, J. D. Fortner, J. B. Hughes, L. M. Abriola and K. D. Pennell, 2008. Transport and Retention of Nanoscale C_{60} Aggregates in Water-Saturated Porous Media. Environmental Science & Technology 42(10), 3588-3594.

Wang, Y., Y. Li, J. Costanza, L. M. Abriola and K. D. Pennell, 2012. Enhanced Mobility of Fullerene (C_{60}) Nanoparticles in the Presence of Stabilizing Agents. Environmental Science & Technology 46(21), 11761-11769.

Wei, Y.-T. and S.-c. Wu, 2010. Development of a Trajectory Model for Predicting Attachment of Submicrometer Particles in Porous Media: Stabilized NZVI as a Case Study. Environmental Science & Technology 44(23), 8996-9002.

Wiesner, M. R., G. V. Lowry, P. Alvarez, D. Dionysiou and P. Biswas, 2006. Assessing the risks of manufactured nanomaterials. Environmental Science & Technology 40(14), 4336-4345.

Xu, S. P., Q. Liao and J. E. Saiers, 2008. Straining of nonspherical colloids in saturated porous media. Environmental Science & Technology 42(3), 771-778.

Yao, K.-M., M. T. Habibian and C. R. O'Melia, 1971. Water and waste water filtration. Concepts and applications. Environmental Science & Technology 5(11), 1105-1112.

Yuan, H. and A. A. Shapiro, 2011. A mathematical model for non-monotonic deposition profiles in deep bed filtration systems. Chemical Engineering Journal 166(1), 105-115.

Zhang, H., J. A. Smith and V. Oyanedel-Craver, 2012. The effect of natural water conditions on the anti-bacterial performance and stability of silver nanoparticles capped with different polymers. Water Research 46(3), 691-699.

Zhang, L., L. Hou, L. Wang, A. T. Kan, W. Chen and M. B. Tomson, 2012. Transport of Fullerene Nanoparticles (nC_{60}) in Saturated Sand and Sandy Soil: Controlling Factors and Modeling. Environmental Science & Technology 46(13), 7230-7238.

Zhou, D., A. I. Abdel-Fattah and A. A. Keller, 2012. Clay Particles Destabilize Engineered Nanoparticles in Aqueous Environments. Environmental Science & Technology 46(14), 7520-7526.

Zook, J. M., R. I. MacCuspie, L. E. Locascio, M. D. Halter and J. T. Elliott, 2011. Stable nanoparticle aggregates/agglomerates of different sizes and the effect of their size on hemolytic cytotoxicity. Nanotoxicology 5(4), 517-530.

List of Figures

List of Tables

Band / Volume 199
Improved characterization of river-aquifer interactions through data assimilation with the Ensemble Kalman Filter
W. Kurtz (2013), xxv, 125 pp
ISBN: 978-3-89336-925-6

Band / Volume 200
Innovative SANEX process for trivalent actinides separation from PUREX raffinate
A. Sypula (2013), 220 pp
ISBN: 978-3-89336-927-0

Band / Volume 201
Transport and deposition of functionalized multi-walled carbon nanotubes in porous media
D. Kasel (2013), 103 pp
ISBN: 978-3-89336-929-4

Band / Volume 202
Full-waveform inversion of surface ground penetrating radar data and coupled hydrogeophysical inversion for soil hydraulic property estimation
S. Busch (2013), 112 pp
ISBN: 978-3-89336-930-0

Band / Volume 203
Politikszenarien für den Klimaschutz VI – Treibhausgas-Emissionsszenarien bis zum Jahr 2030
Advances in Systems Analysis 5
P. Hansen, S. Gores und F. Chr. Matthes (Hrsg.)
(2013), XX, 257 pp
ISBN: 978-3-89336-932-4

Band / Volume 204
Effect of Composition, Microstructure and Component Thickness on the Oxidation Behaviour of Laves Phase Strengthened Interconnect Steel for Solid Oxide Fuel Cells (SOFC)
C. Asensio Jimenez (2014), 210 pp
ISBN: 978-3-89336-935-5

Band / Volume 205
Airborne VOC measurements on board the Zeppelin NT during the PEGASOS campaigns in 2012 deploying the improved Fast-GC-MSD System
J. Jäger (2014), VIII, 182 pp
ISBN: 978-3-89336-936-2

Band / Volume 206
Pulvermetallurgische Funktionsbauteile aus NiTi- und NiTi-X Legierungspulvern
M. Bitzer (2014), III, 144 pp
ISBN: 978-3-89336-937-9

Band / Volume 207
Zinkoxid: Einfluss von Dotierung und Legierungen auf elektro-optische Eigenschaften, auf das Ätzverhalten und auf die Tempernachbehandlung
M. Warzecha (2014), 8, vii, 170 pp
ISBN: 978-3-89336-938-6

Band / Volume 208
SGSreco - Radiologische Charakterisierung von Abfallfässern durch Segmentierte γ-Scan Messungen
T. H. Krings (2014), ix, 181, XI
ISBN: 978-3-89336-945-4

Band / Volume 209
Kühlkonzepte für Hochtemperatur-Polymerelektrolyt-Brennstoffzellen-Stacks
J. Supra (2014), III, 191 pp
ISBN: 978-3-89336-946-1

Band / Volume 210
Eigenschaften des Phosphorsäure-Polybenzimidazol-Systems in Hochtemperatur-Polymerelektrolyt-Brennstoffzellen
A. Majerus (2014), viii, 141 pp
ISBN: 978-3-89336-947-8

Band / Volume 211
Study on the Complex Li-N-H Hydrogen Storage System
L. Du (2014), I, 132 pp
ISBN: 978-3-89336-952-2

Band / Volume 212
Transport and Retention of Stabilized Silver Nanoparticles in Porous Media
Y. Liang (2014), IV, 109 pp
ISBN: 978-3-89336-957-7

Energie & Umwelt / Energy & Environment
Band / Volume 212
ISBN 978-3-89336-957-7

JÜLICH
FORSCHUNGSZENTRUM